Aus der

Universitätsklinik für Hals-, Nasen- und Ohrenheilkunde
Tübinger Hörforschungszentrum
Molekulare Hörphysiologie

in Zusammenarbeit mit

der Radiologischen Universitätsklinik Tübingen
Abteilung Diagnostische und Interventionelle Neuroradiologie
Bereich MR-Forschung

Resting-state BOLD fMRI connectivity in central auditory circuitries and predefined associated regions of interest in young, healthy subjects

Inaugural-Dissertation
zur Erlangung des Doktorgrades
der Medizin

der Medizinischen Fakultät
der Eberhard Karls Universitäts
zu Tübingen

vorgelegt von

Mendola, Giulio

2025

Dekan:	Professor Dr. B. Pichler
1. Berichterstatter:	Professorin Dr. M. Knipper-Breer
2. Berichterstatter:	Professor Dr. H. Lerche
Tag der Disputation:	09.05.2025

To my little son Aureliano, torn away far too early from this world.

You are loved beyond measure.

List of Tables

List of Figures

A	anterior
AAL	Anatomical Automatic Labelling
ABR	auditory brainstem response
AC	anterior commissure *or* Auditory cortex
Amyg	amygdala
AN	auditory nerve
AVCN	anterior ventral cochlear nucleus
BA	Brodmann area
BM	basilar membrane
BOLD	blood oxygen level-dependent
CBF	cerebral blood flow
CBV	cerebral blood volume
CM	cochlear microphonic
CN	cochlear nucleus
dB	decibel
DCN	dorsal cochlear nucleus
dHb	deoxyhemoglobin
DL	dorsolateral
DNLL	dorsal nuclei of the lateral lemniscus
EAM	external auditory meatus
EEG	electroencephalography
EPI	echo-planar-imaging
FA	Flip angle
FDR	false discovery rate
fMRI	functional magnetic resonance imaging
FWHM	full width at half maximum
GRE	gradient echo
Hipp	hippocampus
HPA	hypothalamic-pituitary-adrenal
Hz	hertz
IC	inferior colliculus
IHC	inner hair cell
K^+	potassium
L	left
LL	lateral lemniscus
LORETA	low-resolution electromagnetic tomography analysis
LSO	lateral superior olive
M	medial
MGB	medial geniculate body
mm	millimetre

MNI	Montreal Neurological Institute
MNTB	medial nuclei of trapezoid body
MRI	magnetic resonance imaging
ms	millisecond
MSO	medial superior olive
MTG	middle temporal gyrus
NLL	nuclei of the lateral lemniscus
OHC	outer hair cell
P	posterior
PC	posterior commissure
PVCN	posterior ventral cochlear nucleus
R	right
ROI	region of interest
rs	resting-state
sec	second
sLORETA	standardised low-resolution electromagnetic tomography analysis
SOC	superior olivary complex
SP	summating potential
T	tesla
T1	T1-weighted
TE	echo time
TM	tympanic membrane
TR	repetition time
VNLL	ventral nuclei of the lateral lemniscus
x, y, z	3D Cartesian coordinates in the brain coordinate system

Table of contents

1 Introduction

1.1 Principles of BOLD signal activity

Brain functional connectivity is not a static value. Dynamic neural oscillations at specific frequencies mirror a variety of brain states, such as cognitive tasks, rest, and sleep (Buzsáki 2006). Blood oxygen level-dependent (BOLD) fluctuations measured with functional Magnetic Resonance Imaging (fMRI) have recently been demonstrated to reflect dynamic functional connectivity between different brain nodes (Chang and Glover, 2010; Tagliazucchi et al., 2011; Handwerker et al., 2012; Hutchison et al., 2013; Smith et al., 2012). MRI allows accurate spatial resolution and coverage of the entire brain (Tagliazucchi et al., 2012b). Spontaneous fluctuations of the BOLD signal range between approximately 0.01 and 0.1 Hz (Biswal et al., 2010).

Previous EEG-fMRI analysis outlines the presence of specific neural scalp oscillations and their specific correlation to increased or decreased temporal synchronisation of BOLD signals from different cortical and subcortical brain regions (Tagliazucchi et al., 2012a). Although the effects of spontaneous correlation could not be eliminated, the authors proved that cardiac and motion time series did not correlate with alterations in functional connectivity. In contrast, respiratory time series only correlated with a very limited extent over the possible connections (Tagliazucchi et al., 2012a). Yet, the precise physiological mechanisms underlying resting state fMRI (rs-fMRI) remain unclear.

Goelman et al. (2014) concluded that “negative and positive correlations have distinct physiological properties”, differing “with respect to the structures they connect”. In their study, Goelman et al. (2014) outline a clear distinction between positive and negative correlations. Positive correlations between two brain nodes are obtained if their time courses show similar periodical fluctuations with a short time lag (Goelman et al., 2014). “Time lags of more than a few seconds reduced positive correlations” and make negative correlations even more significant (Figure 1). More specifically, a zero-time lag was strongly correlated with the most and more significant positive connections,

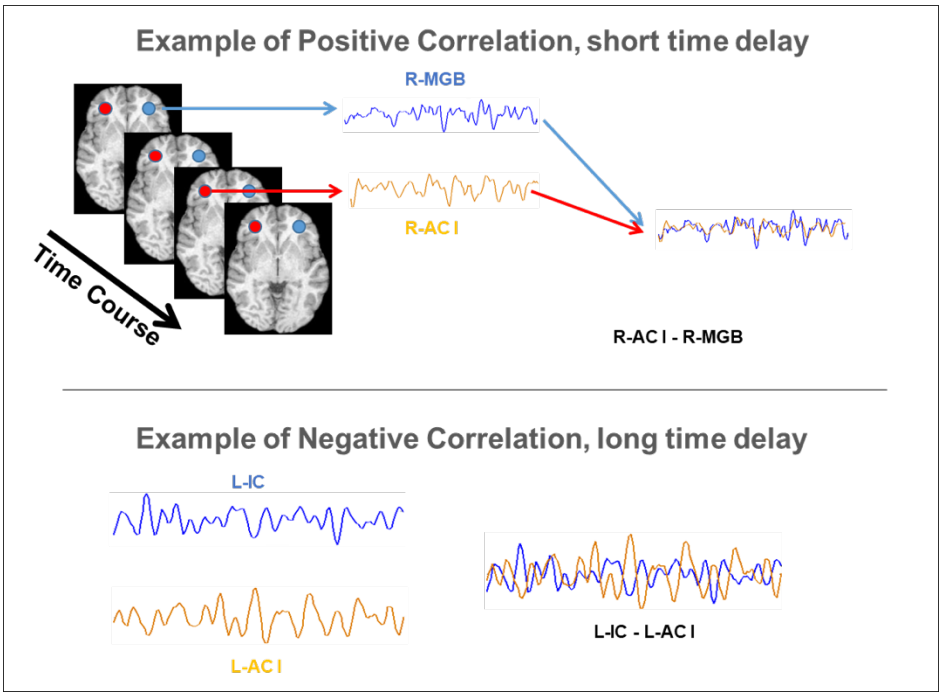

Figure 1 The pictures show exemplarily the rs-fMRI BOLD signal time courses of R-AC (auditory cortex) l and R-MGB with a short-time delay and so a positive correlation and of L-IC and L-AC l with a long-time delay and so a negative correlation between each other.

while a non-zero time-lag was strongly correlated with the most and more significant negative connections. Here, a time-lag of 4 sec resulted to be the turning point at which more negative than positive connections became more significant (Goelman et al., 2014). Furthermore, properties of negative and positive BOLD signals have been shown not to be the mere inverse of one another. Rather, negative BOLD signals are the result of an excess of deoxyhemoglobin (dHb). This phenomenon takes place at high levels of O_{2-} consumption and, accordingly, insufficient net inflow of fresh blood (Goense et al., 2012). Overall, regions exhibiting positive BOLD signal showed an increase in cerebral blood flow (CBF) and cerebral blood volume (CBV), while regions exhibiting negative BOLD signal showed a decreased CBF but an increase in CBV (Goelman et al., 2014).

The coupling between neural activity and CBF (neurovascular coupling) is the core function of neurovascular the unit (NVU): the concept of NVU points out the close bond between the brain and its vessels (Iadecola, 2017). Brain regions with higher energy consumption demand higher arterial blood flow (Sokoloff, 2013, from Iadecola, 2017). Increases in neural activity of a certain brain area are correlated to increased CBF in that brain area only (functional hyperthermia) (Chaigneau et al., 2003; Cox et al., 1993; Freygang and Sokoloff, 1958; Iadecola, 1993; LeDoux et al., 1983; from Iadecola.

2017). The CBF increase, at the microvascular level, might even exceed the activated area in some regions, such as the auditory, the visual or the cerebellar cortex (Harrison et al., 2002; Iadecola et al., 1997; O´Herron et al., 2016; from Iadecola, 2017). The maintenance of homeostasis of the cerebral microenvironment is the key function of the neurovascular coupling: the energy substrates needed for neural activity are hereby delivered and potentially toxic by-products, including heat, of brain metabolism are cleared (Iadecola, 2017). Evidence suggests that the vascular response process leading to increased CBF is initiated through neural activity. On the other hand, the implementation of the hemodynamic response is a carefully orchestrated interaction of other NVU cells of the cerebrovascular network (Iadecola, 2017). Moreover, the authors discovered that mechanisms of neurovascular coupling do not only differ with regard to positive and negative BOLD signals but show substantial differences depending on the cortical layer. More precisely, within the cortical surface and the superficial layers, negative BOLD signals were correlated with a decrease in CBF and only a small and irrelevant decrease in CBV, whereas CBV increased within the deeper layers (Goense et al., 2012). It turns out that the complex, non-linear and spatially inhomogeneous balance between CBF and CBV is probably responsible for the overall resulting BOLD signal (Goelman et al., 2014). Goelman et al. (2014) concluded that ROIs of two separated, highly synchronised brain regions will show a negative correlation in BOLD signals if one is CBV- and the other CBF-dominated. They suggest a model where positive connections in BOLD signals between two different brain nodes are the result of synchronised neuronal activity and homogeneous hemodynamic mechanisms. On the other hand, negative correlations are expected to show non-similar neuronal activity and, accordingly, heterogeneous hemodynamic processes.

Connectome (Sporns et al., 2005) is the term used to describe connectivity mapping of the brain through imaging techniques such as rs-fMRI: subjects lie at rest in the scanner while spontaneous time-series of functionally correlated brain regions are detected (Smith et al., 2013; Biswal et al., 1995; De Luca et al., 2005; Fox and Raichle, 2007; Fox et al., 2005; Greicius et al., 2003). Sufficient quantity and quality of fMRI data serve to generate maps of brain functional networks reflecting networks' spontaneous fluctuations over time (Smith et al., 2009). Thus, the analysis of correlation values, meant as the time courses between two brain regions, allows to

observe if these are functionally connected with each other (Smith et al., 2012). However, the analysis of the BOLD signal cannot differentiate between direct (anatomical) and indirect connectivity (Marrelec et al., 2006). Furthermore, the analysis is limited by spatial resolution, voxel size, and spatial relationships associated with neurovascular coupling. The latter represents a problem especially in gradient echo (GRE) BOLD fMRI, which is the most used imaging technique for functional brain imaging and the only successful procedure applied so far in rs-fMRI. The largest functional signals can be measured in draining vessels (Van Essen and Ugurbil, 2012; Menon et al., 1993; Uludag et al., 2009). These are found on the pial surface of the cerebral cortex, especially when scanning at magnetic fields ranging from 1.5 to 4T (Van Essen and Ugurbil, 2012; Duong et al., 2003). This represents a major issue when detecting signals from buried cortical areas such as the insula, as it could lead to the detection of neural activity exhibited rather by the more superficial surrounding cortical areas (Van Essen and Ugurbil, 2012). Such detection errors can be reduced through restriction to grey-matter voxels (Kolster et al., 2010). Unfortunately, complete elimination is not possible due to the extension of BOLD effects outside the blood vessel borders of approximately the blood vessel diameter (ca. 1 mm) (Ogawa et al., 1993). Only a magnetic field of 7T and above allows for signal detection of precise cortical origin by exploiting microvascular blood flow from capillaries, small post-capillary venules, and small intracortical veins (Uludag et al., 2009; Yacoub et al., 2005).

1.2 Overview of the anatomy and physiology of hearing

The aim of the present study is to use the resting-state functional MRI method presented above for the analysis of the physiological functional connectivity at rest in the auditory system. It follows a brief introduction in its anatomical structures and physiological functions. Sound perception in humans involves a wide range of complicated anatomical structures and physiological processes. The human auditory system can differentiate sounds on the basis of intensities (dB) and frequencies (Hz), as well as little changes within these scales (Pickles, 1989). Although no detailed understanding of the anatomical and pathophysiological processes of many hearing disorders has been discovered, studies suggest these might originate and occur in

both the peripheral and the central auditory system (Kiang et al., 1970, Eggermont and Roberts, 2004). Hence, knowledge of the basics of the auditory anatomy and physiology is essential. The auditory system is made up of a peripheral and a central part. Significant structures of the peripheral auditory system are the temporal bone, the outer and the middle ear, the cochlea, and the auditory nerve (AN). The temporal bone hosts and supports many relevant structures of the peripheral auditory system (Anson and Donaldson, 1981).

After travelling through the external auditory meatus (EAM), the sound wave hits the tympanic membrane (TM). The hereby created vibrations are transmitted to the ossicular chain. The vibrations are then directed through the footplate of the stapes and the oval window to the cochlear fluid of the inner ear. The stapes also strengthens the vibrations, which are transmitted to the cochlea (Musiek and Baran, 2020; Gelfand, 2004). The cochlea is part of the inner ear and is made up of two structures: the osseous and the membranous structure. It contains endolymph and perilymph, hair cells and supporting cells, as well as basilar, tectorial, and Reissner's membrane, along with blood vessels, nerve fibres, and a specialised epithelium. The main functions of the osseous cochlea are the support and protection of auditory nerve fibres and the membranous cochlea. The membranous cochlea consists of the scala vestibuli, the scala tympani, and the cochlear duct or scala media. These ducts extend for the whole length of the cochlea, ending together at the Helicotrema, where scala vestibuli and scala tympani fuse. The cochlear duct, on the other hand, communicates with the vestibular system. Scala vestibuli and scala tympani are filled with perilymph high in sodium and low in potassium. Endolymph fills the cochlear duct and consists of opposite chemical concentrations compared to perilymph (Sahley and Musiek, 2016).

Vibrations are conducted to the cochlear fluid of the inner ear through the footplate of the stapes and the oval window. Vibrations flow across the scala vestibuli and up to the peak of the cochlea. Thereby receptors of the Organ of Corti are aroused. At its inferior side, the Organ of Corti (Figure 2) is supported by the basilar membrane (BM) with about 25.000 auditory nerve fibres. The tectorial membrane, on the other hand, is placed on its superior side. The tectorial membrane interacts with the stereocilia of the outer hair cells (OHC). The inner and outer hair cells are the sensory receptor cells of

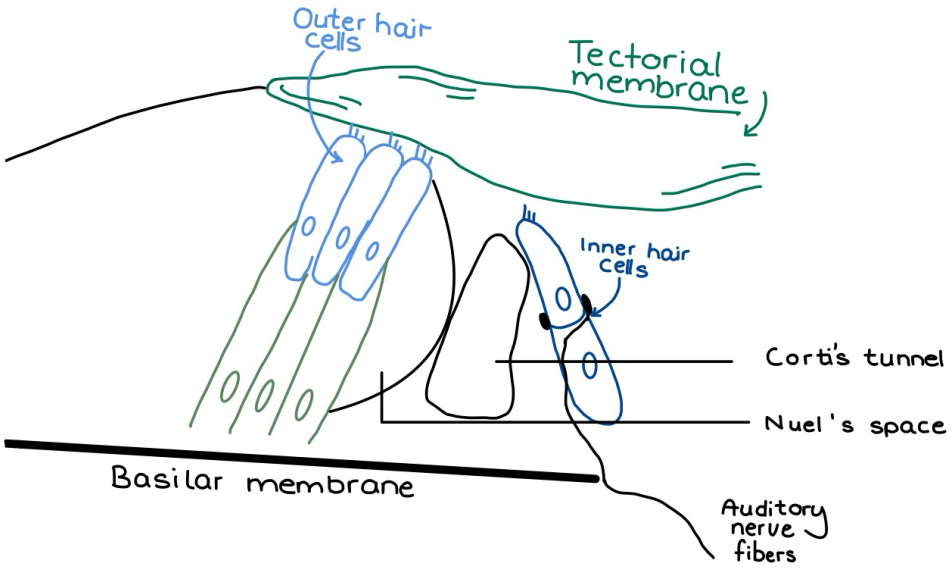

Figure 2 Schematic representation of a cross-section of the Corti's organ.

the auditory system. At their basal sides, they are connected to afferent and efferent neurons through synapses. Each of the hair cells holds about 50-100 stereocilia at its apical side. There are about 12,000 OHCs in the whole cochlea. These are organized in multiple lines of ca. 3-5 units in the Organ of Corti. In total, there are only 3,500 inner hair cells (IHC) which lie on a single row in the Organ of Corti (Geisler, 1998). In the cochlea, the process of mechanoelectrical transduction takes place. Through mechanical and electrophysiological processing, mechanical vibrations are turned into an electrical neural code. This code transmits intensity, frequency, and time-related information. Frequencies are decoded based on their location in the cochlea and their periodicity. High frequencies are processed by basally placed hair cells, while low frequencies are processed by apically based hair cells. Temporally changes in frequency lead to fast shifting of the BM and, at the same rate, to auditory nerve-firing and consequent stimulation of the hair cells. At higher intensities, the hair cells are stimulated more strongly, resulting in an increase of neural activity with decreased sharpness and reduced frequency selectivity (Amunts et al., 2012; Hudspeth et al, 2000). Only once the vibratory energy has been turned into an electrical impulse the nervous system can process the signal. This process begins with the activity of the

OHCs stereocilia, which are located at the bottom of the tectorial membrane. A travelling wave can reach the cochlea either as a compression wave or as a rarefaction wave. The former will shift the BM downwards, resulting in the closing of the channels of the stereocilia. Thus, no chemical transduction will occur, and consequently, the hair cells will not depolarise. The latter, on the other hand, will push the BM upwards, leading to the opening of the channels of the stereocilia. As a result, potassium (K^+)-ions stream into the cells beginning with the depolarisation, i.e., the firing of the hair cells (Geisler, 1998). Both inner and outer hair cells are involved in this transduction process. However, different mechanisms are used, and different functions are pursued. The expansion and contraction of OHCs are achieved due to contractile proteins and cellular wall structures. Up- and downward movements lead to an enhanced shifting of the BM and, thereby, to a higher sound intensity simulating an amplifier system. This is called the “biological-” or “cochlear amplifier”, which is triggered by low intensity-sound (Salvi et al., 2007). IHCs do not have contractile characteristics (Ashmore, 2008), and it appears that they are involved in the signal processing of high-intensity sound signals following amplification through OHCs (Dallos, 2008).

Cellular depolarisation involves three cochlear potentials: the endocochlear or resting potential, the cochlear microphonic potential (CM), and the summating potential (SP). The endocochlear electrical gradient can only be observed throughout the states of hyperpolarisation, recovery from hyperpolarisation, and non-depolarisation of the hair cells and results in the streaming of K^+-ions through the channels (pores). This shifting of ions is responsible for the induction of depolarisation. This significant difference in electrical potential is sustained by the intermediate cells of the stria vascularis. Hence, the so-called “battery model” of stria vascularis as the primary energy source maintains an electrical potential difference between the intra- and extracellular field in the cochlea (Davis 1965; Wangemann 2002).

The CM is the overall hair cell reaction beginning in the BM after an acoustic stimulus. The main source of the CM are OHCs, but IHCs are involved, too (Salvi et al., 2007, Dallos, 1983).

The summating potential, which represents a direct current potential (DC), occurs after the CM. The source of the SP is primarily the IHCs, but OHCs are also involved in its generation (Dallos, 1983).

Hair cells and auditory nerve are connected by synapses, whereby glutamate acts as the neurotransmitter of the afferent hair cells (Clark and Ohlemiller, 2008).

After the successful transduction of the acoustic signal into electrical impulses, these are transmitted to the AN. The AN fibres converge with those from the peripheral vestibular system to form the eight cranial nerve, commonly referred to as the vestibulocochlear nerve, which connects the cochlea with the central auditory pathways in the brainstem. The AN is organized tonotopically. Considering a cross-section of the nerve, low frequencies are transported along the outer side of the nerve, while high frequencies are transported along the central side. The AN fires during the time of an acoustic stimulus. The phenomenon of adaptation of the AN takes place when the sound signal is steady, and no change in frequency and intensity occurs, resulting in a reduction of the amplitude of the action potential in the AN. Adaptation is more likely to be observed at higher frequencies than at low frequencies as well as after impairment of the AN (Keidel et al., 1983; Sahley and Musiek, 2016).

In contrast to the AN, which is composed of several thousands of neurons, the central auditory system is made up of millions of these, a characteristic which is called “neural arborisation” (Ternaux, 2001). The first structure of the central auditory system is the cochlear nucleus (CN) (Figure 3). The CN is located in the caudal lateral side of the pons, close to the superior edge of the medulla. It is made up of three main groups of nuclei: the anterior ventral cochlear nucleus (AVCN), the posterior ventral cochlear nucleus (PVCN), and the dorsal cochlear nucleus (DCN). The AN reaches the CN at the “root entry zone” just between the AVCN and the PVCN. Neural fibres from the CN are mostly passed to the contralateral but also to the ipsilateral side: the ventral and intermediate stria begin in the AVCN and the PVCN and end in the contralateral SOC. The dorsal stria starts in the DCN and reaches the contralateral lateral lemniscus (LL) (Pickles, 1988). The CN is tonotopically organised with low frequencies on the lateral side and high frequencies on the medial dorsal side of the AVCN, PVCN, and DCN (Musiek and Baran, 2020; Romand and Avan, 1997, Shaley and Musiek, 2016). Just

like the tuning curves (TC) of the AN, those of the CN show an analogous trend (Shaley and Musiek, 2016).

The superior olivary complex (SOC) represents the second centre of the central auditory system which is responsible for the sound elaboration and further transmission. As mentioned above, the contralateral CN is the main anatomical structure that provides the SOC with nervous inputs. The SOC is located deep in the pons, approximately at the same height as the CN, but at a different depth. It is composed of the lateral superior olive (LSO), the medial superior olive (MSO), the medial nuclei of the trapezoid body (MNTB), and conglomerates of nuclei in the periolivary field of the lateral and medial olive. In the LSO, high frequencies are processed in its medial side, whereas low frequencies are processed in its lateral side. In the MSO, on the other hand, high frequencies are processed in its ventral side, while low frequencies are processed in its dorsal side (Møller, 2000; Moore, 2000; Musiek and Baran, 2020). Both SOCs process monaural acoustic input perceived from both ears. In this way, a more specific comparison between ipsilateral and contralateral inputs in terms of time, intensity, and frequency is guaranteed to allow sound lateralisation and localisation functions. The SOC can also gather and combine different information from both ears, such as low frequencies from one ear and high frequencies from the other ear. Consequently, the whole frequency spectrum can be perceived (Hirsh, 1952; Moore, 2013).

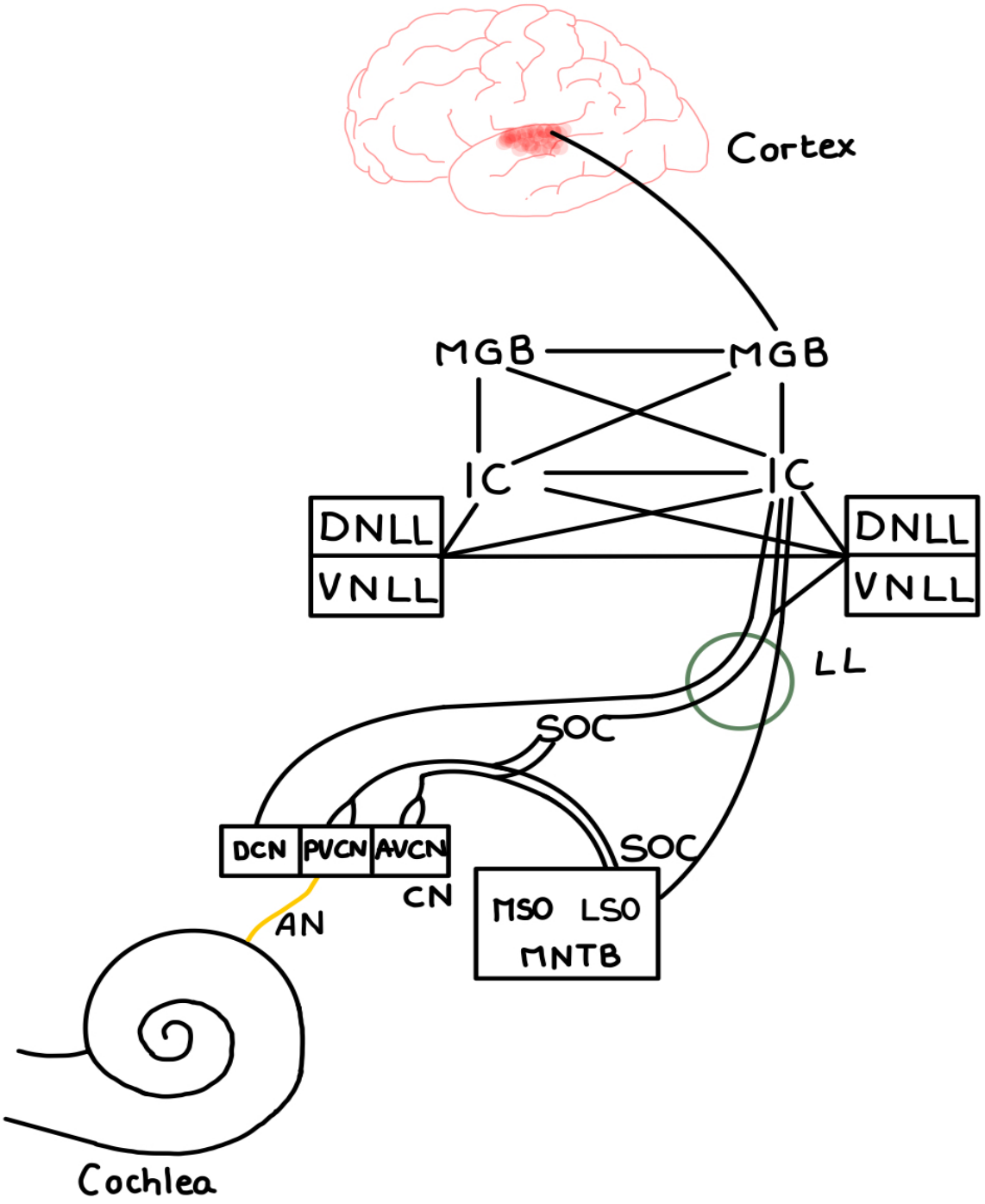

Figure 3 Schematic representation of the ascending auditory pathways beginning in the Cochlea and ending in the auditory cortex. The auditory pathway crosses the medulla, the pons and the midbrain (here not clearly subdivided) before approaching the auditory cortex.

Next, neural impulses run through the (LL) and the nuclei of the lateral lemniscus (NLL). The LL carries more contralateral than ipsilateral fibres. The NLL is made up of a ventral (VNLL) and a dorsal part (DNLL) (Møller, 2000; Schwartz, 1992).

Further on the rostral path of the central auditory system lays the inferior colliculus (IC). It is placed in the midbrain and, compared to the other central nuclei, it is the biggest in width. It is divided into three parts: the central nucleus, which plays the greatest role in signal elaboration, and the lateral and the dorsal nucleus (Morest and Oliver, 1984). Neural inputs are sent to the IC from most pons-located caudal ipsilateral and contralateral nuclei. Most IC efferent fibres reach the ipsilateral medial geniculate body (MGB) in the thalamus after running through the brachium colliculi (Ehret, 1997; Musiek and Baran, 2020). The IC shows a tonotopic organisation, with frequencies being processed by the dorsolateral to the ventromedial side (Winer, 1992). In case of intensity raising, most of the IC fibres react with an increase in firing, while some fibres, in contrast, respond with a loss in firing at a loudness of 10 dB or less (Popelàr and Syka, 1982). Thanks to a high number of neurons, the IC is sensitive to changes in sound amplitude and frequency. It is also a relevant structure for sound-source localisation and binaural hearing (Ehret, 1997; Erulkar, 1959).

The MGB functions as a prominent structure in the thalamus. The MGB is functionally subdivided into a ventral, a dorsal, and a medial segment. The main activity of the ventral segment is the elaboration of signals from the auditory pathway, while a multisensory representation can be observed in the dorsal and the medial pathway. Most of the neural inputs are received from the ipsilateral central nucleus of the IC, and these projections reach the ventral side of the MGB (Morest, 1965; Winer, 1992). Efferent projections of the MGB reach different structures within the central nervous system. Fibres from the ventral side are sent to the insula, while fibres from the dorsal side proceed to the primary and secondary auditory cortex as well as to the insula (Musiek and Baran, 2020; Streitfeld, 1980). The tonotopic organisation of the ventral MGB processes low frequencies on its lateral side and high frequencies on its medial side. At high intensities, the MGB shows a reduced coding activity and a loss in temporal processing, while an enhanced activity can be observed at low frequencies. Moreover, the MGB shows a high sensitivity regarding the interaural time and intensity differences. Further on the path of the auditory cortex lays the subcortex with its auditory projection fibres, such as the capsula interna, which is placed within the lenticular lemniscus. The external capsule with the acoustic signals-sensitive Claustrum is placed on the lateral side of the lenticular lemniscus (Musiek, 1986). Other

structures that are involved in the elaboration of auditory signals are the central gyri in the inferior parietal lobe, the supramarginal, the angular, as well as parts of the superior temporal gyrus, the central gyri in the inferior parietal lobe, the inferior-posterior frontal lobule, the insula (Bamiou et al., 2003) and, finally, the primary auditory cortex. As much as the previous structures discussed above, this latter structure, also called Heschl's gyrus shows a tonotopic arrangement regarding frequency coding. Increasing intensities trigger an increased firing of the fibres. Moreover, the auditory cortex shows a better response to modulated tones than to steady-state tones (Evans and Whitfield, 1964) and to slow than to fast modulation rates (less than 50 per second). Finally, time and intensity differences are used for detecting and localising sound sources (Musiek and Baran, 2020).

1.3 Tinnitus: a major hearing disorder. Definition, epidemiology, classification, and state of art

Tinnitus is defined as the perception of sound in the absence of an external concrete acoustic stimulus. It may be perceived in one or both ears and the head (Belli et al., 2012). An association with a hearing impairment is often observed (Adams et al., 1999; Lockwood et al., 2002). Since cochlear damage is the principal cause of tinnitus, younger generations show a higher incidence due to exposure to recreational and occupational sounds and inefficient protective standards (Eggermont and Roberts, 2012). White people are usually more likely to be affected than black people (Adams et al., 1999; Lockwood et al., 2002).

Chronic tinnitus is a widespread complaint and affects about 5-15% of the adult population (Vanneste et al., 2011). While most of the affected subjects do not feel bothered by the phantom sound at all, approximately 20% of them (Malouff et al., 2011; Galazyuk at al., 2012) experience tinnitus-related secondary diseases and symptoms. For example, they suffer from depression and insomnia (McCormack et al., 2016), which greatly impacts their quality of life (Nondahl et al., 2007; McCormack et al., 2016). The exact pathophysiological processes which lead to tinnitus remain unknown. Most authors intended to prove "that the generation of elevated spontaneous activity is correlated with the percept of tinnitus through increased central neural gain in lower or higher brain levels" (Marks et al., 2018; Sedley et al., 2016; Noreña, 2015; Yang and

Bao, 2013; Schaette and Kempter, 2012; Schaette and McAlpine, 2011; Yang et al., 2011; cited by Hofmeier et al., 2018). This view supports the idea that, in order to requite deprived auditory inputs, deafferentation in some regions may provoke a higher discharge rate in the brainstem (Noreña, 2015; Schaette and Kempter, 2012; Schaette and McAlpine, 2011; cited by Hofmeier et al., 2018). Consequences would result in elevated spontaneous activity, in terms of increased spontaneous firing rates at cortical levels following disinhibition (Eggermont and Roberts, 2012; Roberts et al., 2010; cited by Hofmeier et al., 2018). A few other authors support the idea "that the elevated spontaneous activity in tinnitus rather leads to failure to increase central neural gain, which is associated with a reduced signal-to-noise ratio and elevated noise levels" (Knipper et al., 2013; Rüttiger et al., 2013; Singer et al., 2013; Zeng 2013; cited by Hofmeier et al., 2018). "A failure to increase central neural gain is hypothesised to be related to a critical loss of high-spontaneous rate, low-thresholds fibres, based on a high degree of IHC ribbon loss in animals with behavioural tinnitus" (Rüttiger et al., 2013; Singer et al., 2013; cited by Hofmeier et al., 2018). A hypothesis about the relation between the deafferentation of IHCs and tinnitus has been mentioned (Rüttiger et al., 2013; Singer et al., 2013). Deafferentation and IHC ribbon loss were detected in high-frequency regions of the cochlea of animals with behaviourally tested tinnitus. In contrast, animals without tinnitus showed a more limited IHCs ribbon loss following noise exposure (Rüttiger et al., 2013).

Discovering the real genesis of tinnitus is relevant for diagnostic and therapeutic intervention strategies. No standard diagnostic criterion has been developed yet. Therefore, it is impossible to define the true prevalence of tinnitus (McCormack et al., 2016). Furthermore, correlations have been shown between the prevalence and onset of symptoms and an aging process (McCormack et al., 2016).

Tinnitus is usually sub-classified into a subjective and an objective form. The objective (or somatic) one is based on a concrete somatic dysfunction where a sound finds its conduction through the body tissues. This form may have, for example, a pulsatile or muscular origin (Lockwood et al., 2002; reviewed in Chan., 2009). The subjective form, on the other hand, shows no association with mechanical pathways, and it is perceived by affected individuals only (Chan, 2009). Genetic pathways leading to the arising of tinnitus have not been effectively demonstrated yet (Sand et al., 2012).

The deafferentation of peripheral and central auditory structures after cochlear injuries appears to play a key role in the perception of tinnitus (Brozoski et al., 2012; Diesch et al., 2012; Langers et al., 2012; Middelton and Tzounopoulos, 2012; Schaette and Kempter, 2012; Stolzberg et al., 2012). It leads to some neural changes such as tonotopic map reorganisation and hyperactivity within the auditory Cortex and the thalamus, abnormal bursting in the subcortical auditory nuclei as well as neural hyperactivity in hearing loss-affected tonotopic regions (Noreña and Eggermont, 2006; Roberts et al., 2010). A progression to severe hearing loss over time is not to be excluded (Kujawa and Liberman, 2009; reviewed in Eggermont and Roberts, 2012). Such a hearing-loss-associated model of tinnitus is to be led back to noise exposure and aging (Lockwood et al., 2002; Saunders, 2007). Map reorganisation was shown through neuromagnetic imagining in patients with detected hearing loss (Wienbruch et al., 2006).

Adaptive compensation in the form of an increased spontaneous neural activity occurs via a reduced stimulation of the auditory periphery and results in the perception of tinnitus. This process may occur within the auditory brainstem first and then in the ascending auditory nuclei (Mulders and Robertson, 2013). Increased spontaneous firing from the cochlear nucleus to the inferior colliculus takes place. Such a hyperstimulation of the IC is believed to lead to a spontaneous, synchronous firing within the auditory cortex. Possibly, these events may, in turn, lead to a reorganization of the cortical map (Schaette and Kemptner, 2012; Eggermont and Roberts, 2012). Response activities of uninjured afferent fibres may also play a key role in the central reaction after auditory trauma (Schaette and McAlpine, 2011). Compensation in central activity due to cochlear damage can be detected through auditory brainstem response (ABR) (Gu et al., 2012; reviewed in Knipper et al., 2013). Animal studies also suggested that, depending on the severity of peripheral deafferentation, the range, and extension of changes in sound-induced activity within the auditory ascending pathway are expected to be different for each individual case (Rüttiger et al., 2013; Singer et al., 2013; reviewed in Knipper et al., 2013).

While the association between tinnitus and cochlear/peripheral afferent fibre damage explained above has generally been considered true (Rüttiger et al., 2013; Singer et al., 2013; Knipper et al., 2013), hypotheses about the association with central auditory

pathway responses are still being discussed controversially. As mentioned above, it has been suggested that an exalted spontaneous activity and an upraised central neural gain might be responsible for the perception of tinnitus (Marks et al., 2018; Noreña 2015; Schaette and Kempter, 2012; Schaette and McAlpine, 2012; Sedley et al., 2016; Yang and Bao, 2013; Yang et al., 2011; cited by Hofmeier et al. 2018). Based on recent animal trials by Rüttiger et al. (2013), where separate groups of rats with and without tinnitus were acoustically exposed to the same noise levels, it has been suggested alternatively that the pathogenesis of tinnitus might instead be associated with a “failure to increase central neural gain” due to a “reduced signal-to-noise ratio and elevated noise levels” (Knipper et al., 2013; Rüttiger et al., 2013; Singer et al., 2013; Zeng, 2013; cited by Hofmeier et al., 2018). Recent findings support the latter: the study conducted by Hofmeier et al. (2018) was based on a multimodal dataset analysis (questionnaire, audiological evaluation, calculation of supra-threshold ABR wave fine structure, salivary cortisol measurement, resting state (rs)- and task-evoked fMRI and statistical analysis). In anatomically predefined ROIs, Hofmeier et al. (2018, 2020) observed “reduced and delayed sound-induced suprathreshold auditory brain response (ABR wave V) and reduced BOLD fMRI activity in the tinnitus group”. Consequently, the studies support the hypothesis about “reduced rather than increased central neural gain” and its association with decreased signal-to-noise ratio and higher levels of noise predicted from studies in animals using behavioural animal models (Knipper et al., 2013, Rüttiger et al., 2013; Singer et al., 2013 and Zeng et al., 2013; cited by Hofmeier et al., 2018).

1.4 Aim of the study

The current study aims to investigate and compare the resting-state connectivities between predefined brain ROIs of the central nervous auditory system and of auditory-correlated brain networks in healthy, hearing-unimpaired, non-tinnitus subjects by measuring the BOLD signal activity and correlation strength.

The correlation strengths between lower and higher-level auditory nuclei (CN, SOC, IC, MGB) and the primary and secondary auditory cortex areas (BA41/42 and BA21/22) were assessed using ROIs associated with three distinct networks:

I. The “Auditory Detection Network”, which includes the posterior insula (BA13P) and the hippocampus, encompasses auditory brain regions involved in sound detection and processing (Sadaghiani et al., 2009; Kraus and White-Schwoch, 2015; Weinberger, 2015; cited by Hofmeier et al., 2018).

II. The “Emotional Distress Network”, comprising the amygdala, entorhinal cortex (BA28), and anterior insula (BA13A), relates to limbic/emotional distress brain regions implicated in fear and anxiety processing, particularly in relations to tinnitus (Chen et al., 2017; Husain 2016; Leaver et al., 2016; cited by Hofmeier et al., 2018).

III. The “Temporofrontal attentional network” (alternatively referred to as the frontoparietal attentional network), which includes BA45 and BA46, associated attention-controlling (Cieslik et al., 2015; cited by Hofmeier et al., 2018), BA47, dorsolateral BA9 (BA9DL), and medial BA9 (BA9M), involved in the regulation of fear, disgust, anger and anxiety (Ardila et al., 2017; cited by Hofmeier et al., 2018), focuses on auditory and attentional brain regions engaged in attention regulation and stress management.

2 Material and methods

2.1 Participants

2.1.1 Recruitment

In the present study, the Queensland's dataset by McMahon K. (http://fcon_1000.projects.nitrc.org/fcpClassic/FcpTable.html) used in Kelly et al. (2009) was chosen. Nineteen adults (11 males and 8 females; mean age = 25,9 years), aged between 20 and 34, with no history of psychiatric or neurological disease as well as psychotropic drug consumption or contraindications to Magnetic resonance imaging (MRI), were employed for the composition of the dataset. The participants filled in a medical survey made of a questionnaire, declaring to have normal hearing and no need for hearing aids or hearing assistance. Furthermore, they were interviewed by paramedic staff. The procedures used by McMahon K. for the composition of the dataset, which was then applied by Kelly et al. (2009), had all received approval from the institutional review board of Queensland University.

During the processing of the files, the data of one participant could not be elaborated on Matlab (MathWork Inc., Natick, MA, USA), which is why it was excluded from the study (18 remaining participants: mean age = 26,2, 11 males and 7 females).

2.1.2 Division of subgroups

The data were first analysed for the whole group. Later, the participants were further divided into seven subgroups based on:

1. age (2 subgroups)
    1. 8 participants ≤ 25 years old: 5 males and 3 females, mean age = 23,3
    2. 10 participants > 25 years old: 6 males and 4 females, mean age = 28,6
2. age (3 subgroups)
    1. 6 participants aged between 21 and 24, mean age = 23
    2. 6 participants aged between 24 and 26, mean age 25,5
    3. 6 participants aged between 27 and 34, mean age = 30,3
3. sex:
    1. 11 males: mean age = 27,2
    2. 7 females: mean age = 24,7

2.2 Functional magnetic resonance imaging

The MRI image collection was carried out using a 4 T Bruker MedSpec system with a transverse electromagnetic head coil equipment (Vaughan et al., 2002; Kelly et al., 2009**)**.

2.2.1 The acquisition of magnetic resonance images

A 4 T scanner was used for rs-fMRI. Volunteers were given no task during the scan and were only asked to relax and keep their eyes open. In the first instance, in order to correct geometric distortions in the Echo-planar imaging (EPI) volumes, a point-spread function (PSF) mapping sequence was carried out (Zeitsev et al., 2003; Kelly et al., 2009).

Whole brain rs-fMRI images were gathered as 200 contiguous echo planar images (repetition time (TR) = 2100 ms; echo time (TE) = 30ms; flip angle (FA) > 90°; 36 slices, matrix = 64 x 64; acquisition voxel size = 3.6 x 3.6 x 3.6 mm) (Kelly et al.; 2009). A T1-weighted (T1) high-resolution anatomical image was collected through a GRE-sequence (TR = 2500 ms; TE = 3.83 ms; T1 = 1500 ms; FA = 8°; 256 slices; acquisition voxel size = 0.9 x 0.9 x 0.9 mm) for magnetisation (Kelly et al., 2009).

2.2.2 Anatomical and resting-state functional magnetic resonance imaging analysis

With the intention of targeting and measuring functional connectivity among predefined brain regions of interest in hearing and healthy subjects without tinnitus, the anatomical and resting state functional images were collected, as mentioned above. The pre-processing and analysis were carried out using the MATLAB programming system (MathWork Inc., Natick, MA, USA).

Anatomical and functional images were divided into two separate folders. Data of every participant were again organised in single distinct folders. Resting-state raw functional images were turned from DICOM into the NFTI format using the Statistical Parametric Mapping software to examine “differences in brain activity recorded during functional neuroimaging experiments” (SPM8 Wellcome Trust Centre for Neuroimaging, London http://www.fil.ion.ucl.ac.uk./spm/software/spm8/).

Functional MRI data were prepared using the SPM software. At first, the zero point of the anatomical T1 image was placed on the anterior commissure (AC). Subsequently, the T1 and the functional image were reoriented together through precise overlapping.

The head was then turned on the sagittal plane to move the posterior commissure (PC) on the x-axis (AC-PC line essential for MNI (Montreal Neurological Institute)-coordinates application). Finally, anatomical and functional MRI images were co-registered.

The further pre-processing and time course extraction of resting state functional images were carried out through DPARSF (DPARSF_V4.3 Advanced Edition) Matlab Toolbox (Data Processing Assistant for Resting-State fMRI), (Chao-Gan and Yu-Feng, 2010). Parameters were set for: Slice Number (36), Slice Order (1 to 33, 35, 34, and 36), Time Points (190), TR, Realignment, Normalization Voxel Size (3x3x3), Smoothing of FWHM (full width at half maximum) (5x5x5), Filter (0.01 Hz to 0.08 Hz). Afterwards, the regions of interest for processing and analysis were determined (auditory cortex region, auditory and limbic system region, auditory and prefrontal cortex region) and entered with the (X, Y, Z) MNI coordinates and radius range.

All participants' ROIs, time courses, as well as the correlation matrix and AAL (Anatomical Automatic Labelling) time courses, were successfully gathered in MATLAB files.

2.2.3 Statistical analysis of rs-fMRI correlations between predefined ROIs

Rs-fMRI results were corrected for False Discovery Rate (FDR) (Hofmeier et al., 2018).

Statistical significance was set to be tested at a level of $\alpha = 5\%$. The Pearson Correlation coefficients (*r*-values) between the targeted brain regions (ROIs or regions of interest) were successfully extracted as described under "Anatomical and resting-state functional magnetic resonance imaging analysis" above (see chapter 2.2.2). It is crucial to distinguish this *r*-value from the Significance value (*p*-value) associated with the correlation.

The analysis of functional connectivity was carried out in three different sets of defined ROIs. The **first** set includes auditory brain regions only, beginning with the cochlear nucleus and progressing to higher-level auditory nuclei, cortical and subcortical regions (Figure 3). The **second** set includes the emotional distress network, analysing both auditory regions and different limbic (distress) regions of interest to investigate any kind of correlation in terms of functional connectivity between the auditory and the limbic regions. The **third** and last set includes the temporofrontal attentional network

for the analysis of different attentional and auditory brain regions of interest. Statistical-relevant functional connectivities between both the right and the left-brain hemisphere, as well as within one brain hemisphere only, were considered in all sets.

Significance in the results of time course correlation analysis was considered when the Significance correlation value (p) of the Pearson correlation coefficient (r) resulted in being smaller than 0,05 ($p < 0,05$, FDR corrected).

The correlation was evaluated depending on the results of p: (i) when $p > 0,05$, no correlation was considered; (ii) positive connectivity, in terms of significant correlation between two regions, when $p < 0,05$ and positive r-value; (iii) negative connectivity, in terms of significant though negative correlation between two regions when $p < 0,05$ and negative r-value.

All statistical test evaluations were extracted using MATLAB (MathWork Inc., Natick, MA, USA).

All MRI – Results must be considered as FDR-corrected with a correction of $p < 0,05$.

2.3 Research of Resting-State fMRI – Data from the "1000 Functional Connectomes Project"

2.3.1 Characteristics of the "1000 Functional Connectomes Project" (http://fcon_1000.projects.nitrc.org/fcpClassic/FcpTable.html)

The "1000 Functional Connectomes Project" includes rs-fMRI datasets of more than 1000 subjects from more than 30 independent studies worldwide (Kalcher et al., 2012).

All datasets were donated by the principal investigators in order to provide complete access to a large-scale functional imaging dataset. The aim was to create a comprehensive mapping of the functional connectome to facilitate corresponding research related to brain disorders (Biswal et a., 2010).

For this study, the "1000 Functional Connectomes Project" databank was chosen.

It was searched for rs-fMRI images for the analysis of BOLD signal activities with respect to the auditory brainstem and thalamus, as well as to auditory cortical areas, prefrontal cortex, and limbic system.

These data were used to recreate the same map of ROIs examined in Hofmeier et al. (2018) for the evaluation of synchronicity (or connectivity as a function of time) in hearing-unimpaired non-tinnitus individuals only.

2.3.2 Description of the datasets

All datasets belonging to the "1000 Functional Connectome Project" (Biswal et al., 2010) are available for download at its webpage (http://fcon_1000.projects.nitrc.org/).

The website offers brain images and resulting volumes of 1000 participants (age 28 +/- 13, 561 females) randomly sampled by centres in North America, Europe, Asia and Australia.

2.3.3 Application of Queensland dataset by McMahon K.

In the present study the Queensland's dataset by McMahon K., used in Kelly et al. (2009), was chosen to generate the correlation matrix between the above cited ROIs (see chapter 1.4) as similarities in participants' characteristics used by Hofmeier et al. (2018), such as the number of participants and sex distribution, were observed. Moreover, the rs-fMRI parameters and settings applied also showed some affinities, such as repetition time and the number of slices.

2.4 Selection of Regions of Interest (ROIs) and brain networks

To generate most comparable results as possible, the following ROIs (Table 1), as in Hofmeier et al. (2018), were considered for the generation of the Pearson Correlation Matrix. A graph illustration of their functional connectivity pattern is shown in Figure 6-20.

Importantly, the results of the time course correlation analysis were considered significant only when the Pearson correlation coefficient value and the *p*-value of the correlation amounted to less than 0.05 ($p < 0.05$, FDR corrected), and by doing so one out of three possibilities can be obtained:

i. no correlation (with $p > 0.05$)
ii. positive connectivity (with a positive *r*-value and $p < 0.05$) as a result of two functionally related regions
iii. negative connectivity (with a negative *r*-value and $p < 0.05$) as a result of a significant but negative correlation.

Next, to better frame the BOLD fMRI activity, positive rs-fMRI correlations were differentiated from negative ones.

Brain Region (Brodmann area)	MNI Coordinates			Radius
	X	Y	Z	
CN-R/CN-L	10/-10	-39	-45	3
SOC-R/SOC-L	13/-13	-35	-41	3
IC-R/IC-L	6/-6	-33	-11	3
MGB-R/MGB-L	18/-18	-24	1	3
BA41-R/BA41-L	46/-46	-25	7	3
BA42-R/BA42-L	64/-63	-22	9	3
BA22A-R/BA22A-L	54/-54	-6	-6	3
BA21A-R/BA21A-L	66/-66	-13	-5	3
BA22P-R/BA22P-L	67/-67	-27	3	3
BA21P-R/BA21P-L	66/-66	-22	-5	3
Hipp-R/Hipp-L	13/-13	-36	8	3
BA13P-R/BA13P-L	33/-33	-16	19	3
BA13A-R/BA13A-L	36/-36	20	7	3
BA28-R/BA28-L	18/-18	-13	-22	3
Amyg-R/Amyg-L	22/-22	-5	-18	3
BA45-R/BA45-L	57/-57	26	14	3
BA46-R/BA46-L	46/-46	41	18	3
BA47-R/BA47-L	33/-33	32	-10	3
BA9M-R/BA9M-L	7/-7	50	30	3
BA9DL-R/BA9DL-L	50/-50	14	32	3

Table 1 Predefined ROIs for resting-state fMRI.

The connectivity of defined brain nodes/ROIs belonging to the auditory pathway (CN, SOC, IC, MGB, BA41/42 and BA21/22) were calculated with ROIs associated with:

i. the posterior insula (BA13P) and hippocampus named “Auditory Detection Network”.
ii. the amygdala (Amyg), entorhinal cortex (BA28) and the anterior insula (BA13A) named “Emotional Distress Network”.
iii. BA45, BA46, BA47, dorsolateral BA9 (BA9DL) and medial BA9 (BA9M) named “Temporofrontal Attentional Network”.

For this analysis, correlations among all ROIs within each detection network were initially examined for the entire participant cohort (Figure 6, Figure 11, Figure 16). Subsequently, these correlations were assessed with respect to age (Figure 8, Figure 9, Figure 13, Figure 14, Figure 18, Figure 19) and sex (Figure 10, Figure 15, Figure 20) subgroups for all ROIs. To facilitate a streamlined presentation of results,

correlations were the specifically analysed between individual ROIs from the targeted brain networks (auditory, limbic and attentional) and selected auditory cortical (BA21, BA22, BA41, BA42) and subcortical (CN, SOC, IC, MGN) ROIs (Figure 7, Figure 12, Figure 17). This separate analysis was conducted in the context of the whole group rather than on a subgroup basis. To maintain clarity in the overview of findings, correlations between homologous ROIs or between two ROIs both situated within the traditional auditory subcortical/cortical pathway (CN, SOC, IC, MNG, BA21, BA22, BA41, BA42) were deliberately omitted from this part of the study.

3 Results

3.1 Recruitment and analysis of the dataset

Data were extracted from the dataset of McMahon K., Queensland University, Australia, stored in the databank of the "1000 Connectome Project" (detailed description in "Material and Methods" chapter 2.3).

The functional connectivity between all regions of interest (Table 1) was successfully identified after the generation of the Pearson Correlation Matrix (detailed description in "Material and Methods" chapter 2.2.3).

The Correlation Matrix (with *r* as the value of the Pearson correlation coefficient and *p* as the value of the Significance of the correlation) was generated for each subject of the group. The mean-values of correlation strength between each brain node are provided in the appendix for convenient reference. The graph analysis between defined brain nodes grants an overview of the average functional connectivity of the group and, hereby, show different connectivity patterns.

In a next step, variations of correlation-strength were analysed between the above selected ROIs of the 18 subjects. For illustrative purposes, these are here exemplary shown for the correlation-strength between CN-R/SOC and BA13P-L and CN-L (Figure 4).

A

Mean-Value of Correlation Strength (*r*) ≈ 0,66

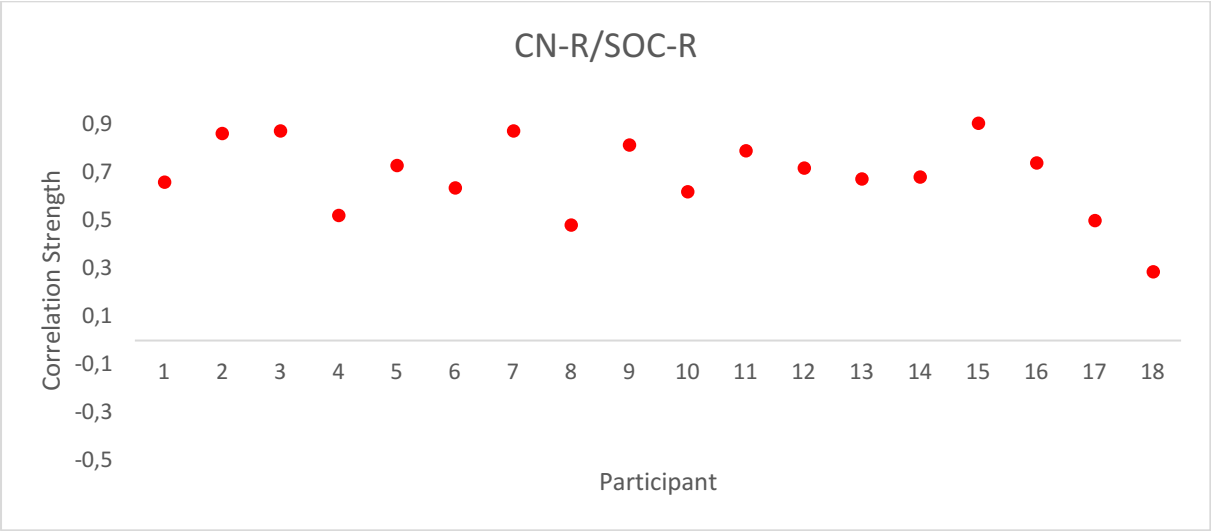

B

Mean-Value of Correlation Strength (*r*) ≈ -0,15

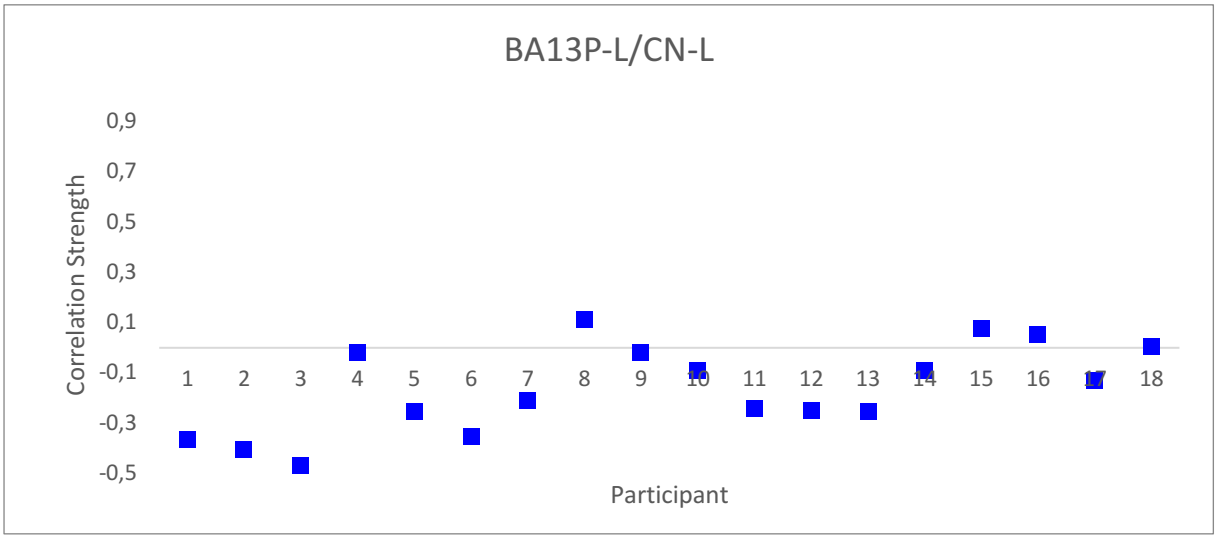

Figure 4 The diagrams (A, B) represent the correlation strength (*y*-axis) between two coordinates of the considered predefined ROIs for each individual subject (*x*-axis) (*n*=18).

The value recorded for every single participant is shown. The mean value was then drawn as a functional connectivity pattern (Figure 5), where the thickness of lines corresponds to the group mean of the correlation strength between two coordinates of the above-mentioned predefined ROIs.

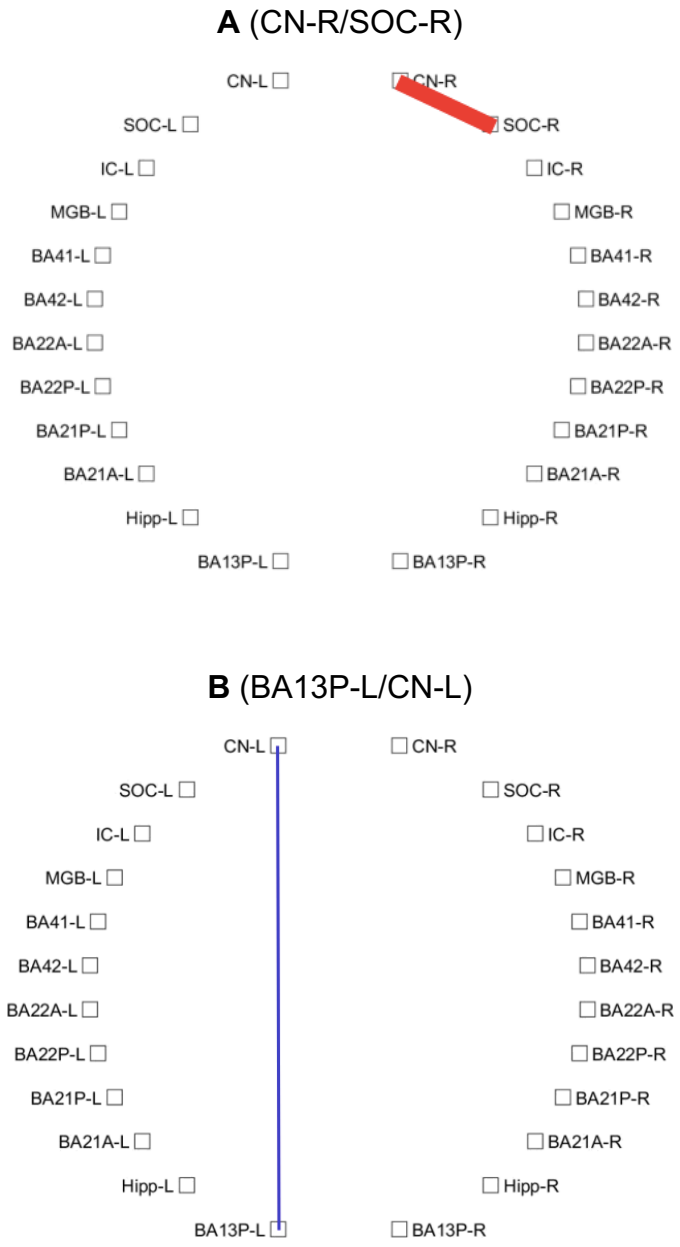

Figure 5 The graphs (A, B) show the mean correlation strength for all participants involved, pertaining exclusively to the correlation pathways featured in Figure 4. Correlations involving other ROIs have been intentionally excluded.

3.2 Auditory Detection Network

Next, calculations of functional connectivity were performed, as described above, for the auditory detection network first. Here the connectivity is calculated between specific regions involved primarily in sound detection and processing, from the cochlear nucleus onward until the primary auditory cortex (BA41, BA42), the secondary auditory association cortex (BA22) in the superior temporal gyrus, and the multi-modal

area (BA21) in the middle temporal gyrus (MTG). The hippocampus (Hipp) and the posterior insular cortical region were also considered (BA13P).

The time course correlation matrix between all tested regions of interest was generated. A graphical illustration of their functional connectivity patterns can be found below.

3.2.1 Description of correlations in the entire group of participants

All homologous bilateral connectivities exhibit positive correlations, with correlation strength values ranging from 0,18 and 0,45 (Appendix) and a mean value of 0,33. No negative connectivity was observed between non-cortical structures (Figure 6).

Additionally, within the auditory cortex and auditory brainstem, a significant number of correlations between brain nodes on both the ipsilateral and contralateral sides can be observed. Higher correlation strengths can be observed between CNL-L and SOC-L ($r \approx 0{,}76$), as well as between CN-R and SOC-R ($r \approx 0{,}68$) (Figure 6). This suggests an extensive level of interconnectivity and synchronicity between these areas.

Auditory detection network. Whole group. All correlations

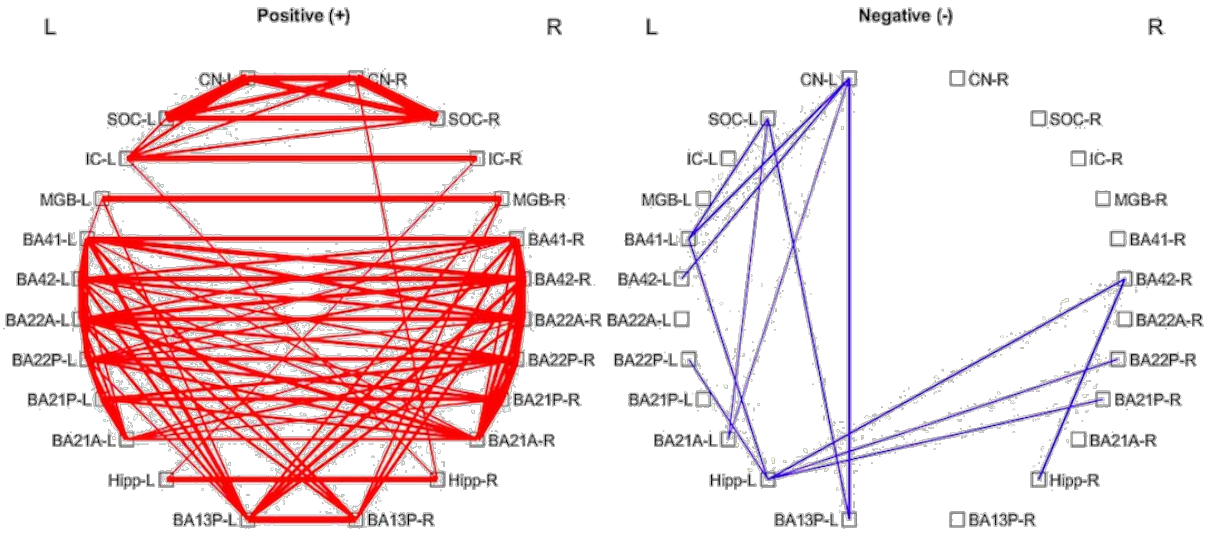

Figure 6 Significant mean rs-fMRI BOLD connectivity patterns of defined auditory brain regions of interest. Significant Pearson correlations of BOLD time courses of different brain regions are shown for the whole group (n=18) for positive (left red panel; ∑99 patterns) and negative (right blue panel; ∑13 patterns) connectivities.

Both the right and the left posterior insular regions (BA13P-L and BA13P-R) show numerous significant positive correlations with the ipsilateral and contralateral auditory cortex (*r* up to 0,3) and auditory thalamus (*r* up to 0,17), but none with lower auditory

brainstem nuclei (CN, SOC, and IC). The latter exhibit positive connectivity only with the hippocampus (Hipp-R to CN-R and IC-L; Hipp-L to IC-R) (Figure 7).

Vice versa, negative functional connectivity (anti-correlations) can be observed between left and right hippocampus and auditory cortical areas (Hipp-L to BA41-L, BA22P-L, BA42-R, BA22P-R, BA21P-R, BA42-R and Hipp-R to BA42-R) as well as between the left posterior insula and the ipsilateral auditory brainstem (BA13P-L to CN-L and SOC-L) (Figure 7).

Auditory detection network. Whole group. Auditory regions of interest

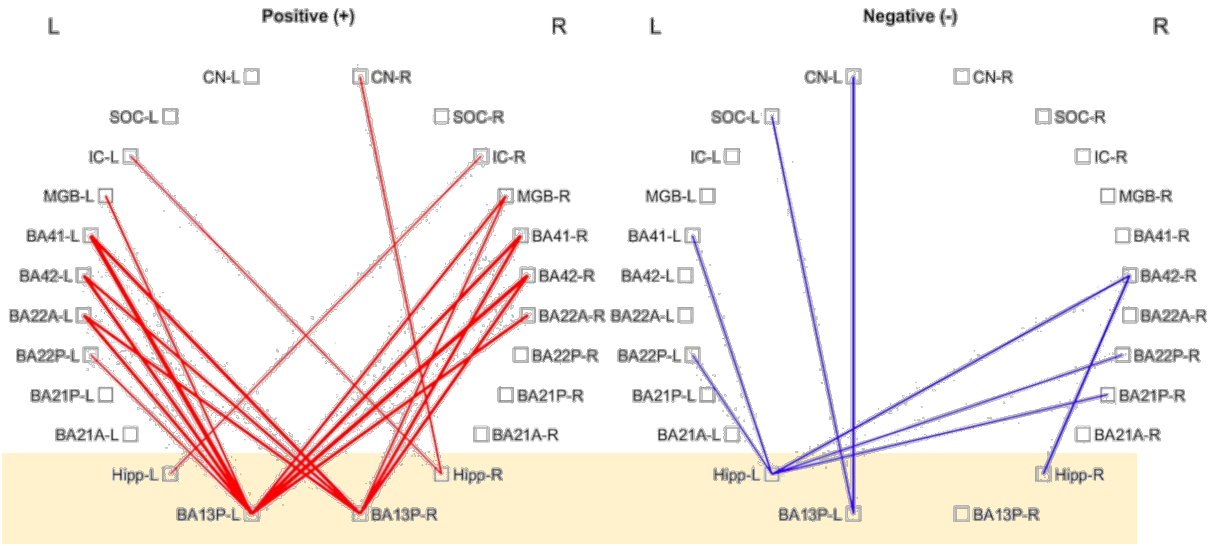

Figure 7 Auditory brain regions of interest: for a simplified overview the yellow panel displays correlations from specific auditory brain nodes (BA13P and Hippocampus) to brain nodes of the auditory cortex and auditory brainstem. Other correlations have been intentionally excluded. ∑18 positive, ∑8 negative patterns.

To resume, regions of the auditory cortex and auditory brainstem demonstrate positive correlations with homologous, ipsilateral and contralateral brain areas (Figure 6), displaying correlation strengths ranging from low to moderate. Even the hippocampus and BA13P exhibit significant positive correlation with their homologous regions (Figure 6). Within the auditory detection network, the posterior insula shows positive correlations with the ipsilateral and contralateral auditory cortices and auditory thalamus on both sides (Figure 7), albeit with relatively low correlation strengths. At the same time, lower auditory brainstem nuclei do not show any significant functional connectivity with the posterior insula. In fact, they tend to ben anti-correlated (Figure 7).

3.2.2 Age- and sex-related description of correlations

Regarding the subgroup of participants sorted by age (until and over 25 years of age), a far higher number of both positive and negative correlations within the older subgroup can be observed (Figure 8).

Auditory detection network. Participants sorted by age (until and over 25 years of age)

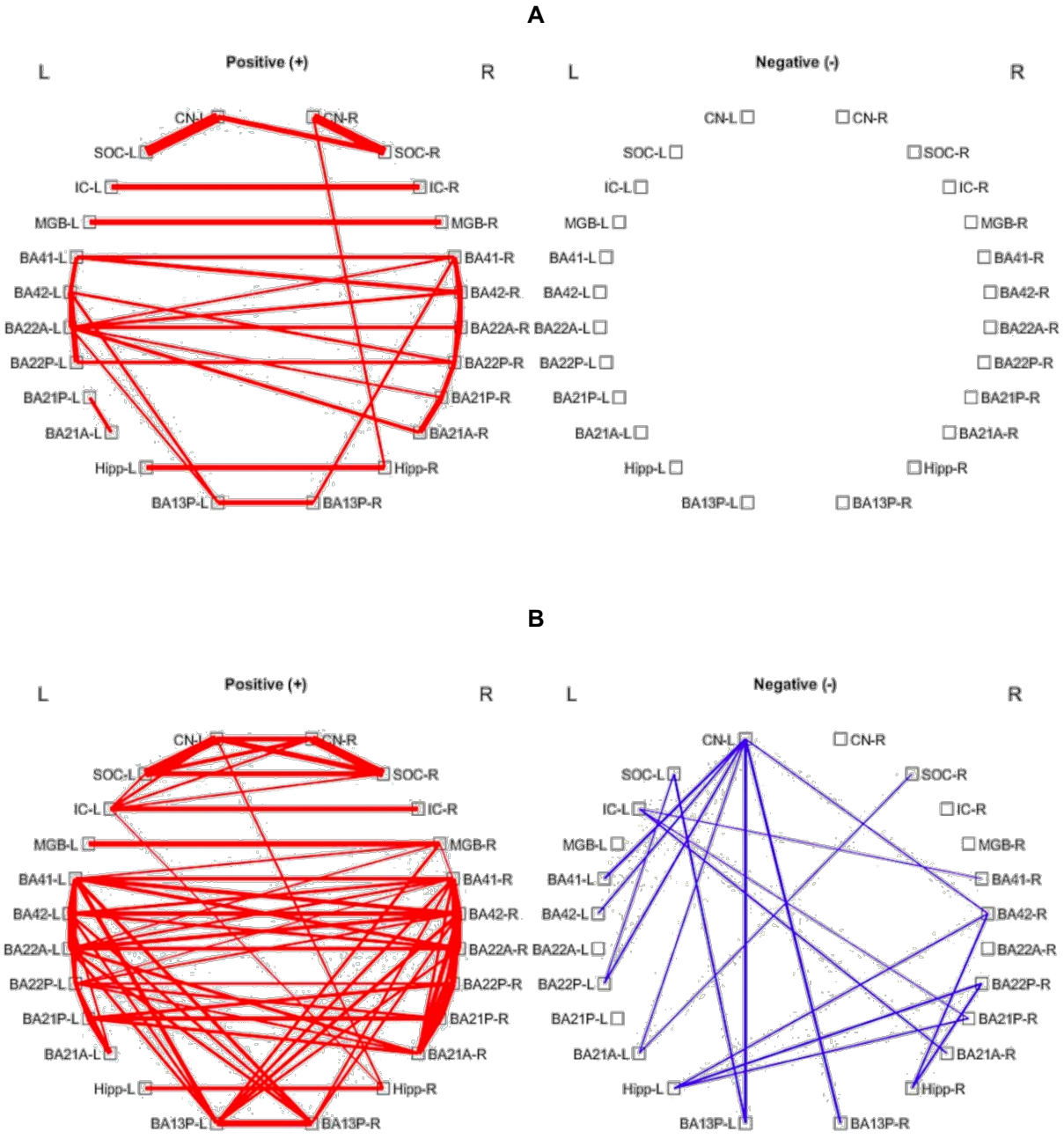

Figure 8 Auditory brain regions of interest: significant Pearson correlations of BOLD time courses of different brain regions are shown for the subgroups of participants until the age of 25 (Fig. A; n=8; ∑43 positive, ∑0 negative patterns) and over the age of 25 (Fig. B; n=10; ∑85 positive, ∑19 negative patterns).

Network-specific relevant differences between the two subgroups could not be specified. Therefore, the entire group was arranged into three homogeneous subgroups, each made up of six participants in ascending order of age (Figure 9).

Auditory detection network. Participants sorted by age (subgroups 21-24, 24-26, 27-34)

A

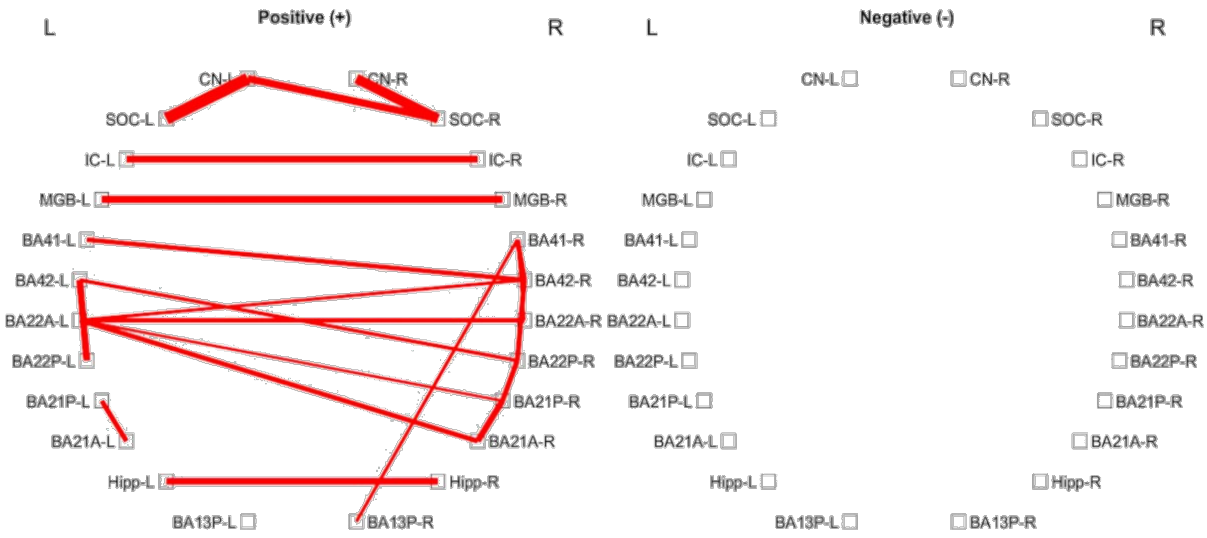

B

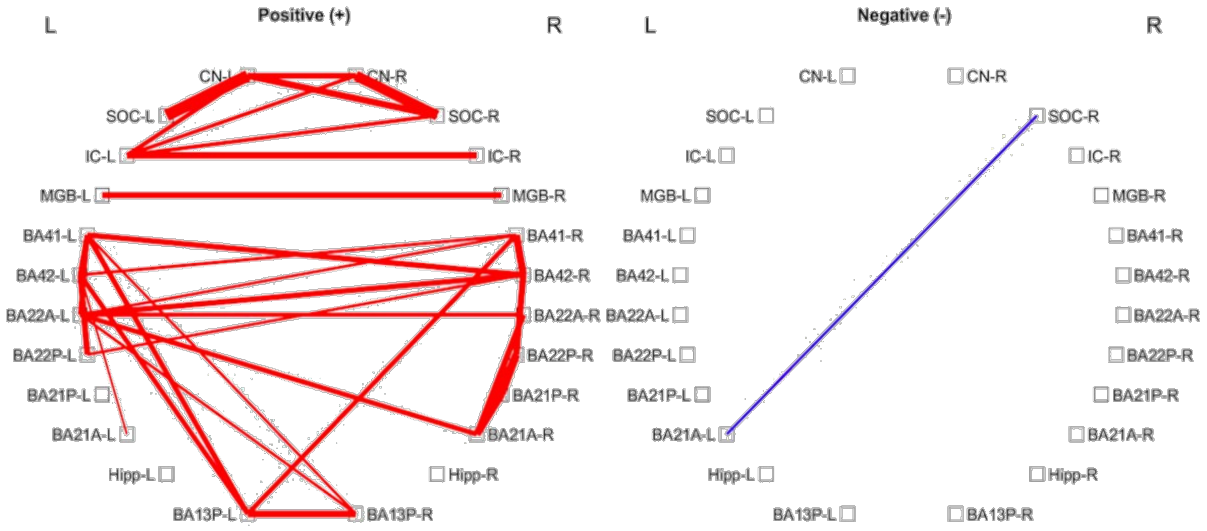

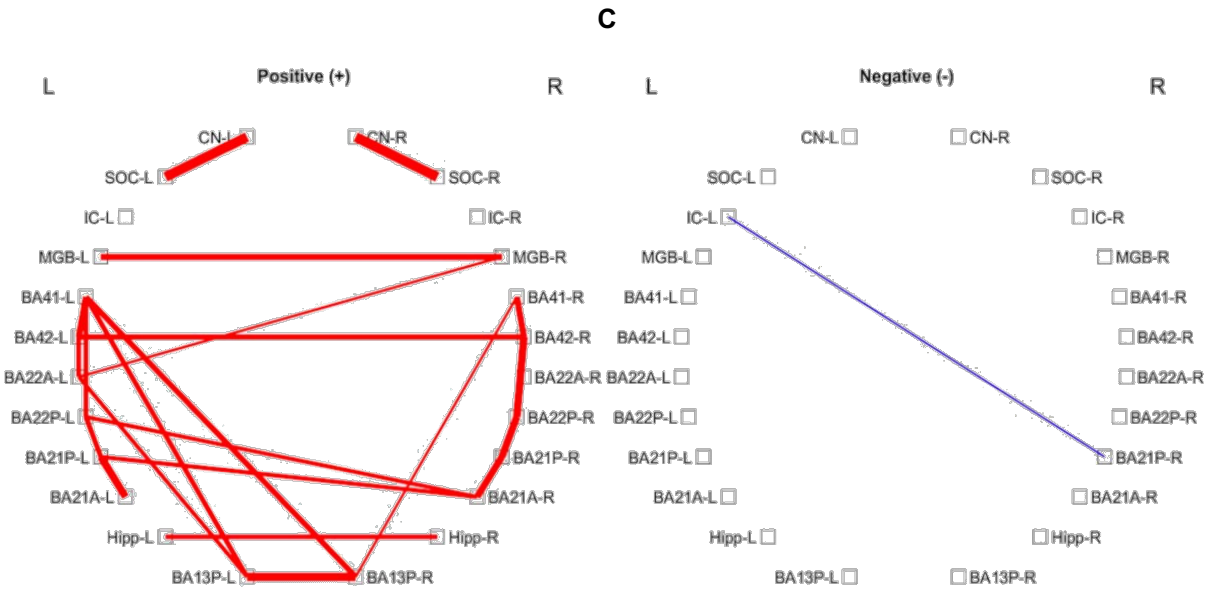

Figure 9 Auditory brain regions of interest: significant Pearson correlations of BOLD time courses of different brain regions are shown for the three subgroups of participants between the age of 21 and 24 (Fig. A; n=6;), 24 and 26 (Fig. B; n=6), 27 and 34 (Fig. C; n=6) for positive (left red panel) and negative (right blue panel) connectivities.

Contrary to expectations, the subgroup of the oldest participants shows similar number of positive correlations as the youngest one. At the same time, the subgroup of participants aged 24-26 exhibits the highest number of positive functional connectivities (Figure 9).

Auditory detection network. Participants sorted by sex

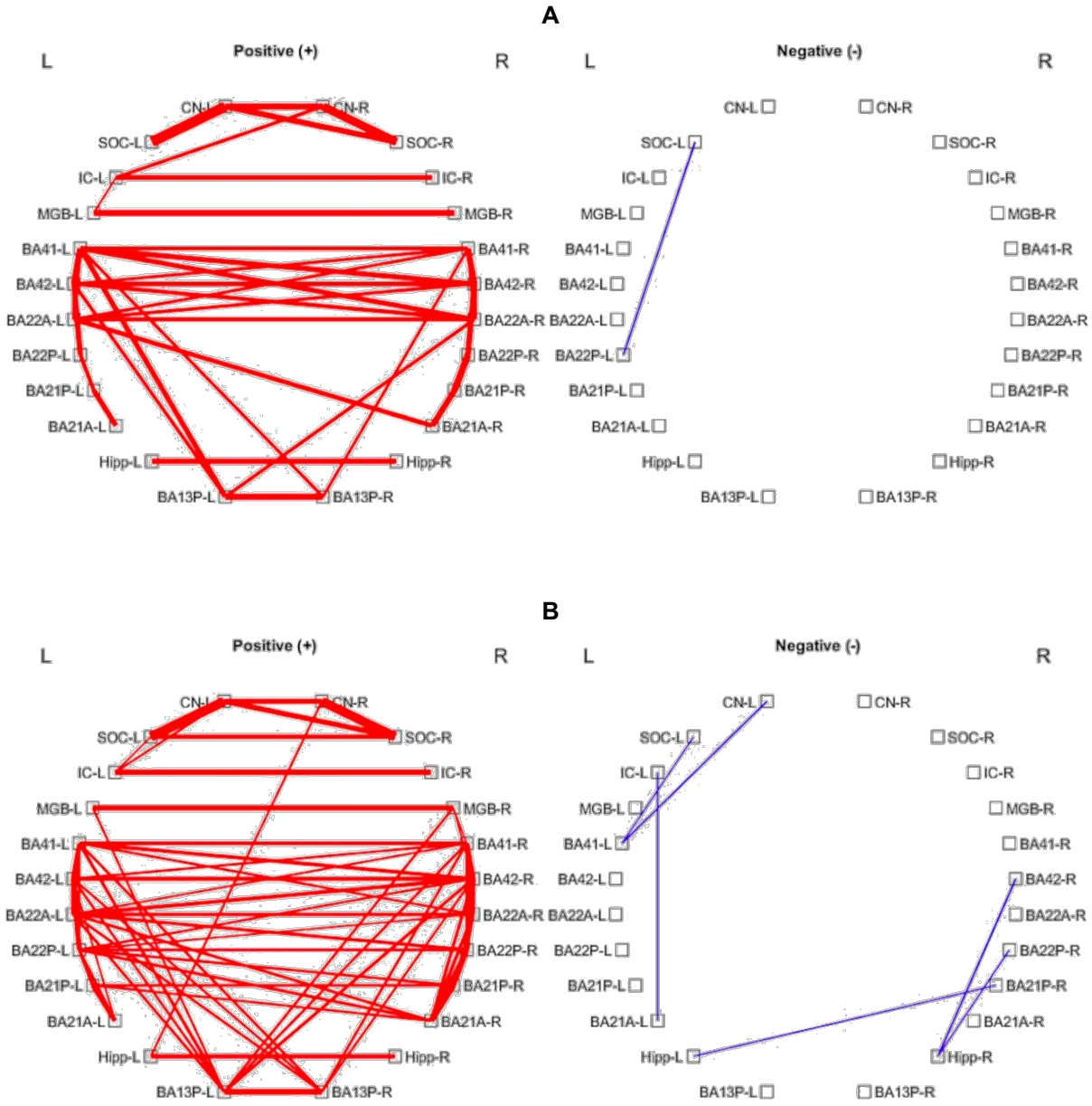

Figure 10 Auditory brain regions of interest: significant Pearson correlations of BOLD time courses of different brain regions are shown for the subgroups of female (Fig. A; n=7; ∑49 positive, ∑1 negative patterns) and male participants (Fig. B; n=11; ∑76 positive, ∑6 negative patterns).

The subgroups of participants sorted by sex exhibit a relevant discrepancy in the absolute number of positive correlations, with male participants showing a higher number of functional correlations than females (Figure 10).

3.3 Emotional Distress Network

In this part of the study, correlations between the auditory brainstem, auditory midbrain, auditory cortex, and structures related to limbic regions such as the amygdala, the entorhinal cortex (BA28), and the anterior insula (BA13A) were analysed.

3.3.1 Description of correlations in the entire group of participants

The entire group shows positive functional connectivities between all homologous left and right regions (Amyg, BA28, BA13A) with correlation strength values ranging from 0,28 and 0,42 and a mean value of 0,36. No negative connectivities were observed between non-cortical structures (Figure 11). Non-homologous regions such as Amyg-L and BA28-R and vice versa, as well as ipsilateral brain nodes of the limbic network, (BA28-R to Amyg-R ($r \approx 0,41$), BA28-L to Amyg-L ($r \approx 0,54$)) also show positive correlations (Figure 11). ROIs of the emotional distress network exhibit primarily positive connectivity with brain areas belonging to the left primary and secondary auditory cortex, thus, outlining a left-hemisphere dominance in this network´s functional architecture (Figure 12). Both the left and the right anterior insular regions appear to be correlated with the left primary auditory cortex (BA13A-L and BA13A-R both to BA41-L and BA42-L, with a correlation strength of approximately 0,1). At the same time, the right and left amygdala show positive functional connectivities with the ipsilateral and the contralateral auditory cortices (Amyg-R to BA22A-R, BA22A-L, BA42-L, with $r \approx 0,1$) (Figure 12).

Emotional distress network. Whole group. All correlations

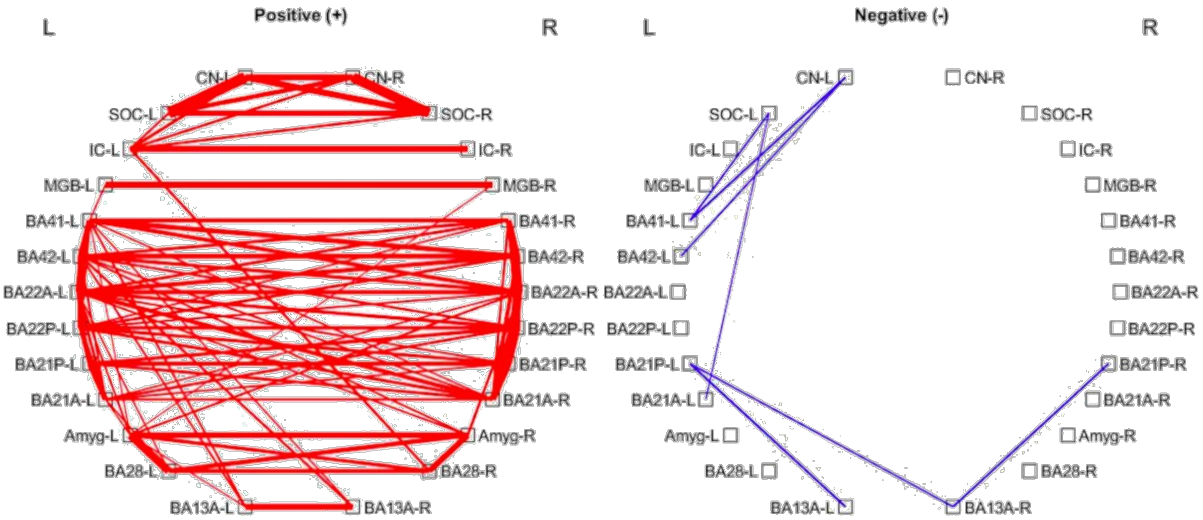

Figure 11 Significant mean rs-fMRI BOLD connectivity patterns of defined auditory and distress brain regions of interest. Significant Pearson correlations of BOLD time courses of different brain regions are shown for the whole group (n=18) for positive (left red panel; ∑103 patterns) and negative (right blue panel; ∑7 patterns) connectivities.

The right entorhinal cortex demonstrates to be the only limbic-specific brain area correlated with the lower auditory brainstem (BA28-R to IC-L, $r \approx 0{,}17$). The left amygdala, contrarily, shows connectivity with the right auditory thalamus and the auditory and multi-modal cortex (Amyg-L to MGB-R, BA22A-R, BA21A-L, BA41-L, with values of correlation strength $r \leq 0{,}15$) (Figure 12).

Emotional distress network. Whole group. Limbic regions of interest

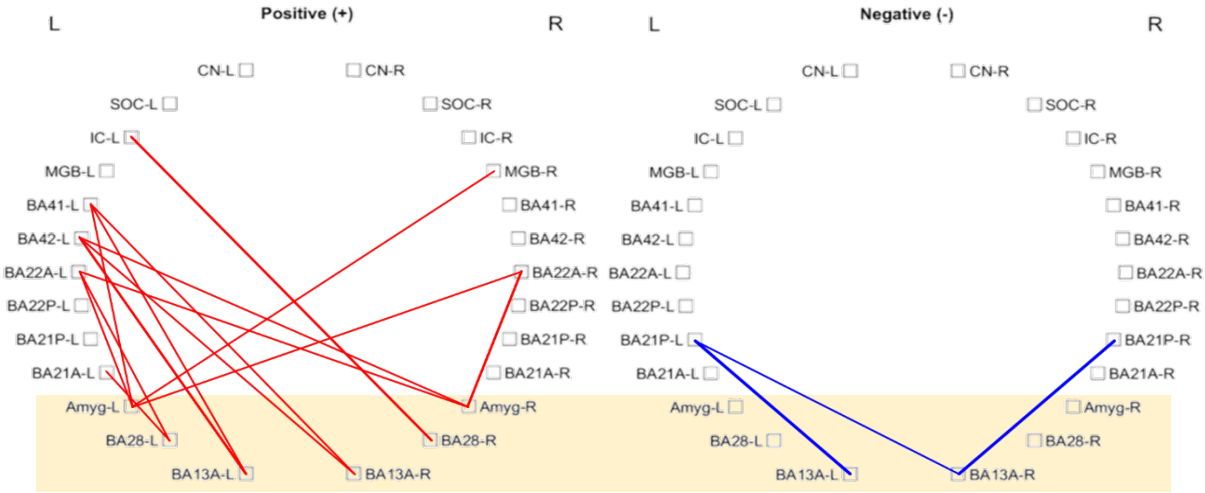

Figure 12 Auditory and limbic/emotional distress brain regions of interest: for a simplified overview the yellow panel displays correlations from specific limbic/distress brain nodes (Amygdala, BA28, BA13A) to brain nodes of the auditory cortex and auditory brainstem. Other correlations have been intentionally excluded. ∑14 positive, ∑3 negative patterns.

Anti-correlations appear solely between the anterior insula and posterior multimodal cortex in MTG (BA13A-L to BA21P-L and BA13A-R to BA21P-L, BA21P-R) (Figure 12).

To sum up, only a few significant positive functional connectivities can be observed between the auditory cortex and ROIs of the emotional-distress network (Figure 12), displaying relatively low correlation strengths. They correlate primarily with regions of the left hemisphere. In contrast, the auditory brainstem, the midbrain, and the right auditory cortex are only poorly correlated (Figure 12).

3.3.2 Age- and sex-related description of correlations

The older participants, as in the above-mentioned case, show more positive functional correlations than the younger ones (Figure 13).

Emotional distress network. Participants sorted by age (until and over 25 years of age)

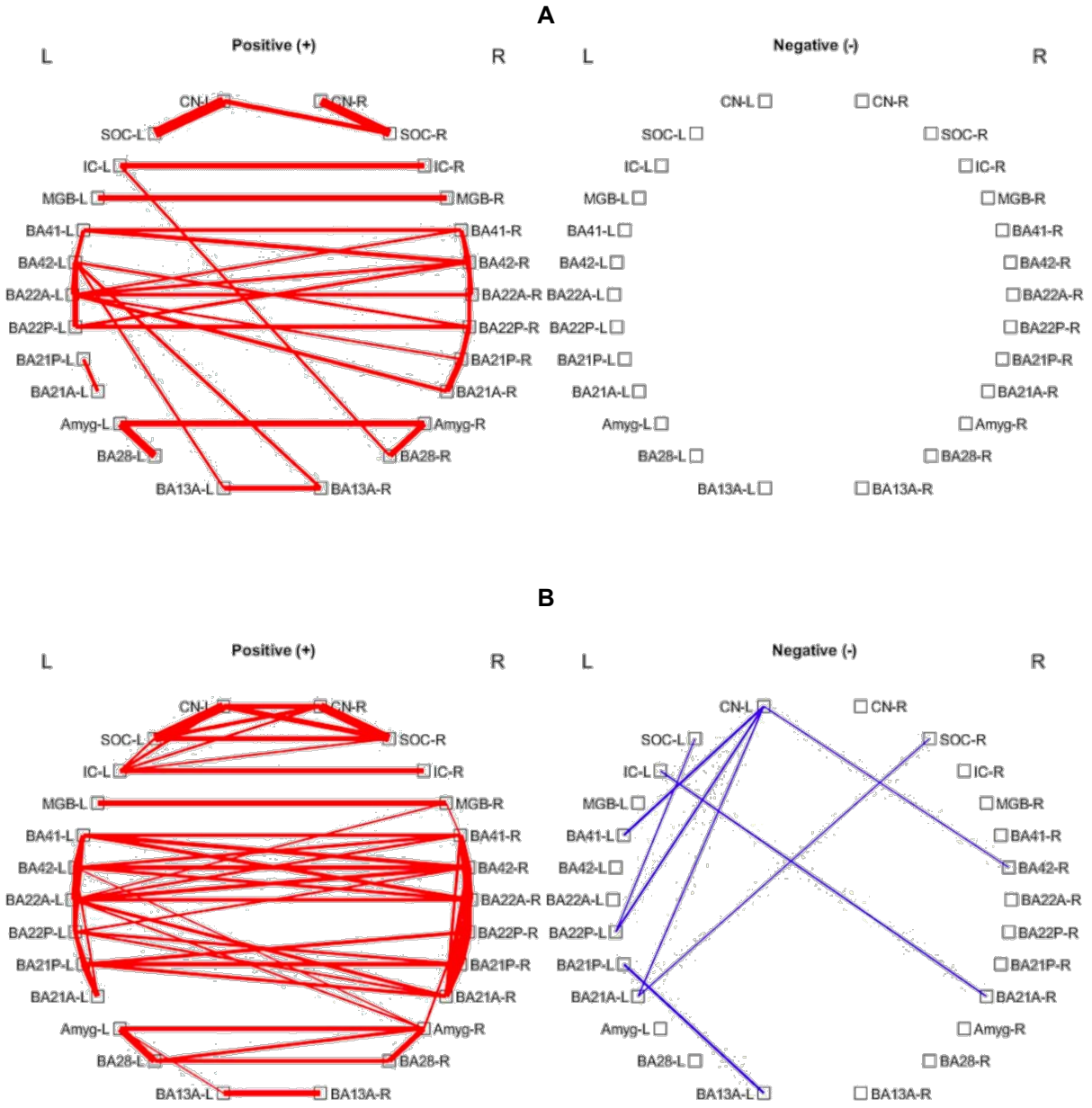

Figure 13 Auditory and limbic/distress brain regions of interest: significant Pearson correlations of BOLD time courses of different brain regions are shown for the subgroups of participants until the age of 25 (Fig. A; n=8; ∑ 45 positive and ∑ 0 negative patterns) and over the age of 25 (Fig. B; n=10; ∑74 positive, ∑8 negative patterns).

Differences between the two subgroups could not be specified here too. Accordingly, the entire group was divided into three homogenous subgroups sorted by age in ascending order. As expected, the same result, as with regard to the auditory network, was obtained: participants between 24 and 26 exhibit the highest number of positive correlation-paths in comparison to the younger (21-24) and older (27-34) subgroups (Figure 14).

Emotional distress network. Participants sorted by age (subgroups 21-24, 24-26, 27-34)

A

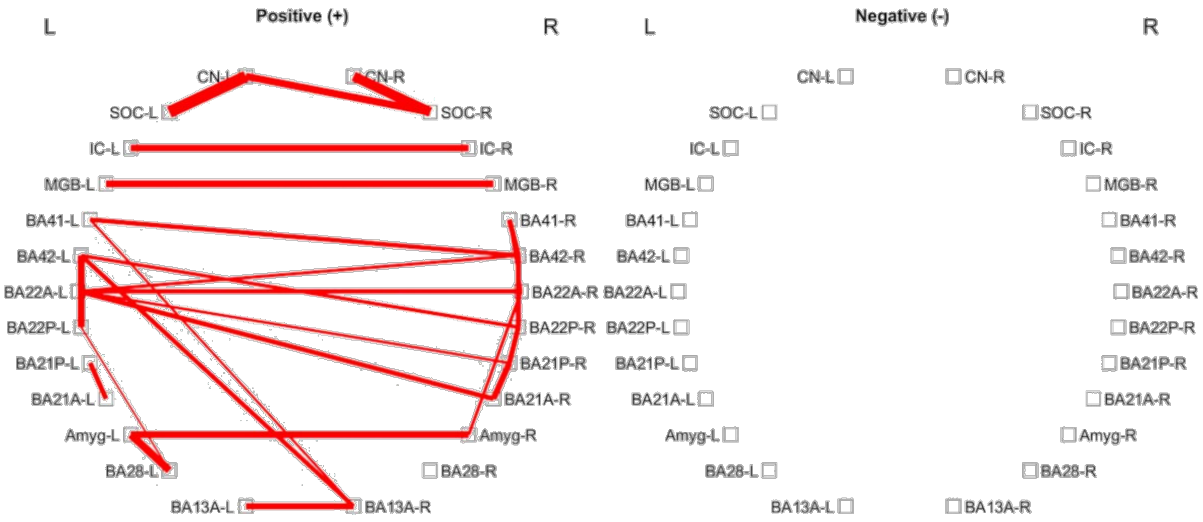

B

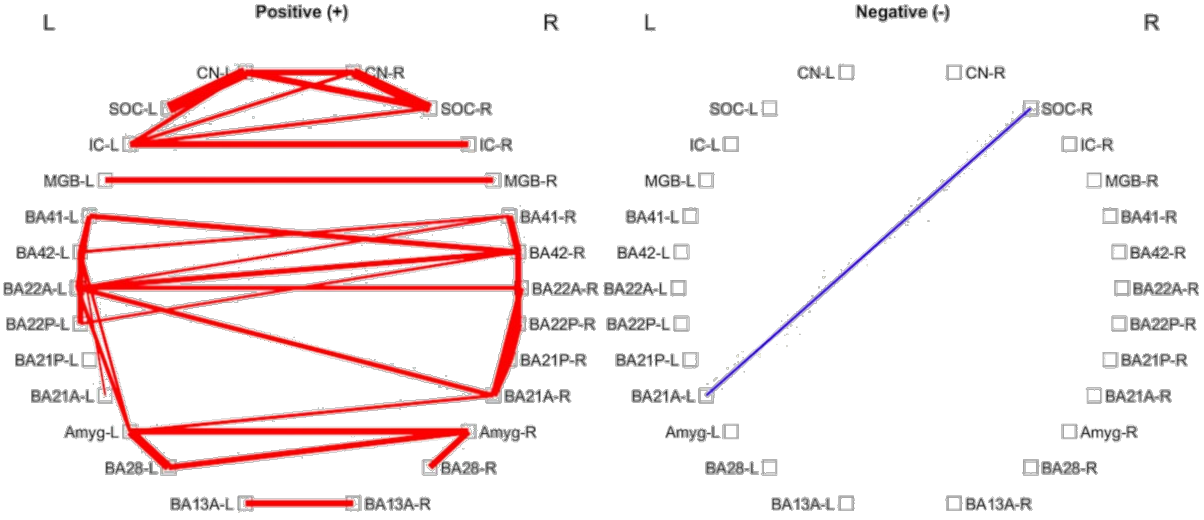

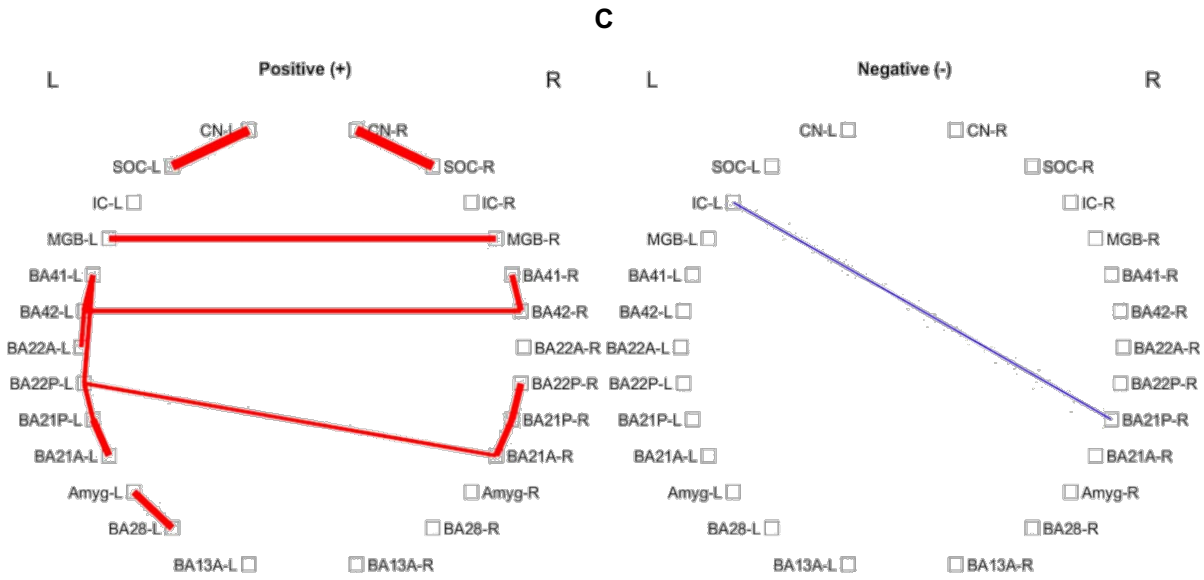

Figure 14 Auditory and limbic/distress brain regions of interest: significant Pearson correlations of BOLD time courses of different brain regions are shown for the three subgroups of participants between the age of 21 and 24 (Fig. A; n=6), 24 and 26 (Fig. B; n=6), 27 and 34 (Fig. C; n=6) for positive (left red panel) and negative (right blue panel) connectivities.

Emotional distress network. Participants sorted by sex

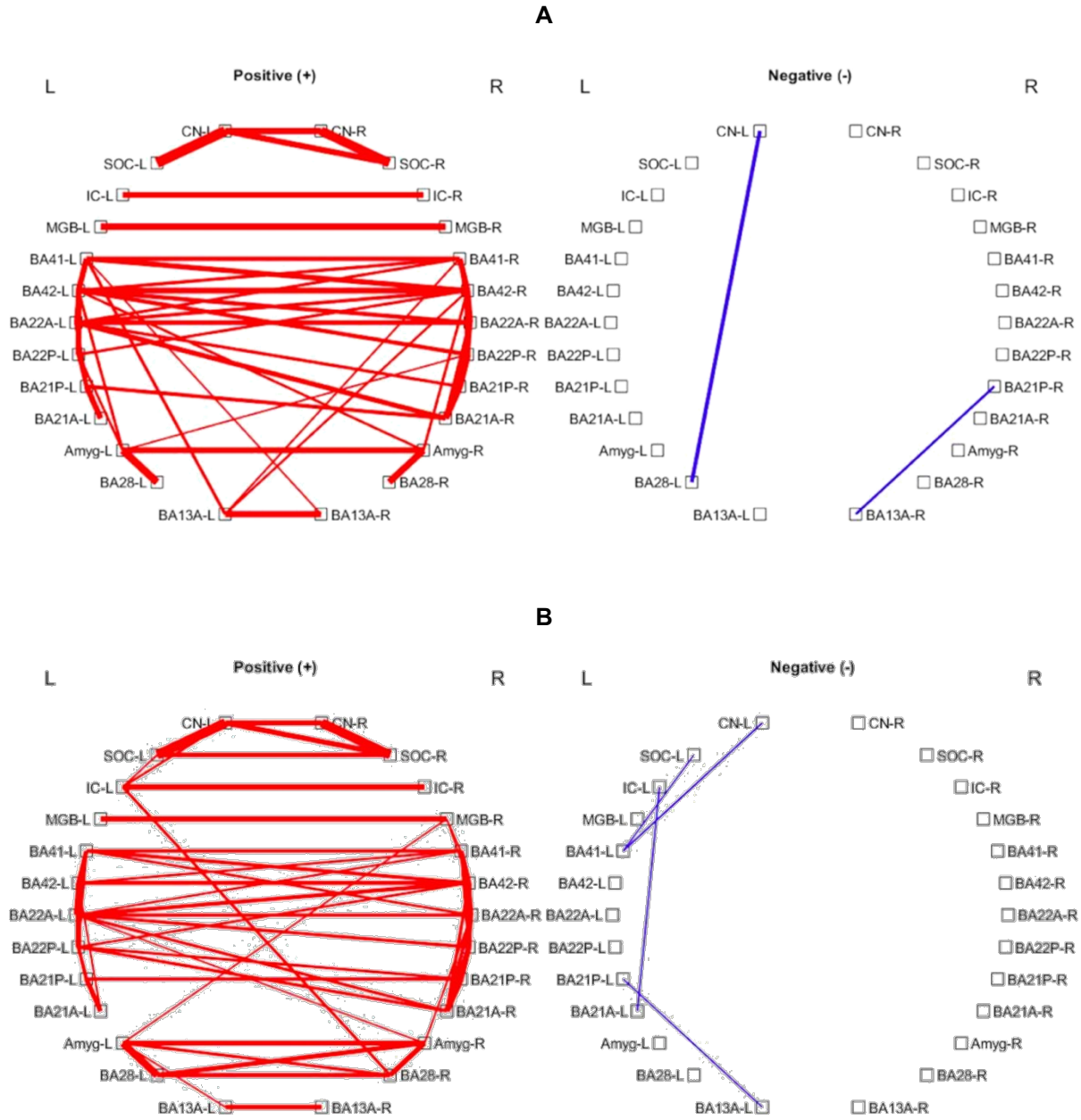

Figure 15 Auditory and limbic/emotional distress brain regions of interest: significant Pearson correlations of BOLD time courses of different brain regions are shown for the subgroups of female (Fig. A; n=7; ∑60 positive, ∑2 negative patterns) and male participants (Fig. B; n=11; ∑103 positive, ∑4 negative patterns).

Regarding the subgroups arranged by sex, the same similarities as in the results obtained in the auditory network, with males exhibiting a higher number of positive functional correlations than females, can be observed (Figure 15).

3.4 Temporofrontal Attentional Network

Functional connectivity between different auditory pathway regions and some temporofrontal network regions were explored as well. In addition to the considered auditory pathway regions from the auditory brainstem and auditory cortex, now regions of the temporofrontal attentional network such as the prefrontal cortex (BA9 and BA46), BA45, and BA47 were also regarded in the analysis.

3.4.1 Description of correlation in the entire group of participants

The entire group shows positive functional connectivity between all homologous left and right brain nodes (BA45, BA46, BA47, BA9DL, BA9M), with correlation strength values ranging from 0,18 and 0,57 and a mean value of 0,32 (Figure 16).

Specific areas of the temporofrontal attentional network (BA45, BA46, BA47, BA9DL and BA9M) exhibit numerous positive functional connectivity with each other ipsilaterally and contralaterally (Figure 16).

Temporofrontal attentional network. Whole group. All correlations

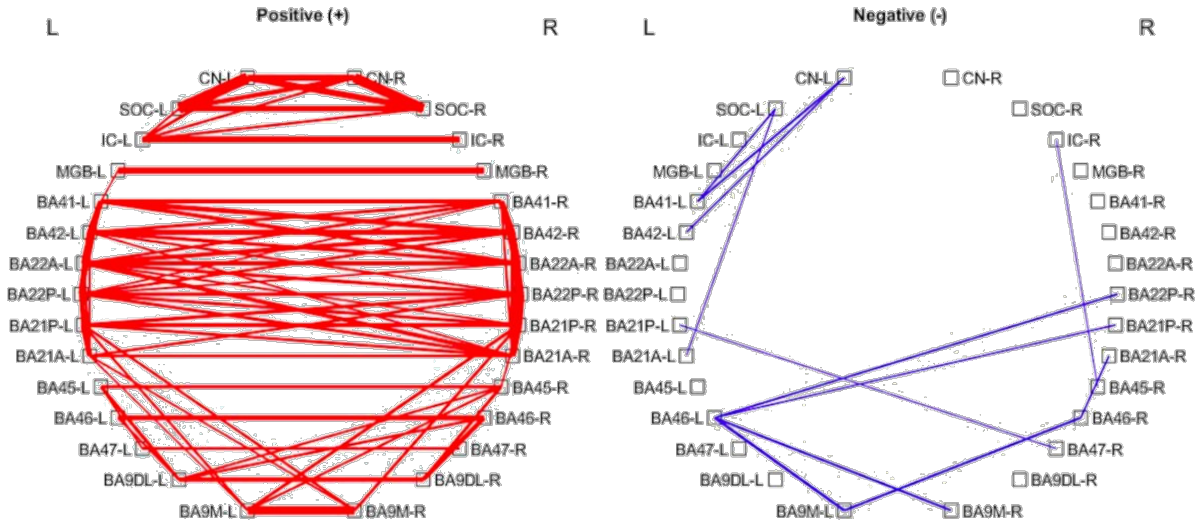

Figure 16 Significant mean rs-fMRI BOLD connectivity patterns of defined auditory and temporofrontal/attentional brain regions of interest. Significant Pearson correlations of BOLD time courses of different brain regions are shown for the whole group (n=18) for positive (left red panel; ∑99 patterns) and negative (right blue panel; ∑12 patterns) connectivities.

On the other hand, these areas appear to be only poorly correlated with cortical auditory areas and subcortical auditory nuclei (Figure 17). In this case, correlations are solely observed between the medial prefrontal cortex and the multi-modal area in MTG (BA9M-L to BA21P-L, BA21A-L, BA21P-R, and BA9M-R to BA21P-L, BA21P-R respectively) (Figure 17).

Temporofrontal attentional network. Whole group. Attentional regions of interest

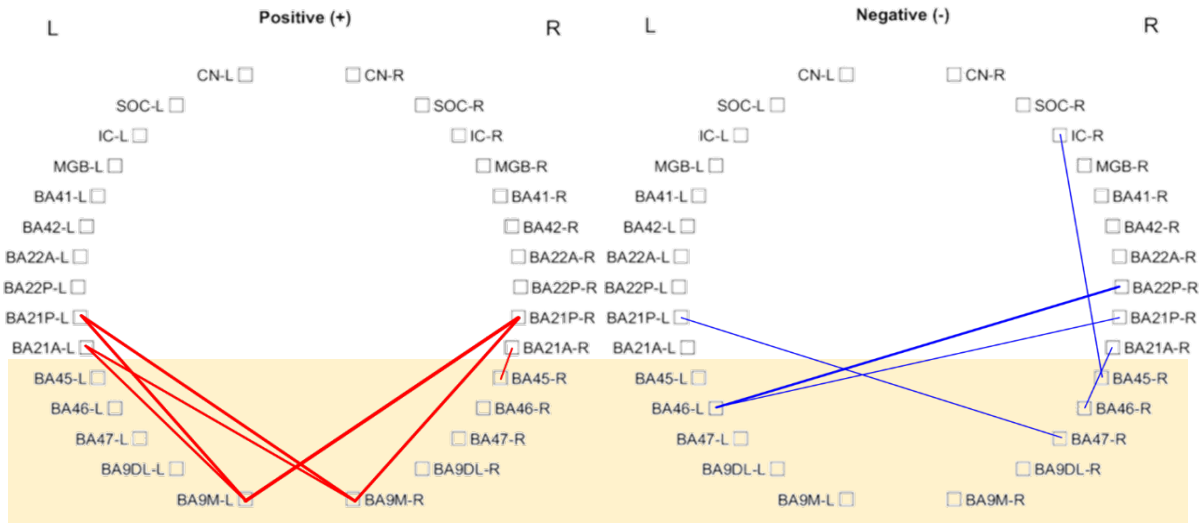

Figure 17 Auditory and attentional brain regions of interest: for a simplified overview the yellow panel displays correlations from specific attentional brain nodes (BA45, BA46, BA47, BA9DL, BA9M) to brain nodes of the auditory cortex and auditory brainstem. Other correlations have been intentionally excluded. ∑7 positive, ∑5 negative patterns.

Anti-correlations can be found between prefrontal cortical areas (BA9M-L to BA46-L, BA46-R, and BA9M-R to BA46-L). At the same time, BA46-R, BA46-L, and BA47-R are the only attentional ROIs negatively correlated with brain nodes of the auditory association cortex (BA46-L to BA22P-R, BA21P-R; BA46-R to BA21A-R; BA47-R to BA21P-L). The only negative correlation between the brainstem and the attentional circuit is between IC-R and BA45-R (Figure 17).

Overall, ROIs within the temporofrontal attentional network demonstrate numerous positive correlations among themselves (Figure 16). In contrast, these ROIs have fewer correlations with auditory specific brain regions, such as the auditory association cortex, and no correlation at all with the primary auditory cortex, auditory thalamus and auditory brainstem. This study identified only a limited number of negative correlations. These involved primarily the areas BA9M and BA46 (Figure 17).

3.4.2 Age- and sex- related description of correlations

With respect to the temporofrontal-attentional network, the results are similar to the auditory and limbic network. Older participants exhibit positive functional correlation-paths than younger participants (Figure 18), whereas, following the subdivision of the entire group into three subgroups sorted by age in ascending order, participants

between the age of 24 and 27 show more positive connectivity than the younger and the older subjects (Figure 19).

Temporofrontal attentional network. Participants sorted by age (until and over 25 years of age)

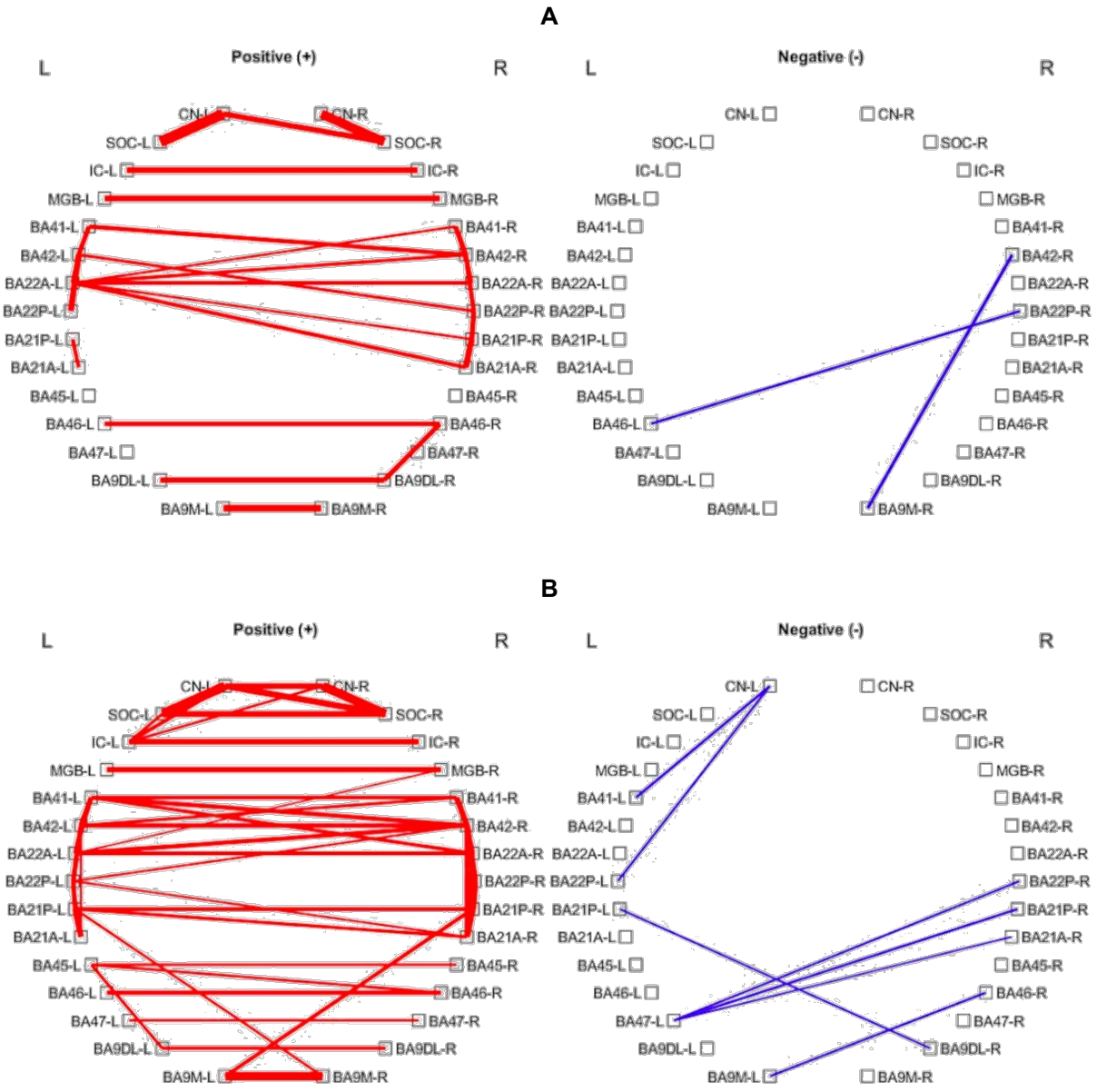

Figure 18 Auditory and attentional brain regions of interest: significant Pearson correlations of BOLD time courses of different brain regions are shown for the subgroups of participants until the age of 25 (Fig. A; n=8; ∑ 41 positive and ∑ 2 negative patterns) and over the age of 25 (Fig. B; n=10; ∑62 positive, ∑7 negative patterns).

Temporofrontal attentional network. Participants sorted by age (subgroups 21-24, 24-26, 27-34)

A

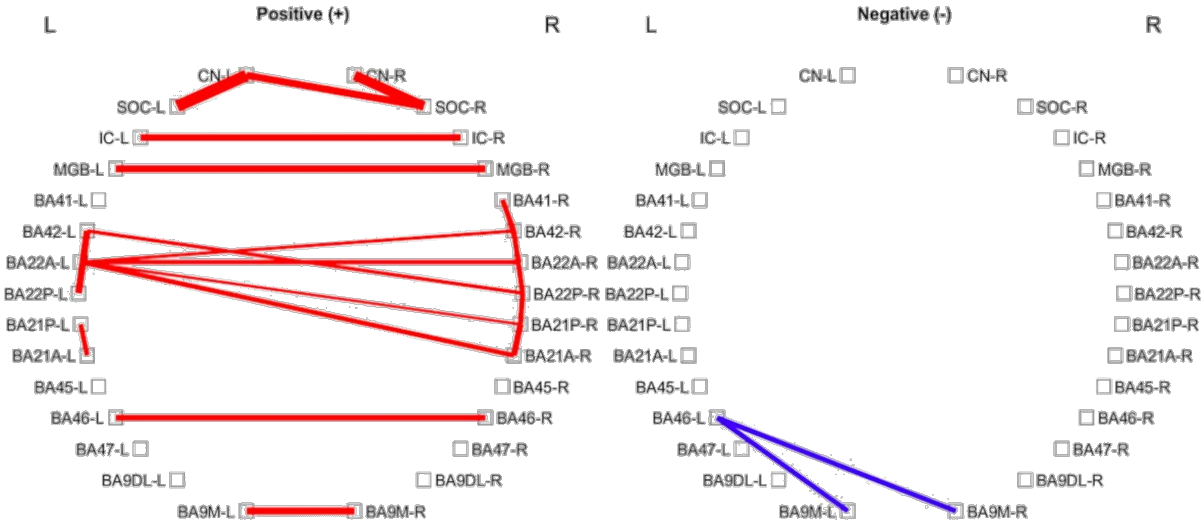

B

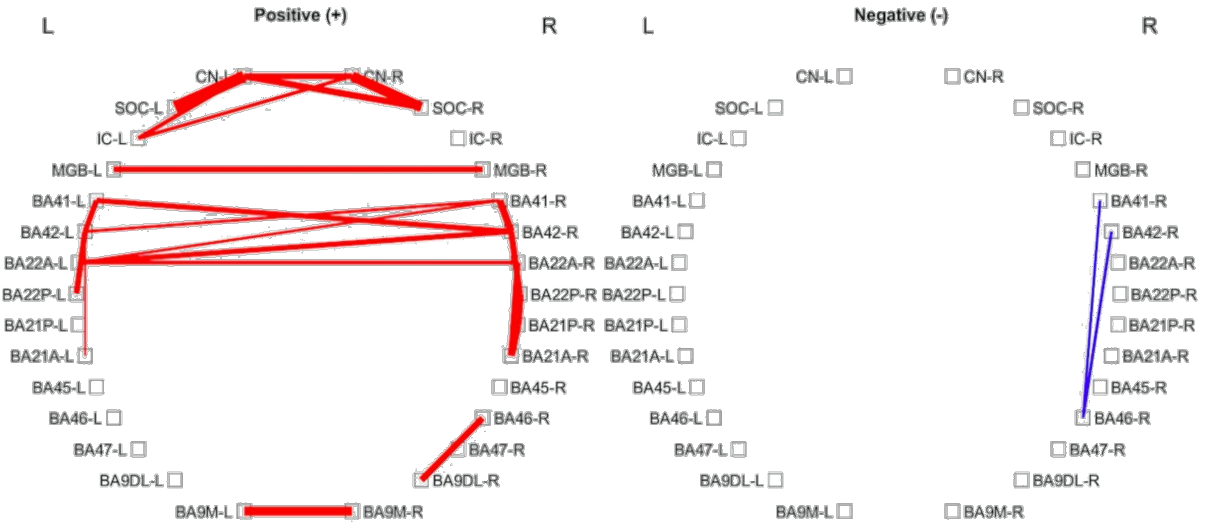

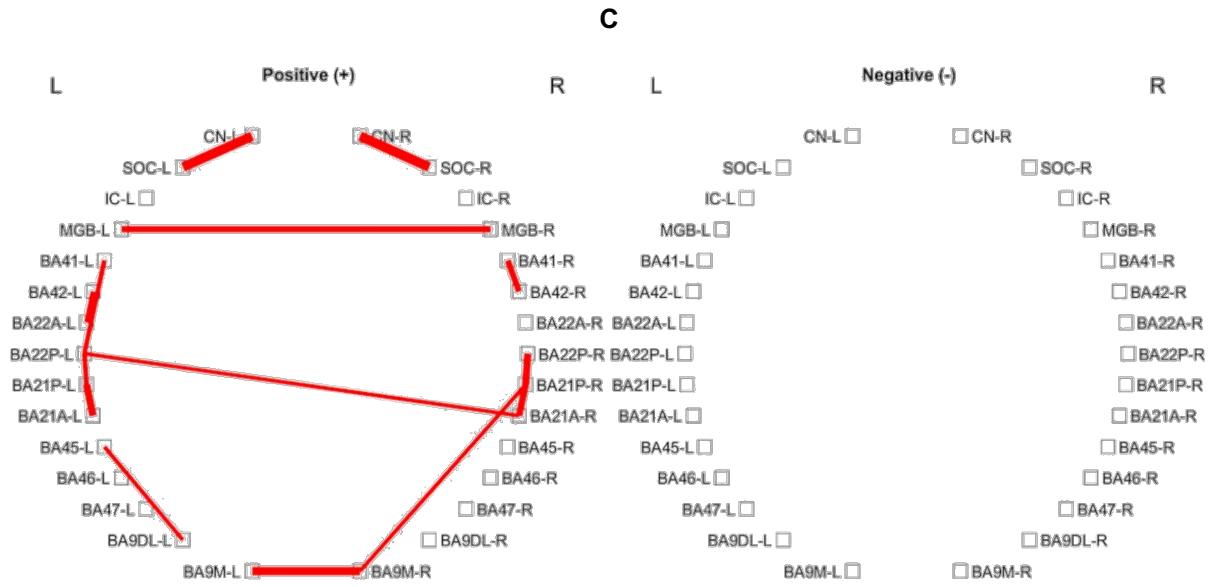

Figure 19 Auditory and attentional brain regions of interest: significant Pearson correlations of BOLD time courses of different brain regions are shown for the three subgroups of participants between the age of 21 and 24 (Fig. A; n=6), 24 and 26 (Fig. B; n=6), 27 and 34 (Fig. C; n=6) for positive (left red panel) and negative (right blue panel) connectivities.

Temporofrontal attentional network. Participants sorted by sex

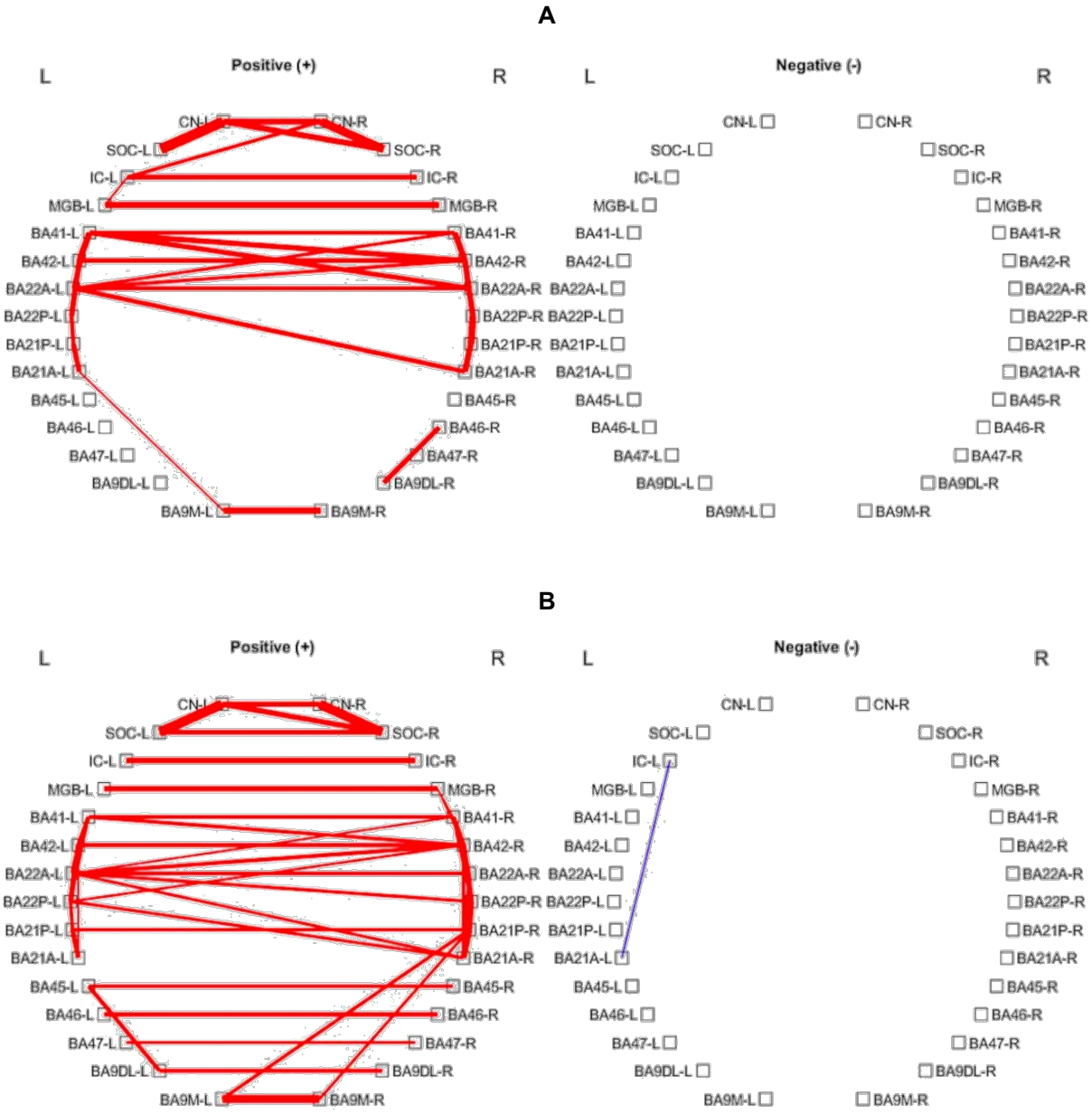

Figure 20 Auditory and attentional brain regions of interest: significant Pearson correlations of BOLD time courses of different brain regions are shown for the subgroups of female (Fig. A; n=7; ∑45 positive, ∑0 negative patterns) and male participants (Fig. B; n=11; ∑62 positive and ∑1 negative patterns).

Regarding the sex subgroups males exhibit more positive functional connectivities than females (Figure 20).

3.5 Analysis of age- and sex-subgroups

Though the significant differences in correlation numbers, all age- and sex-sorted subgroups reflect a similar template of positive connectivities in comparison to the entire group of participants, although with a lower absolute number of connectivities.

In regard to all three analysed brain networks, the correlation template of the subgroup of males (Figure 10B, Figure 15B, Figure 20B) is similar to the template of the subgroup of older participants (Figure 8B, Figure 13B, Figure 18B). The same is true for the subgroup of females (Figure 10A, Figure 15A, Figure 20A) and that of younger participants (Figure 8A, Figure 13A, Figure 18A). However, it is relevant to underline that male participants (11 subjects) significantly outnumber female participants (7 subjects) in this study.

In summary, both subgroups (age and sex) are characterized by the dominance of one subgroup (male and older participants) over the other (female and younger participants) in terms of the absolute number of correlations. Yet, all subgroups maintain clear correlation comparability to the entire group of participants (Figure 6, Figure 11, Figure 16). Male and older participants, as well as female and younger participants, share very similar correlation templates.

4 Discussion

4.1 General considerations

In the present study in a group of 18 healthy, hearing unimpaired subjects (11 males, 7 females, between 21 and 34 years of age, mean-age 26,2), significant positive correlation strengths between distinct auditory, limbic and temporofrontal/attentional brain regions were observed. Furthermore, high synchronicity between all homologous cortical and subcortical auditory brain regions was detected. No significant network-specific difference between males and females as well as younger and older subjects was observed.

Neurovascular coupling and an increased local metabolism represent the basis of neural activity detected through BOLD signal (Logothetis et al., 2001; Hofmeier et al., 2018). Positively correlated hemodynamic BOLD signals between two brain areas at rest indicate, for a predefined time frame, a constant spontaneous, highly synchronized, and short-time lagged neural activity (Goelman et al., 2014). In contrast, negative connectivity is represented through a long-time lag and, accordingly, decreased synchronicity between two different populations of neurons (Goelman et al., 2014). Haag et al. (2015) were able to correlate high synchronicity at rest with increased synchronicity in evoked BOLD signals to better sensory performance. Considering this, it was observed in the present study that all homologous ROIs are positively correlated with each other, while no negative connection between non-cortical brain nodes could be observed (Figure 6, Figure 11, Figure 16). Goelman et al. (2014) obtained similar results in their study, although they analysed different brain areas. This indicates that the identified correlation strengths and number of correlations can be considered relevant and significant. In their study, Hofmeier et al. (2018) did not detect any negative correlation between non-cortical regions in their control group either. But they demonstrated relevant negative connections between subcortical auditory nuclei in their tinnitus group. Thereby, they outlined a substantial difference between healthy subjects and tinnitus patients.

4.2 Auditory detection network: high synchronicity of the posterior insular region and reduced hippocampal activity at rest

All homologous left and right ROIs show positive connectivities only (Figure 6). Positive correlations were detected between ipsilateral and contralateral brain regions of the auditory cortex and auditory brainstem (Figure 6). The posterior insular region BA13P shows positive correlations with ipsilateral and contralateral auditory cortex and auditory thalamus over both sides (Figure 7). Regarding the hippocampus, only few positive (with low brainstem nuclei) and negative (with primary and secondary auditory cortex) correlations could be observed (Figure 7). No statistically relevant difference in functional connectivity within the age and sex subgroups could be observed (Figure 8, Figure 9, Figure 10).

The posterior insula is known to be involved in improving sound detection thresholds by forwarding attentional resources towards auditory inputs (Sadaghiani et al., 2009; cited by Hofmeier et al., 2018). The hippocampus is responsible for shaping auditory skills (Kraus and White-Schwoch, 2015; Weinberger, 2015; cited by Hofmeier et al., 2018). Furthermore, the hippocampus has also been suggested to play a key role in the accentuation of behaviourally fundamental sounds (Kilgard and Merzenich, 1998; Kraus and White-Schwoch, 2015; Weinberger, 2015; cited by Hofmeier et al., 2018). Thus, the positive correlations identified in this study between BA13 and auditory cortex, as well as between hippocampus and subcortical auditory nuclei (Figure 7) are significant despite their relatively modest correlation strengths. Considering that positive correlations at rest are associated to synchronicity of neural activity and finer sensory performance (Haag et al., 2015), the high positive interhemispheric functional connectivity of cortical and subcortical auditory areas indicates intact auditory pathway (Figure 6).

As observed by Hofmeier et al. (2018), in contrast to control participants, tinnitus subjects exhibited no involvement of the posterior insula at all. Considering that the control group in Hofmeier et al. (2018) primarily showed correlations with low auditory brainstem centres, these results lead to the assumption that the suppression of posterior insular activity, and so, in turn, the failure to recruit attentional resources for the improvement of sound detection thresholds (Sedaghiani et al., 2009), could set a turning point in the emergence and/or maintenance of tinnitus.

4.3 Emotional distress network: poor involvement of specific limbic brain areas at rest

In this study, multiple significant connectivities with the AC and only few with subcortical regions were observed (Figure 12). Hereby, limbic-specific brain areas, such as the anterior insular region BA13A and the amygdala, correlate primarily with regions of the left auditory cortex. Statistically significant differences between younger and older subjects (Figure 13, Figure 14) as well as between females and males (Figure 15) were not observed.

The limbic system is a brain network responsible for memory, motivation, emotion and attention. It includes both cortical and subcortical brain structures (Sanchez Jimenez and De Jesus, 2022). Areas of the limbic/emotional-distress network, such as the amygdala, the entorhinal cortex (BA28) and the anterior insula (BA13A), constitute a relevant network for the elaboration of fear and anxiety, especially during tinnitus (Chen et al., 2017; Husain 2016; Leaver et al., 2016; cited by Hofmeier et al., 2018). The anterior insular cortex is involved in a generalised distress network, which shows an enhanced activity after real or phantom hearing stimuli or pain (Langguth et al., 2012 and Leaver et al., 2012; reviewed in Galazyuk et al., 2012). The amygdala is a relevant brain structure of the auditory pathway, since it is directly connected with the MGB and auditory secondary association areas (Kapolowicz and Thompson, 2020; Sah et al., 2003; LeDoux, 2007). It plays a key role in a wide range of behavioural functions and psychiatric disorders (De Ridder et al., 2006). The amygdala is a fundamental component of the limbic system, and it is correlated with emotional expression. In animal models, it showed involvement in terms of increased activity (Zhang et al., 2003 and Chen et al., 2012; reviewed in Galazyuk et al., 2012), and so it did in humans suffering from tinnitus (Mirz et al., 2000 and Vanneste et al., 2010; reviewed in Galazyuk et al., 2012). The amygdala was observed to be involved in aversive responses such as distress because of tinnitus (Galazyuk et al., 2012). Yoo et al. (2016) showed reductions in grey matter volumes of bilateral amygdalae in chronic tinnitus patients, while Tae et al. (2018) outlined the presence of wide atrophic regions of the amygdala in tinnitus subjects using surface-based vertex analysis from MRI data. Hence, they suggest that in the presence of a reduced limbic regional volume, the chances of experiencing tinnitus are higher and that specific pathologies affecting

these regions might lead to tinnitus perception. Since the amygdala shows high responsiveness to acoustic trauma and exhibits plasticity far after the end of noise exposure, the hypothesis that non-classical auditory areas, such as the limbic regions, also play a key role in both arising and maintenance of hearing disorders was deduced (Kapolowicz and Thompson, 2020).

The results obtained in the present study strengthen those obtained in Hofmeier et al. (2018). They are representative for a general neuronal distress-free state and apparently reflect a physiological functioning of central non-specific auditory limbic circuitries. Because these limbic brain regions are responsible for “auditory fear conditioning” (Sander et al., 2005; reviewed in Galazyuk et al., 2012) and “emotional response to vocal stimuli” (Sander et al., 2005, Fecteau et al., 2007, Wiethoff et al., 2009, Leitman et al., 2010 Gadziola et al., 2012 and Peterson et al., 2008; reviewed in Galazyuk et al., 2012), this sort of state of quiescence in the emotional distress brain areas likely appears to be an essential neural condition for physiological balance in central auditory circuitries. In support of this, Hofmeier et al. (2018) demonstrated multiple significant positive correlations between emotional distress brain regions and lower brainstem nuclei in tinnitus subjects, as well as elevated BOLD fMRI activities in the anterior insula (BA13A). The “Jastreboff Neurophysiological Model” suggests a “negative emotional reinforcement”: the limbic system is hereby implied to increase and manifest pre-tinnitus activity following aversive emotional states such as fear, anxiety, and tension (Jastreboff, 1990; cited by Hofmeier et al., 2018). Chronic tinnitus and hearing impairment in most cases find the same origin in auditory peripheral and/or central deafferentation (Brozoski et al., 2012; Diesch et al., 2012b; Langers et al., 2012; Middelton and Tzounopoulos, 2012; Schaette and Kempter, 2012; Stolzberg et al., 2012). This explains why we can expect an involvement of ROIs belonging to the limbic system also in hearing-impaired subjects with no history of tinnitus (Hofmeier et al., 2018). Since tinnitus and hearing-impairment are both perceived as a distress condition, with the first one being more bothersome than the other, it can be intuitively understood why young and hearing-unimpaired subjects show an overall poor involvement of emotional distress brain regions. Such differences between healthy controls and tinnitus subjects could mark a turning point for future studies. Yet, current studies still outline controversial results, and future ones could try to investigate further

and clarify possible correlations between changes in volumes of limbic areas and eventually correlated variations of BOLD signal activity.

4.4 Temporofrontal attentional network: reduced synchronicity of specific stress-enhancing brain areas at rest

ROIs within the temporofrontal attentional network exhibit a widespread and uniform pattern of positive functional connectivity among themselves (Figure 16). In contrast only a limited number of these ROIs exhibit such connections with areas of the auditory cortex (Figure 17). Upon further analysis, no statistically significant differences in connectivity between younger and older participants (Figure 18, Figure 19), as well as between males and females (Figure 20) were observed.

The prefrontal cortical region BA9 coordinates the stress response by the hypothalamic-pituitary axis (HPA) (Sullivan and Gratton, 2002). “The medial prefrontal cortex (BA9M), which belongs to the default mode network, has been suggested to play a role in stress excitation” (McKlveen et al., 2016; Utevsky et al., 2014; cited by Hofmeier et al., 2018). In contrast, “the dorsolateral prefrontal cortex (BA9DL and BA46), which is essential for auditory-specific attentional tasks, is linked to stress inhibition” (McKlveen et al., 2013; Rasgon et al., 2017; cited by Hofmeier et al., 2018).

Tinnitus is generally assessed by a few characteristics such as perceived loudness, annoyance, and distress level. In this context, consciousness becomes a crucial aspect of tinnitus. Recent studies have proved that the sole activation of the auditory cortex is mandatory but not enough for an auditory stimulus to access consciousness (Boly et al., 2004). First, Boly et al., (2004) and then Laureys (2005) outlined the involvement of higher-order multimodal association areas required for sound perception. In resting state BOLD fMRI data of chronic tinnitus patients in comparison to control subjects, Maudoux et al. (2012) observed decreased connectivity in non-auditory regions such as the prefrontal cortex. This indicates a change in cortical and subcortical connectivity. Hence, the attentional network is involved. Their results confirm the involvement of non-auditory brain regions in tinnitus pathophysiology, suggesting that various regions of the brain appear to play a role in the perception of the phenomenon, which leads to psychological distress and disabling chronic

conditions. This provides evidence for a distributed cerebral network associated with tinnitus.

The present study provides evidence for homogenously distributed neural activity in regard to the stress-enhancing region BA9M and the stress-inhibiting region BA9DL (Figure 16). This reflects HPA axis balance in healthy, non-tinnitus hearing-unimpaired subjects.

Remarkably, the current study did not reveal any correlation between attentional ROIs and subcortical auditory nuclei. This stands in contrast to the findings of Hofmeier et al.´s (2018) tinnitus group where positive correlations were primarily identified between attentional ROIs and subcortical auditory nuclei. These observations lend support to the hypothesis that an increased, stress-induced, attention-modulated synchronicity between attentional regions, such as BA9M and BA45, and auditory brainstem nuclei may underlie or contribute to certain sensorineural imbalances, such as tinnitus.

4.5 Age and sex analysis

The dominance of one subgroup (male (Figure 10B, Figure 15B, Figure 20B) and older (Figure 8B, Figure 13B, Figure 18B) participants) over the other (female (Figure 10A, Figure 15A, Figure 20A) and younger (Figure 8A, Figure 13A, Figure 18A) participants) was observed in terms of absolute number of correlations. Furthermore, male and older participants share a very similar correlation template. The same is true for female and younger participants. Finally, both subgroups maintain clear correlation comparability with the entire group of participants (Figure 6, Figure 11, Figure 16).

Females are more susceptible to stress than males, as pain and depression appear to entail more grievous consequences for female tinnitus patients (Vanneste et al., 2012; Erlandsson and Holgers, 2001). Through rs-EEG, Vanneste et al. (2012) detected differences in activities and connectivity between male and female tinnitus patients. Their results suggest that “sex influences in tinnitus cannot be ignored and should be taken into account in functional imaging studies related to tinnitus” (Vanneste et al., 2012). Regarding tinnitus patients, sLORETA (standardized low-resolution brain electromagnetic tomography) showed differences between the two sexes, confirming that females are generally more sensitive to symptoms, their intensity, and overall distress than males (Frank et al., 2012).

Tomasi and Volokow (2012) analysed MRI data of a pool of 561 healthy subjects and suggest sex differences in the functional organization of the brain: female subjects showed 14% higher local function connectivity density and up to 5% more grey matter density than male subjects in cortical and subcortical regions. Voxel Based Morphometry analysis showed a higher grey matter density in women than in men concerning the occipital, parietal, temporal, and ventral prefrontal cortices. In men, on the other hand, a significantly larger total brain volume than in women was observed. Such differences in brain functional connectivity may also contribute to sex differences in the development of neurological diseases (Tomasi and Volokow, 2012).

Gong et al. (2009) observed age and sex differences through diffusion MRI-tractography, where the cerebral cortex was represented as a weighted network of connected regions. Their study analysed the network efficiency on the basis of age- and sex-related dynamics within the anatomical network: the aim of the investigation was to observe how well information is carried within the cerebral cortex. Differences in the neuroanatomy between men and women were already observed by Sowell et al. (2007). In Gong et al. (2009), the two sexes showed differences in regional efficiency: women appeared to own a greater overall cortical connectivity and, at the same time, more dynamic cortical networks, both regionally and globally. Thus, they seem to have an overall better-skilled cortical network. The same was already hypothesized by Gur et al. (1999), who suggested that the female brain might be more flexible and efficient than the male brain, also due to a better exploiting of available white matter. Older brains showed a reduction in global cortical connectivity as well as a shift of local efficiency from the parieto-occipital to the temporofrontal neocortex. The decay in the aging brain leads to a disorder in the functional integration between brain nodes, resulting in specific cognition declines (Gong et al., 2009). O'Sullivan et al. (2001) suggested that cognitive deficits in older brains arise as a consequence of structural disconnection on the cortex level as well as a decay of specific grey matter areas.

In this study, a predominance of positive correlations was observed between most cortical and subcortical ROIs across all three detection network analysed, with males exhibiting a higher number of such correlations compared to females (Figure 10, Figure 15, Figure 20). This finding appears to contradict previous research suggesting more robust functional connectivity between brain regions in females (Tomasi and Volokow,

2012; Gong et al., 2009). The discrepancy may be attributed to an imbalance in the sex distribution within the participant sample, which comprises 11 males and 7 females. To gain a deeper understanding of potential sex-related differences in (sub-)cortical network reorganisation, particularly in response to disrupted somatosensory input such as that caused by peripheral deafferentation, further research with a more balanced representation of sexes is warranted.

Contrary to expectations, this study found a greater synchronicity of BOLD signals in the older subgroups compared to the younger ones (Figure 8, Figure 13, Figure 18). These results may be more reflective of individual variability in neural synchronicity rather than indicative of age-related changes. It is possible that the small sample size within each subgroup limits the statistical power and significance of these findings.

Additionally, considering the younger mean age of females and the older mean age of males, the similarities observed between the subgroups of male and older participants and the similarities between the subgroups of female and younger participants are likely not coincidental. Rather, they can be attributed to the differing average ages within each sex subgroup. More precisely, it was not possible in this study to detect significant differences between males and females because both subgroups do not have comparable mean ages.

Future studies could try to analyse larger subgroups that are balanced in terms of both number of participants and average age across sexes. This approach would help to isolate sex differences from age effects and provide clearer understanding of the underlying neural mechanisms.

5 Summary

In this study, rs-fMRI data were used to investigate BOLD functional connectivities between multiple auditory-correlated, cortical and subcortical brain regions of interest (ROIs). The data were extracted from the dataset of McMahon K., Queensland University, Australia, stored in the databank of the "1000 Functional Connectome Project" (http://fcon_1000.projects.nitrc.org/fcpClassic/FcpTable.html). The dataset includes recordings from 19 healthy subjects with normal hearing, encompassing both females and males, ranging in age from 20 to 34 years. Due to issues with the data quality, information from one female participant was deemed unsuitable for analysis and consequently excluded. This resulted in a final sample of 18 subjects, whose ages ranged from 21 to 34 years, being included in the study.

The analysis included brain ROIs that are considered to play a significant role in the genesis and maintenance of hearing disorders such as tinnitus, a phantom sound whose neurophysiological mechanisms remain open to scientific debate (Hofmeier et al., 2018).

High synchronicity was observed between all homologous regions as well as within subcortical auditory brain nuclei. Additionally, all ROIs within the aforementioned (auditory, limbic/emotional distress, temporofrontal/attentional) brain networks demonstrated a significant degree of synchronicity with one another.

The posterior insula region BA13P exhibited wide interconnectivity with auditory cortical areas. This extensive network of functional correlations suggests a robust level of synchronicity, which may reflect effective auditory processing capabilities and potentially contribute to the optimization of sound detection thresholds.

In contrast, regions of the limbic/emotional distress network showed comparatively lower levels of involvement, indicating minimal auditory-related distress. This suggests a state of physiological equilibrium in auditory processing, reflective of a balanced emotional response to auditory stimuli. Remarkably, the current study revealed the absence of connectivity between auditory limbic regions, such as the amygdala and the anterior insula, and subcortical auditory nuclei. This finding is noteworthy because previous research (Hofmeier et al., 2018) had identified such connections as a possible underlying cause for auditory distress.

Similarly, in regard to the temporofrontal attentional network, both the stress-enhancing medial prefrontal cortex BA9M and the stress-inhibiting dorsolateral prefrontal cortex BA9DL exhibit a sparse yet uniformly distributed pattern of functional connectivity. Notably, when compared to tinnitus participants from prior studies (Hofmeier et al., 2018), no correlations were observed between regions of the attentional network and regions of the auditory brainstem in this research. This absence of connectivity not only lends support to the notion of HPA axis balance but also supports the hypothesis that synchronicity between temporofrontal areas (such as BA9M and BA45) and auditory brainstem regions might be implicated in, or contribute to certain sensorineural disorders, including tinnitus.

In this study, a higher prevalence of positive correlations was found in male and older participants compared to female and younger ones across cortical and subcortical ROIs in the aforementioned brain networks. This contradicts earlier studies suggesting stronger connectivity in females. The observed discrepancy might be due to the uneven sex distribution in the sample (11 males vs. 7 females). Additionally, older participants showed higher BOLD-signal synchronicity than younger ones, which could reflect individual variability rather than age-related changes, potentially influenced by the small group sizes. The similarities between male and older participants, as well as between female and younger participants, suggest that differences in average ages within the sex subgroups may have affected the results. Consequently, it was challenging to discern significant sex differences due to this age disparities. Future research should aim for larger, age-balanced subgroups to better distinguish sex differences from age effects and clarify the neural mechanisms involved.

These findings highlight potential neural mechanisms that could differentiate between normal auditory processes and pathological conditions like tinnitus. These findings provide an overview of physiological functional connectivity patterns between auditory regions and auditory-correlated areas of interest in the brain, as measured by BOLD activity, reflecting the inherent neural processes associated with normal auditory functions. The results presented here can serve as a comparative basis for future research aiming to identify and characterise alterations in functional connectivity that may arise following the onset of auditory disorders as hearing loss and tinnitus.

German summary

In dieser Studie wurden rs-fMRT-Daten verwendet, um BOLD-funktionellen Verbindungen zwischen mehreren auditorisch-korrelierten kortikalen und subkortikalen Gehirnregionen von Interesse (ROIs) zu untersuchen. Die Daten wurden aus dem Datensatz von McMahon K., Queensland Universität, Australien, entnommen, der in der Datenbank des „1000 Functional Connectome Project“ gespeichert ist (http://fcon_1000.projects.nitrc.org/fcpClassic/FcpTable.html). Der Datensatz umfasst Aufnahmen von 19 gesunden Probanden mit normalen Hörvermögen, darunter Frauen und Männer im Alter von 20 bis 34 Jahren. Aufgrund von Problemen mit der Datenqualität wurden die Informationen einer weiblichen Teilnehmerin als ungeeignet für die Analyse erachtet und folglich ausgeschlossen. Dies führte zu einer endgültigen Stichprobe von 18 Probanden im Alter von 21 bis 34 Jahren, die in die Studie einbezogen wurden.

Die Analyse umfasst Gehirn-ROIs, denen eine bedeutende Rolle bei der Entstehung und Aufrechterhaltung von Hörstörungen wie Tinnitus zugeschrieben wird, einem Phantomgeräusch, dessen neurophysiologische Mechanismen weiterhin Gegenstand wissenschaftlicher Debatten sind (Hofmeier et al., 2018).

Es wurde eine hohe Synchronizität zwischen allen homologen Regionen sowie innerhalb subkortikaler auditorischer Hirnkerne beobachtet. Darüber hinaus zeigten alle ROIs innerhalb der genannten (auditorischen, limbischen/emotionalen Disstress-, temporofrontalen/Aufmerksamkeits-) Gehirnnetzwerke einen signifikanten Grad an Synchronizität miteinander.

Die hintere Inselregion BA13P zeigte eine weite Vernetzung mit auditorischen kortikalen Bereichen. Dieses umfangreiche Netzwerk funktioneller Korrelationen deutet auf ein robustes Maß an Synchronizität hin, das effektive auditorische Verarbeitungsfähigkeiten widerspiegeln und möglicherweise zur Optimierung der Schwellenwerte für die Schallerkennung beitragen kann.

Im Gegensatz dazu zeigten Regionen des limbischen/emotionalen Disstress-Netzwerks vergleichsweise geringere Beteiligungsgrade, was auf minimale hörbezogene Disstress hindeutet. Dies deutet auf einen Zustand physiologischen Gleichgewichts in der auditorischen Verarbeitung hin, der eine ausgeglichene emotionale Reaktion auf auditorische Reize widerspiegelt. Bemerkenswerterweise offenbarte die aktuelle Studie das

Fehlen von Verbindungen zwischen limbischen Regionen wie der Amygdala und der vorderen Insel sowie subkortikalen auditorischen Kernen. Dieser Befund ist bemerkenswert, da frühere Forschungen (Hofmeier et al., 2018) solche Verbindungen als mögliche Ursache für auditorische Disstress identifiziert hatten.

Ähnlich verhält es sich mit dem temporofrontalen Aufmerksamkeitsnetzwerk: sowohl der stressverstärkende mediale präfrontale Kortex BA9M als auch der stresshemmende dorsolaterale präfrontale Kortex BA9DL zeigen ein spärliches, aber gleichmäßig verteiltes Muster an funktionelle Konnektivität. Insbesondere im Vergleich zu Tinnitus-Teilnehmern aus früheren Studien (Hofmeier et al., 2018) wurden in dieser Forschung keine Korrelationen zwischen Regionen des Aufmerksamkeitsnetzwerks und Regionen des auditorischen Hirnstamms beobachtet. Das Fehlen dieser Konnektivität stützt nicht nur die Vorstellung eines Gleichgewichts der HPA-Achse, sondern unterstützt auch die Hypothese, dass Synchronizität zwischen temporofrontalen Bereichen (wie BA9M und BA45) und auditorischen Hirnstammregionen bei bestimmten sensorineuralen Störungen einschließlich Tinnitus beteiligt sein könnte oder dazu beiträgt.

In dieser Studie wurde eine höhere Prävalenz positiver Korrelationen bei männlichen und älteren Teilnehmern im Vergleich zu weiblichen und jüngeren Teilnehmern über kortikale und subkortikale ROIs in den zuvor genannten Gehirnnetzwerken festgestellt. Dies steht im Widerspruch zu früheren Studien, die eine stärkere Konnektivität bei Frauen nahelegen. Die beobachtete Diskrepanz könnte auf die ungleiche Geschlechterverteilung in der Stichprobe (11 Männer gegenüber 7 Frauen) zurückzuführen sein. Zudem zeigten ältere Teilnehmer eine höhere Synchronizität des BOLD-Signals als jüngere, was individuelle Variabilität anstelle von altersbedingten Veränderungen widerspiegeln könnte, möglicherweise beeinflusst durch die geringe Gruppengröße. Die Ähnlichkeiten zwischen männlichen und älteren Teilnehmern sowie zwischen weiblichen und jüngeren Teilnehmern lassen vermuten, dass Unterschiede im Durchschnittsalter innerhalb der Geschlechtsuntergruppen die Ergebnisse beeinflusst haben könnten. Folglich war es schwierig, signifikante Geschlechtsunterschiede aufgrund dieser Altersunterschiede zu erkennen. Zukünftige Forschungen sollten größere, altersausgeglichene Untergruppen anstreben, um Geschlechtsunterschiede besser von Alterseffekten unterscheiden zu können und die zugrundeliegenden neuralen Mechanismen zu klären.

Diese Ergebnisse heben potenzielle neuronale Mechanismen hervor, die zwischen normalen auditorischen Prozessen und pathologischen Zustände wie Tinnitus unterscheiden könnten. Diese Ergebnisse bieten einen Überblick über physiologische Muster funktioneller Konnektivität zwischen auditorischen Regionen und auditorisch-korrelierten Gehirnbereiche von Interesse, gemessen durch BOLD-Aktivität, welche die inhärenten neuralen Prozesse im Zusammenhang mit normaler auditorischen Funktion widerspiegeln. Die hier präsentierten Resultate können als vergleichende Grundlage für zukünftige Forschungen dienen, die darauf abzielen, Veränderungen in der funktionellen Konnektivität zu identifizieren und zu charakterisieren, die nach dem Auftreten von Hörstörungen wie Hörverlust und Tinnitus entstehen können.

6 References

Adams PF, Hendershot GE, Marano MA. Current estimates from the National Health Interview Surevey, 1996. Hyattsville, Md.: National Center for Health Statistics, 1999.

Amunts K, Morosan P, Hilbig H,Zilles K. Chapter 36 - Auditory System. In “The Human Nervous System” (Third Edition), Jürgen K. Mai, Paxinos G. Academic Press, 2012

Anson BJ, Donaldson JA. The surgical anatomy of the temporal bone and ear (3rd ed.). Philadelphia, PA: W.B. Saunders, 1981

Amaral DG, Price JL. Amygdalo-cortical projections in the monkey (Macaca fascicularis). J Comp Neurol. 1984 Dec 20;230(4):465-96. doi: 10.1002/cne.902300402.

Ardila A, Bernal B, Rosselli M. The language area of the brain: a functional reassessment. Rev Neurol. 2016 Feb 1;62(3):97-106. doi: 10.33588/rn.6203.2015286

Ashmore J. Cochlear outer hair cell motility. Physiol Rev. 2008 Jan;88(1):173-210. doi: 10.1152/physrev.00044.2006.

Badre D, Wagner AD. Semantic retrieval, mnemonic control, and prefrontal cortex. Behav Cogn Neurosci Rev. 2002 Sep;1(3):206-18. doi: 10.1177/1534582302001003002.

Bamiou DE, Musiek FE, Luxon LM. The insula (Island of Reil) and its role in auditory processing. Literature review. Brain Res Brain Res Rev. 2003 May;42(2):143-54. doi: 10.1016/s0165-0173(03)00172-3.

Baxter MG, Murray EA (2002). The amygdala and reward. Nat Rev Neurosci. 2002 Jul;3(7):563-73. doi: 10.1038/nrn875.

Belli H, Belli S, Oktay MF, Ural C. Psychopathological dimensions of tinnitus and psychopharmacologic approaches in its treatment. Gen Hosp Psychiatry. 2012 May-Jun;34(3):282-9. doi: 10.1016/j.genhosppsych.2011.12.006.

Biswal BB, Mennes M, Zuo XN, Gohel S, Kelly C, Smith SM, Beckmann CF, Adelstein JS, Buckner RL, Colcombe S, Dogonowski AM, Ernst M, Fair D, Hampson M, Hoptman MJ, Hyde JS, Kiviniemi VJ, Kötter R, Li SJ, Lin CP, Lowe MJ, Mackay C, Madden DJ, Madsen KH, Margulies DS, Mayberg HS, McMahon K, Monk CS, Mostofsky SH, Nagel BJ, Pekar JJ, Peltier SJ, Petersen SE, Riedl V, Rombouts SA, Rypma B, Schlaggar BL, Schmidt S, Seidler RD, Siegle GJ, Sorg C, Teng GJ, Veijola J, Villringer A, Walter M, Wang L, Weng XC, Whitfield-Gabrieli S, Williamson P, Windischberger C, Zang YF, Zhang HY, Castellanos FX, Milham MP. Toward discovery science of human brain function. Proc Natl Acad Sci U S A. 2010 Mar 9;107(10):4734-9. doi: 10.1073/pnas.0911855107.

Biswal B, Yetkin FZ, Haughton VM, Hyde JS. Functional connectivity in the motor cortex of resting human brain using echo-planar MRI. Magn Reson Med. 1995 Oct;34(4):537-41. doi: 10.1002/mrm.1910340409.

Boly M, Faymonville ME, Peigneux P, Lambermont B, Damas P, Del Fiore G, Degueldre C, Franck G, Luxen A, Lamy M, Moonen G, Maquet P, Laureys S. Auditory processing in severely brain injured patients: differences between the minimally conscious state and the persistent vegetative state. Arch Neurol. 2004 Feb;61(2):233-8. doi: 10.1001/archneur.61.2.233.

Brozoski T, Odintsov B, Bauer C. Gamma-aminobutyric acid and glutamic acid levels in the auditory pathway of rats with chronic tinnitus: a direct determination using high resolution point-resolved proton magnetic resonance spectroscopy (H-MRS). Front Syst Neurosci. 2012 Feb 24;6:9. doi: 10.3389/fnsys.2012.00009.

Buzsáki G. Rythms of the Brain. New York, NY: Oxford University Press, 2006.

Chaigneau E, Oheim M, Audinat E, Charpak S. Two-photon imaging of capillary blood flow in olfactory bulb glomeruli. Proc Natl Acad Sci U S A. 2003 Oct 28;100(22):13081-6. doi: 10.1073/pnas.2133652100.

Chan Y. Tinnitus: etiology, classification, characteristics, and treatment. Discov Med.2009 Oct;8(42):133-6. PMID: 19833060.

Chang C, Glover GH. Time-frequency dynamics of resting-state brain connectivity measured with fMRI. Neuroimage. 2010 Mar;50(1):81-98. doi: 10.1016/j.neuroimage.2009.12.011.

Chao-Gan Y, Yu-Feng Z. DPARSF: a MATLAB Toolbox for "Pipeline" Data Analysis of Resting-State fMRI. Front Syst Neurosci. 2010 May 14;4:13. doi: 10.3389/fnsys.2010.00013.

Chen GD, Manohar S, Salvi R. Amygdala hyperactivity and tonotopic shift after salicylate exposure. Brain Res. 2012 Nov 16;1485:63-76. doi: 10.1016/j.brainres.2012.03.016.

Chen YC, Xia W, Chen H, Feng Y, Xu JJ, Gu JP, Salvi R, Yin X. Tinnitus distress is linked to enhanced resting-state functional connectivity from the limbic system to the auditory cortex. Hum Brain Mapp. 2017 May;38(5):2384-2397. doi: 10.1002/hbm.23525.

Cieslik EC, Mueller VI, Eickhoff CR, Langner R, Eickhoff SB. Three key regions for supervisory attentional control: evidence from neuroimaging meta-analyses. Neurosci Biobehav Rev. 2015 Jan;48:22-34. doi: 10.1016/j.neubiorev.2014.11.003.

Clark WW, Ohlemiller KK. Anatomy and physiology of hearing for audiologists. Clifton Park, NY: Thomson Delmar Learning, 2008.

Coles RR. Epidemiology of tinnitus: (1) prevalence. J Laryngol Otol Suppl. 1984;9:7-15. doi: 10.1017/s1755146300090041.

Cox SB, Woolsey TA, Rovainen CM. Localized dynamic changes in cortical blood flow with whisker stimulation corresponds to matched vascular and neuronal architecture of rat barrels. J Cereb Blood Flow Metab. 1993 Nov;13(6):899-913. doi: 10.1038/jcbfm.1993.113.

Dallos P. Cochlear amplification, outer hair cells and prestin. Curr Opin Neurobiol. 2008 Aug;18(4):370-6. doi: 10.1016/j.conb.2008.08.016.

Dallos P. Some electrical circuit properties of the organ of Corti. I. Analysis without reactive elements. Hear Res. 1983 Oct;12(1):89-119. doi: 10.1016/0378-5955(83)90120-x.

Dallos P. The Auditory Periphery. Biophysics and Physiology. New York : Academic Press, 1973.

Davis H. A model for transducer action in the cochlea. Cold Spring Harb Symp Quant Biol. 1965;30:181-90. doi: 10.1101/sqb.1965.030.01.020.

De Luca M, Beckmann CF, De Stefano N, Matthews PM, Smith SM. fMRI resting state networks define distinct modes of long-distance interactions in the human brain. Neuroimage. 2006 Feb 15;29(4):1359-67. doi: 10.1016/j.neuroimage.2005.08.035.

De Ridder D, Fransen H, Francois O, Sunaert S, Kovacs S, Van De Heyning P. Amygdalohippocampal Involvement in tinnitus and auditory memory. Acta Otolaryngol Suppl. 2006 Dec;(556):50-3. doi: 10.1080/03655230600895580.

Diesch E, Schummer V, Kramer M, Rupp A. Structural changes of the corpus callosum in tinnitus. Front Syst Neurosci. 2012 Mar 26;6:17. doi: 10.3389/fnsys.2012.00017.

Duong TQ, Yacoub E, Adriany G, Hu X, Ugurbil K, Kim SG. Microvascular BOLD contribution at 4 and 7 T in the human brain: gradient-echo and spin-echo fMRI with suppression of blood effects. Magn Reson Med. 2003 Jun;49(6):1019-27. doi: 10.1002/mrm.10472.

Eggermont JJ, Roberts LE. The neuroscience of tinnitus: understanding abnormal and normal auditory perception. Front Syst Neurosci. 2012 Jul 11;6:53. doi: 10.3389/fnsys.2012.00053.

Eggermont JJ, Roberts LE. The neuroscience of tinnitus. Trends Neurosci. 2004 Nov;27(11):676-82. doi: 10.1016/j.tins.2004.08.010.

Ehret G. The auditory midbrain, a "shunting-yard" of acoustical information processing. In “The Central Auditory System” (G. Ehret, R. Romand, eds.), New York, Oxford University Press, pp. 259-316, 1997.

Erlandsson SI, Holgers KM. The impact of perceived tinnitus severity on health- related quality of life with aspects of gender. Noise Health. 2001;3(10):39-51. PMID: 12689455.

Erulkar SD (1959). The responses of single units of the inferior colliculus of the cat to acoustic stimulation. Proc R Soc Lond B Biol Sci. 1959 Apr 21;150(940):336-55. doi: 10.1098/rspb.1959.0026.

Evans EF, Whitfield IC. Classification of unit responses in the auditory cortex of the unanaesthetized and unrestrained cat. J Physiol. 1964 Jun;171(3):476-93. doi: 10.1113/jphysiol.1964.sp007391.

Fecteau S, Belin P, Joanette Y, Armony JL. Amygdala responses to nonlinguistic emotional vocalizations. Neuroimage. 2007 Jun;36(2):480-7. doi: 10.1016/j.neuroimage.2007.02.043.

Fox MD, Raichle ME. Spontaneous fluctuations in brain activity observed with functional magnetic resonance imaging. Nat Rev Neurosci. 2007 Sep;8(9):700-11. doi: 10.1038/nrn2201.

Fox MD, Snyder AZ, Vincent JL, Corbetta M, Van Essen DC, Raichle ME. The human brain is intrinsically organized into dynamic, anticorrelated functional networks. Proc Natl Acad Sci U S A. 2005 Jul 5;102(27):9673-8. doi: 10.1073/pnas.0504136102.

Frank E, Schecklmann M, Landgrebe M, Burger J, Kreuzer P, Poeppl TB, Kleinjung T, Hajak G, Langguth B. Treatment of chronic tinnitus with repeated sessions of prefrontal transcranial direct current stimulation: outcomes from an open-label pilot study. J Neurol. 2012 Feb;259(2):327-33. doi: 10.1007/s00415-011-6189-4.

Freygang WH Jr, Sokoloff L. Quantitative measurement of regional circulation in the central nervous system by the use of radioactive inert gas. Adv Biol Med Phys. 1958;6:263-79. doi: 10.1016/b978-1-4832-3112-9.50011-6.

Fuster, JM. The prefrontal cortex: Anatomy, physiology and neuropsychology of the frontal lobe. 3rd ed. Philadelphia, Lippincott Williams and Wilkins, 1997.

Gadziola MA, Grimsley JM, Shanbhag SJ, Wenstrup JJ. A novel coding mechanismfor social vocalizations in the lateral amygdala. J Neurophysiol. 2012 Feb;107(4):1047-57. doi: 10.1152/jn.00422.2011.

Galazyuk AV, Wenstrup JJ, Hamid MA. Tinnitus and underlying brain mechanisms. Curr Opin Otolaryngol Head Neck Surg. 2012 Oct;20(5):409-15. doi: 10.1097/MOO.0b013e3283577b81.

Geisler CD. From sound to synapse: Physiology of the mammalian ear. New York, NY: Oxford University Press, 1998.

Gelfand SA. Hearing: An introduction to psychological and physiological acoustics. New York: Marcel Dekker, 2004.

Goelman G, Gordon N, Bonne O. Maximizing negative correlations in resting-state functional connectivity MRI by time-lag. PLoS One. 2014 Nov 14;9(11):e111554. doi: 10.1371/journal.pone.0111554.

Goense J, Merkle H, Logothetis NK. High-resolution fMRI reveals laminar differences in neurovascular coupling between positive and negative BOLD responses. Neuron. 2012 Nov 8;76(3):629-39. doi: 10.1016/j.neuron.2012.09.019.

Goldman-Rakic PS. Circuitry of primate prefrontal cortex and regulation of behavior by representational memory. In F. Plum and V. Mountcastle (Eds.), Handbook of physiology, section 1: The nervous system – Higher functions of the brain, part 1 (Vol. 5, pp. 373-417). Behesda, MD: American Physiological Society, 1987

Gong G, Rosa-Neto P, Carbonell F, Chen ZJ, He Y, Evans AC (2009). Age- and gender- related differences in the cortical anatomical network. J Neurosci. 2009 Dec 16;29(50):15684-93. doi: 10.1523/JNEUROSCI.2308-09.2009.

Greicius MD, Krasnow B, Reiss AL, Menon V (2003). Functional connectivity in the resting brain: a network analysis of the default mode hypothesis. Proc Natl Acad Sci U S A. 2003 Jan 7;100(1):253-8. doi: 10.1073/pnas.0135058100.

Gu JW, Herrmann BS, Levine RA, Melcher JR. Brainstem auditory evoked potentials suggest a role for the ventral cochlear nucleus in tinnitus. J Assoc Res Otolaryngol. 2012 Dec;13(6):819-33. doi: 10.1007/s10162-012-0344-1.

Gur RC, Turetsky BI, Matsui M, Yan M, Bilker W, Hughett P, Gur RE. Sex differences in brain gray and white matter in healthy young adults: correlations with cognitive performance. J Neurosci. 1999 May 15;19(10):4065-72. doi: 10.1523/JNEUROSCI.19-10-04065.1999.

Haag LM, Heba S, Lenz M, Glaubitz B, Höffken O, Kalisch T, Puts NA, Edden RA, Tegenthoff M, Dinse H, Schmidt-Wilcke T. Resting BOLD fluctuations in the primary somatosensory cortex correlate with tactile acuity. Cortex. 2015 Mar;64:20-8. doi: 10.1016/j.cortex.2014.09.018.

Handwerker DA, Roopchansingh V, Gonzalez-Castillo J, Bandettini PA. Periodic changes in fMRI connectivity. Neuroimage. 2012 Nov 15;63(3):1712-9. doi: 10.1016/j.neuroimage.2012.06.078.

Harrison RV, Harel N, Panesar J, Mount RJ. Blood capillary distribution correlates with hemodynamic-based functional imaging in cerebral cortex. Cereb Cortex. 2002 Mar;12(3):225-33. doi: 10.1093/cercor/12.3.225.

Hirsch IJ. The measurement of hearing. New York, NY: McGraw-Hill Book Company, Inc., 1952

Hofmeier B, Wertz J, Refat F, Hinrichs P, Saemisch J, Singer W, Rüttiger L, Klose U, Knipper M, Wolpert S. Functional biomarkers that distinguish between tinnitus with and without hyperacusis. Clin Transl Med. 2021 May;11(5):e378. doi: 10.1002/ctm2.378.

Hofmeier B, Wolpert S, Aldamer ES, Walter M, Thiericke J, Braun C, Zelle D, Rüttiger L, Klose U, Knipper M. Reduced sound-evoked and resting-state BOLD fMRI connectivity in tinnitus. Neuroimage Clin. 2018 Aug 31;20:637-649. doi: 10.1016/j.nicl.2018.08.029.

Hudspeth AJ, Choe Y, Mehta AD, Martin P. Putting ion channels to work: mechanoelectrical transduction, adaptation, and amplification by hair cells. Proc Natl Acad Sci U S A. 2000 Oct 24;97(22):11765-72. doi: 10.1073/pnas.97.22.11765.

Husain FT. Neural networks of tinnitus in humans: Elucidating severity and habituation. Hear Res. 2016 Apr;334:37-48. doi: 10.1016/j.heares.2015.09.010.

Hutchison RM, Womelsdorf T, Gati JS, Everling S, Menon RS. Resting-state networks show dynamic functional connectivity in awake humans and anesthetized macaques. Hum Brain Mapp. 2013 Sep;34(9):2154-77. doi: 10.1002/hbm.22058.

Iadecola C. The Neurovascular Unit Coming of Age: A Journey through Neurovascular Coupling in Health and Disease. Neuron. 2017 Sep 27;96(1):17-42. doi: 10.1016/j.neuron.2017.07.030.

Iadecola C. Regulation of the cerebral microcirculation during neural activity: is nitric oxide the missing link? Trends Neurosci. 1993 Jun;16(6):206-14. doi: 10.1016/0166-2236(93)90156-g.

Iadecola C, Yang G, Ebner TJ, Chen G. Local and propagated vascular responses evoked by focal synaptic activity in cerebellar cortex. J Neurophysiol. 1997 Aug;78(2):651-9. doi: 10.1152/jn.1997.78.2.651.

Jastreboff PJ. Phantom auditory perception (tinnitus): mechanisms of generation and perception. Neurosci Res. 1990 Aug;8(4):221-54. doi: 10.1016/0168-0102(90)90031-9.

Kalcher K, Huf W, Boubela RN, Filzmoser P, Pezawas L, Biswal B, Kasper S, Moser E, Windischberger C. Fully exploratory network independent component analysis of the 1000 functional connectomes database. Front Hum Neurosci. 2012 Nov 6;6:301. doi: 10.3389/fnhum.2012.00301.

Kapolowicz MR, Thompson LT (2020). Plasticity in Limbic Regions at Early Time Points in Experimental Models of Tinnitus. Front Syst Neurosci. 2020 Jan 24;13:88. doi: 10.3389/fnsys.2019.00088.

Keidel WD, Kallert S, Korth M. The Physiological Basis of Hearing: a Review. New York: Thieme-Stratton Corp, 1983.

Kelly C, de Zubicaray G, Di Martino A, Copland DA, Reiss PT, Klein DF, Castellanos FX, Milham MP, McMahon K (2009). L-dopa modulates functional connectivity in striatal cognitive and motor networks: a double-blind placebo-controlled study. J Neurosci. 2009 Jun 3;29(22):7364-78. doi: 10.1523/JNEUROSCI.0810-09.2009.

Kiang NY, Moxon EC, Levine RA. Auditory-nerve activity in cats with normal and abnormal cochleas. In: Sensorineural hearing loss. Ciba Found Symp. 1970:241-73. doi: 10.1002/9780470719756.ch15.

Kilgard MP, Merzenich MM. Plasticity of temporal information processing in the primary auditory cortex. Nat Neurosci. 1998(a) Dec;1(8):727-31. doi: 10.1038/3729.

Kilgard MP, Merzenich MM. Cortical map reorganization enabled by nucleus basalis activity. Science. 1998(b) Mar 13;279(5357):1714-8. doi: 10.1126/science.279.5357.1714.

Kleinjung T, Eichhammer P, Landgrebe M, Sand P, Hajak G, Steffens T, Strutz J, Langguth B. Combined temporal and prefrontal transcranial magnetic stimulation for tinnitus treatment: a pilot study. Otolaryngol Head Neck Surg. 2008 Apr;138(4):497-501. doi: 10.1016/j.otohns.2007.12.022.

Knipper M, Van Dijk P, Nunes I, Rüttiger L, Zimmermann U. Advances in the neurobiology of hearing disorders: recent developments regarding the basis of tinnitus and hyperacusis. Prog Neurobiol. 2013 Dec;111:17-33. doi: 10.1016/j.pneurobio.2013.08.002.

Kolster H, Peeters R, Orban GA. The retinotopic organization of the human middle temporal area MT/V5 and its cortical neighbors. J Neurosci. 2010 Jul 21;30(29):9801-20. doi: 10.1523/JNEUROSCI.2069-10.2010.

Kraus KS, Canlon B. Neuronal connectivity and interactions between the auditory and limbic systems. Effects of noise and tinnitus. Hear Res. 2012 Jun;288(1-2):34-46. doi: 10.1016/j.heares.2012.02.009.

Kraus N, White-Schwoch T. Unraveling the Biology of Auditory Learning: A Cognitive-Sensorimotor-Reward Framework. Trends Cogn Sci. 2015 Nov;19(11):642- 654. doi: 10.1016/j.tics.2015.08.017.

Kujawa SG, Liberman MC. Adding insult to injury: cochlear nerve degeneration after “temporary" noise-induced hearing loss. J Neurosci. 2009 Nov 11;29(45):14077-85. doi: 10.1523/JNEUROSCI.2845-09.2009.

Langers DR, de Kleine E, van Dijk P. Tinnitus does not require macroscopic tonotopic map reorganization. Front Syst Neurosci. 2012 Feb 1;6:2. doi: 10.3389/fnsys.2012.00002.

Langguth B, Schecklmann M, Lehner A, Landgrebe M, Poeppl TB, Kreuzer PM, Schlee W, Weisz N, Vanneste S, De Ridder D. Neuroimaging and neuromodulation: complementary approaches for identifying the neuronal correlates of tinnitus. Front Syst Neurosci. 2012 Apr 9;6:15. doi: 10.3389/fnsys.2012.00015.

Laureys S. The neural correlate of (un)awareness: lessons from the vegetative state. Trends Cogn Sci. 2005 Dec;9(12):556-9. doi: 10.1016/j.tics.2005.10.010.

Leaver AM, Turesky TK, Seydell-Greenwald A, Morgan S, Kim HJ, Rauschecker JP. Intrinsic network activity in tinnitus investigated using functional MRI. Hum Brain Mapp. 2016 Aug;37(8):2717-35. doi: 10.1002/hbm.23204.

Leaver AM, Seydell-Greenwald A, Turesky TK, Morgan S, Kim HJ, Rauschecker JP. Cortico-limbic morphology separates tinnitus from tinnitus distress. Front Syst Neurosci. 2012 Apr 5;6:21. doi: 10.3389/fnsys.2012.00021.

LeDoux J. The amygdala. Curr Biol. 2007 Oct 23;17(20):R868-74. doi: 10.1016/j.cub.2007.08.005.

LeDoux JE, Thompson ME, Iadecola C, Tucker LW, Reis DJ. Local cerebral blood flow increases during auditory and emotional processing in the conscious rat. Science. 1983 Aug 5;221(4610):576-8. doi: 10.1126/science.6867731.

Lee MH, Smyser CD, Shimony JS. Resting-state fMRI: a review of methods and clinical applications. AJNR Am J Neuroradiol. 2013 Oct;34(10):1866-72. doi: 10.3174/ajnr.A3263.

Leitman DI, Wolf DH, Ragland JD, Laukka P, Loughead J, Valdez JN, Javitt DC, Turetsky BI, Gur RC. "It's Not What You Say, But How You Say it": A Reciprocal Temporo-frontal Network for Affective Prosody. Front Hum Neurosci. 2010 Feb 26;4:19. doi: 10.3389/fnhum.2010.00019.

Liu L, Shen P, He T, Chang Y, Shi L, Tao S, Li X, Xun Q, Guo X, Yu Z, Wang J. Noise induced hearing loss impairs spatial learning/memory and hippocampal neurogenesis in mice. Sci Rep. 2016 Feb 4;6:20374. doi: 10.1038/srep20374.

Lockwood AH, Salvi RJ, Burkard RF. Tinnitus. N Engl J Med. 2002 Sep 19;347(12):904-10. doi: 10.1056/NEJMra013395.

Logothesis NK, Pauls J, Augath M, Trinath T, Oeltermann A. Neurophysiological investigation of the basis of the fMRI signal. Nature 412, 150-157. 2001.

Málková L, Gaffan D, Murray EA. Excitotoxic lesions of the amygdala fail to produce impairment in visual learning for auditory secondary reinforcement but interfere with reinforcer devaluation effects in rhesus monkeys. J Neurosci. 1997 Aug 1;17(15):6011-20. doi: 10.1523/JNEUROSCI.17-15-06011.1997.

Malouff JM, Schutte NS, Zucker LA. Tinnitus-related distress: A review of recentfindings. Curr Psychiatry Rep. 2011 Feb;13(1):31-6. doi: 10.1007/s11920-010-0163-1.

Marks KL, Martel DT, Wu C, Basura GJ, Roberts LE, Schvartz-Leyzac KC, Shore SE. Auditory-somatosensory bimodal stimulation desynchronizes brain circuitry to reduce tinnitus in guinea pigs and humans. Sci Transl Med. 2018 Jan 3;10(422):eaal3175. doi: 10.1126/scitranslmed.aal3175.

Marrelec G, Krainik A, Duffau H, Pélégrini-Issac M, Lehéricy S, Doyon J, Benali H. Partial correlation for functional brain interactivity investigation in functional MRI. Neuroimage. 2006 Aug 1;32(1):228-37. doi: 10.1016/j.neuroimage.2005.12.057.

Marsh RA, Fuzessery ZM, Grose CD, Wenstrup JJ. Projection to the inferior colliculus from the basal nucleus of the amygdala. J Neurosci. 2002 Dec 1;22(23):10449-60. doi: 10.1523/JNEUROSCI.22-23-10449.2002.

Maudoux A, Lefebvre P, Cabay JE, Demertzi A, Vanhaudenhuyse A, Laureys S, Soddu A. Auditory resting-state network connectivity in tinnitus: a functional MRI study. PLoS One. 2012;7(5):e36222. doi: 10.1371/journal.pone.0036222.

McKlveen JM, Morano RL, Fitzgerald M, Zoubovsky S, Cassella SN, Scheimann JR, Ghosal S, Mahbod P, Packard BA, Myers B, Baccei ML, Herman JP. Chronic Stress Increases Prefrontal Inhibition: A Mechanism for Stress-Induced Prefrontal Dysfunction. Biol Psychiatry. 2016 Nov 15;80(10):754-764. doi: 10.1016/j.biopsych.2016.03.2101.

McCormack A, Edmondson-Jones M, Somerset S, Hall D. A systematic review of the reporting of tinnitus prevalence and severity. Hear Res. 2016 Jul;337:70-9. doi: 10.1016/j.heares.2016.05.009.

Menon RS, Ogawa S, Tank DW, Uğurbil K. Tesla gradient recalled echo characteristics of photic stimulation-induced signal changes in the human primary visual cortex. Magn Reson Med. 1993 Sep;30(3):380-6. doi: 10.1002/mrm.1910300317.

Middleton JW, Tzounopoulos T. Imaging the neural correlates of tinnitus: a comparison between animal models and human studies. Front Syst Neurosci. 2012 May 4;6:35. doi: 10.3389/fnsys.2012.00035.

Miller EK, Cohen JD. An integrative theory of prefrontal cortex function. Annu Rev Neurosci. 2001;24:167-202. doi: 10.1146/annurev.neuro.24.1.167.

Mirz F, Gjedde A, Sødkilde-Jrgensen H, Pedersen CB. Functional brain imaging of tinnitus-like perception induced by aversive auditory stimuli. Neuroreport. 2000 Feb 28;11(3):633-7. doi: 10.1097/00001756-200002280-00039.

Møller AR. Hearing: Its physiology and pathophysiology. New York, NY: Academic Press, 2000.

Moore BCJ. An introduction to the psychology of hearing. 6th ed. Leiden, the Netherladns: Brill, 2013.

Moore JK. Organization of the human superior olivary complex. Microsc Res Tech. 2000 Nov 15;51(4):403-12. doi: 10.1002/1097-0029(20001115)51:4<403:AID-JEMT8>3.0.CO;2-Q.

Morest DK, Oliver DL. The neuronal architecture of the inferior colliculus in the cat: defining the functional anatomy of the auditory midbrain. J Comp Neurol. 1984 Jan 10;222(2):209-36. doi: 10.1002/cne.902220206.

Morest DK. The laminar structure of the medial geniculate body of the cat. J Anat. 1965 Jan;99(Pt 1):143-60. PMID: 14245341.

Mulders WH, Robertson D (2013). Development of hyperactivity after acoustic trauma in the guinea pig inferior colliculus. Hear Res. 2013 Apr;298:104-8. doi: 10.1016/j.heares.2012.12.008.

Musiek FE. Neuroanatomy, neurophysiology, and central auditory assessment. Part II: The cerebrum. Ear Hear. 1986 Oct;7(5) 283-294. doi:10.1097/00003446-198610000-00001.

Musiek FE and Baran JA. The auditory system: Anatomy, physiology, and clinical correlates. 2nd ed. San Diego: Plural Publishing, 2020.

Nondahl DM, Cruickshanks KJ, Dalton DS, Klein BE, Klein R, Schubert CR, Tweed TS, Wiley TL. The impact of tinnitus on quality of life in older adults. J Am Acad Audiol. 2007 Mar;18(3):257-66. doi: 10.3766/jaaa.18.3.7.

Noreña AJ. Revisiting the cochlear and central mechanisms of tinnitus and therapeutic approaches. Audiol Neurootol. 2015;20 Suppl 1:53-9. doi: 10.1159/000380749.

Noreña AJ, Eggermont JJ. Enriched acoustic environment after noise trauma abolishes neural signs of tinnitus. Neuroreport. 2006 Apr 24;17(6):559-63. doi: 10.1097/00001756-200604240-00001.

O'Herron P, Chhatbar PY, Levy M, Shen Z, Schramm AE, Lu Z, Kara P. Neural correlates of single-vessel haemodynamic responses in vivo. Nature. 2016 Jun 16;534(7607):378-82. doi: 10.1038/nature17965.

O'Sullivan M, Jones DK, Summers PE, Morris RG, Williams SC, Markus HS. Evidence for cortical "disconnection" as a mechanism of age-related cognitive decline. Neurology. 2001 Aug 28;57(4):632-8. doi: 10.1212/wnl.57.4.632.

Ogawa S, Menon RS, Tank DW, Kim SG, Merkle H, Ellermann JM, Ugurbil K. Functional brain mapping by blood oxygenation level-dependent contrast magnetic resonance imaging. A comparison of signal characteristics with a biophysical model. Biophys J. 1993 Mar;64(3):803-12. doi: 10.1016/S0006-3495(93)81441-3.

Peterson DC, Voytenko S, Gans D, Galazyuk A, Wenstrup J. Intracellular recordings from combination-sensitive neurons in the inferior colliculus. J Neurophysiol. 2008 Aug;100(2):629-45. doi: 10.1152/jn.90390.2008.

Pickles JO. An introduction to the physiology of hearing. 2nd ed. London, UK: Elsevier Science Publishing Co Inc, 1989.

Pijnenburg R, Scholtens LH, Mantini D, Vanduffel W, Barrett LF, van den Heuvel MP. Biological Characteristics of Connection-Wise Resting-State Functional Connectivity Strength. Cereb Cortex. 2019 Dec 17;29(11):4646-4653. doi: 10.1093/cercor/bhy342.

Pitkänen A, Jolkkonen E, Kemppainen S . Anatomic heterogeneity of the rat amygdaloid complex. Folia Morphol (Warsz). 2000;59(1):1-23. PMID: 10774087.

Pollmann S, Lepsien J, Hugdahl K, von Cramon DY. Auditory target detection in dichotic listening involves the orbitofrontal and hippocampal paralimbic belts. Cereb Cortex. 2004 Aug;14(8):903-13. doi: 10.1093/cercor/bhh049.

Popelár J, Syka J. Response properties of neurons in the inferior colliculus of the guinea-pig. Acta Neurobiol Exp (Wars). 1982;42(4-5):299-310. PMID: 7184324.

Rasgon A, Lee WH, Leibu E, Laird A, Glahn D, Goodman W, Frangou S. Neural correlates of affective and non-affective cognition in obsessive compulsive disorder: A meta-analysis of functional imaging studies. Eur Psychiatry. 2017 Oct;46:25-32. doi: 10.1016/j.eurpsy.2017.08.001.

Roberts LE, Husain FT, Eggermont JJ (2013). Role of attention in the generation and modulation of tinnitus. Neurosci Biobehav Rev. 2013 Sep;37(8):1754-73. doi: 10.1016/j.neubiorev.2013.07.007.

Roberts LE, Eggermont JJ, Caspary DM, Shore SE, Melcher JR, Kaltenbach JA (2010). Ringing ears: the neuroscience of tinnitus. J Neurosci. 2010 Nov 10;30(45):14972-9. doi: 10.1523/JNEUROSCI.4028-10.2010.

Rodgers KM, Benison AM, Klein A, Barth DS. Auditory, somatosensory, and multisensory insular cortex in the rat. Cereb Cortex. 2008 Dec;18(12):2941-51. doi: 10.1093/cercor/bhn054.

Romand R, Avan P. Anatomical and functional aspects of the cochlear nucleus. In “The Central Auditory System”, Ehret G, Romand R. New York, Oxford: Oxford University Press, 1997.

Rüttiger L, Singer W, Panford-Walsh R, Matsumoto M, Lee SC, Zuccotti A, Zimmermann U, Jaumann M, Rohbock K, Xiong H, Knipper M. The reduced cochlear output and the failure to adapt the central auditory response causes tinnitus in noise exposed rats. PLoS One. 2013;8(3):e57247. doi: 10.1371/journal.pone.0057247.

Sadaghiani S, Hesselmann G, Kleinschmidt A. Distributed and antagonistic contributions of ongoing activity fluctuations to auditory stimulus detection. J Neurosci. 2009 Oct 21;29(42):13410-7. doi: 10.1523/JNEUROSCI.2592-09.2009.

Sah P, Faber ES, Lopez De Armentia M, Power J. The amygdaloid complex: anatomy and physiology. Physiol Rev. 2003 Jul;83(3):803-34. doi: 10.1152/physrev.00002.2003.

Sahley TL, Musiek FE. Basic Fundamentals in Hearing Science. San Diego: Plural publishing Inc, 2016

Salvi RJ, Clock Eddins, AC, Wang J. Cochlear physiology II: Mostly electrophysiology. In “The auditory system: Anatomy, physiology, and clinical correlates” .2nd ed. Musiek FE, Baran JA. Boston. San Diego: Plural Publishing, 2020.

Sanchez Jimenez JG, De Jesus O. Hypothalamic Dysfunction. 2021 Dec 24. In: StatPearls (Internet). Treasure Island (FL): StatPearls Publishing; 2022 Jan-. PMID: 32809578.

Sand PG, Langguth B, Itzhacki J, Bauer A, Geis S, Cárdenas-Conejo ZE, Pimentel V, Kleinjung T. Resequencing of the auxiliary GABA(B) receptor subunit gene KCTD12 in chronic tinnitus. Front Syst Neurosci. 2012 May 25;6:41. doi: 10.3389/fnsys.2012.00041.

Sander D, Grandjean D, Pourtois G, Schwartz S, Seghier ML, Scherer KR, Vuilleumier P. Emotion and attention interactions in social cognition: brain regions involved in processing anger prosody. Neuroimage. 2005 Dec;28(4):848-58. doi: 10.1016/j.neuroimage.2005.06.023.

Saunders JC. The role of central nervous system plasticity in tinnitus. J Commun Disord. 2007 Jul-Aug;40(4):313-34. doi: 10.1016/j.jcomdis.2007.03.006.

Schaette R, Kempter R. Computational models of neurophysiological correlates of tinnitus. Front Syst Neurosci. 2012 May 8;6:34. doi: 10.3389/fnsys.2012.00034.

Schaette R, McAlpine D. Tinnitus with a normal audiogram: physiological evidence for hidden hearing loss and computational model. J Neurosci. 2011 Sep 21;31(38):13452-7. doi: 10.1523/JNEUROSCI.2156-11.2011.

Schwartz IR (1992). Superior olivary complex in the lateral lemniscal nuclei. In Webster DB, Popper AN, and Fey RR (Eds.), The cochlea, (pp. 117-167). New York, NY: Springer-Verlag.

Sedley W, Friston KJ, Gander PE, Kumar S, Griffiths TD (2016). An Integrative Tinnitus Model Based on Sensory Precision. Trends Neurosci. 2016 Dec;39(12):799-812. doi: 10.1016/j.tins.2016.10.004.

Shimamura AP (1995). Memory and frontal lobe function. In M.S. Gazzaniga (Ed.), The cognitive neurosciences (pp. 803-813). Cambridge, MA: MIT Press.

Singer W, Zuccotti A, Jaumann M, Lee SC, Panford-Walsh R, Xiong H, Zimmermann U, Franz C, Geisler HS, Köpschall I, Rohbock K, Varakina K, Verpoorten S, Reinbothe T, Schimmang T, Rüttiger L, Knipper M. Noise-induced inner hair cell ribbon loss disturbs central arc mobilization: a novel molecular paradigm for understanding tinnitus. Mol Neurobiol. 2013 Feb;47(1):261-79. doi: 10.1007/s12035-012-8372-8.

Smith SM, Beckmann CF, Andersson J, Auerbach EJ, Bijsterbosch J, Douaud G, Duff E, Feinberg DA, Griffanti L, Harms MP, Kelly M, Laumann T, Miller KL, Moeller S, Petersen S, Power J, Salimi-Khorshidi G, Snyder AZ, Vu AT, Woolrich MW, Xu J, Yacoub E, Uğurbil K, Van Essen DC, Glasser MF; WU-Minn HCP Consortium (2013). Resting-state fMRI in the Human Connectome Project. Neuroimage. 2013 Oct 15;80:144-68. doi: 10.1016/j.neuroimage.2013.05.039.

Smith SM, Miller KL, Moeller S, Xu J, Auerbach EJ, Woolrich MW, Beckmann CF, Jenkinson M, Andersson J, Glasser MF, Van Essen DC, Feinberg DA, Yacoub ES, Ugurbil K (2012). Temporally-independent functional modes of spontaneous brain activity. Proc Natl Acad Sci U S A. 2012 Feb 21;109(8):3131-6. doi: 10.1073/pnas.1121329109.

Smith SM, Fox PT, Miller KL, Glahn DC, Fox PM, Mackay CE, Filippini N, Watkins KE, Toro R, Laird AR, Beckmann CF (2009). Correspondence of the brain's functional architecture during activation and rest. Proc Natl Acad Sci U S A. 2009 Aug 4;106(31):13040-5. doi: 10.1073/pnas.0905267106.

Sowell ER, Peterson BS, Kan E, Woods RP, Yoshii J, Bansal R, Xu D, Zhu H, Thompson PM, Toga AW. Sex differences in cortical thickness mapped in 176 healthy individuals between 7 and 87 years of age. Cereb Cortex. 2007 Jul;17(7):1550-60. doi: 10.1093/cercor/bhl066.

Sokoloff, L. Circulation in the central nervous system. Windhorst, U., editor. Springer Science & Business Media; Berlin, Heidelberg: 2013 p. 561-578.

Spoendlin H. Innervation densities of the cochlea. Acta Otolaryngol. 1972 Feb-Mar;73(2):235-48. doi: 10.3109/00016487209138937.

Sporns O, Tononi G, Kötter R. The human connectome: A structural description of the human brain. PLoS Comput Biol. 2005 Sep;1(4):e42. doi: 10.1371/journal.pcbi.0010042.

Stolzberg D, Salvi RJ, Allman BL. Salicylate toxicity model of tinnitus. Front Syst Neurosci. 2012 Apr 20;6:28. doi: 10.3389/fnsys.2012.00028.

Streitfeld BD. The fiber connections of the temporal lobe with emphasis on the rhesus monkey. Int J Neurosci. 1980;11(1):51-71. doi: 10.3109/00207458009147579.

Stuss DT, Benson DF (1996). Book reviwes: The frontal lobes. New York: Raven Press, 1987.

Sullivan RM, Gratton A. Prefrontal cortical regulation of hypothalamic-pituitary-adrenal function in the rat and implications for psychopathology: side matters. Psychoneuroendocrinology. 2002 Jan-Feb;27(1-2):99-114. doi: 10.1016/s0306-4530(01)00038-5.

Tae WS, Yakunina N, Lee WH, Ryu YJ, Ham HK, Pyun SB, Nam EC. Changes in the regional shape and volume of subcortical nuclei in patients with tinnitus comorbid with mild hearing loss. Neuroradiology. 2018 Nov;60(11):1203-1211. doi: 10.1007/s00234-018-2093-2.

Tagliazucchi E, von Wegner F, Morzelewski A, Brodbeck V, Laufs H. Dynamic BOLD functional connectivity in humans and its electrophysiological correlates. Front Hum Neurosci. 2012(a) Dec 28;6:339. doi: 10.3389/fnhum.2012.00339.

Tagliazucchi E, Balenzuela P, Fraiman D, Chialvo DR. Criticality in large-scale brain FMRI dynamics unveiled by a novel point process analysis. Front Physiol. 2012(b) Feb 8;3:15. doi: 10.3389/fphys.2012.00015.

Tagliazucchi E, Balenzuela P, Fraiman D, Montoya P, Chialvo DR. Spontaneous BOLD event triggered averages for estimating functional connectivity at resting state. Neurosci Lett. 2011 Jan 20;488(2):158-63. doi: 10.1016/j.neulet.2010.11.020.

Ternaux JP. "Neuronal Arborization." Branching in Nature: Dynamics and Morphogenesis of Branching Structures, from Cell to River Networks. Springer Berlin Heidelberg, 2001.

Tomasi D, Volkow ND (2011). Gender differences in brain functional connectivity density. Hum Brain Mapp. 2012 Apr;33(4):849-60. doi: 10.1002/hbm.21252.

Uludağ K, Müller-Bierl B, Uğurbil K (2009). An integrative model for neuronal activity- induced signal changes for gradient and spin echo functional imaging. Neuroimage. 2009 Oct 15;48(1):150-65. doi: 10.1016/j.neuroimage.2009.05.051.

Van Essen DC, Ugurbil K. The future of the human connectome. Neuroimage. 2012 Aug 15;62(2):1299-310. doi: 10.1016/j.neuroimage.2012.01.032.

Vanneste S, De Ridder D. The auditory and non-auditory brain areas involved in tinnitus. An emergent property of multiple parallel overlapping subnetworks. Front Syst Neurosci. 2012 May 8;6:31. doi: 10.3389/fnsys.2012.00031.

Vanneste S, Joos K, De Ridder D. Prefrontal cortex based sex differences in tinnitus perception: same tinnitus intensity, same tinnitus distress, different mood. PLoS One. 2012;7(2):e31182. doi: 10.1371/journal.pone.0031182.

Vanneste S, van de Heyning P, De Ridder D. The neural network of phantom sound changes over time: a comparison between recent-onset and chronic tinnitus patients. Eur J Neurosci. 2011 Sep;34(5):718-31. doi: 10.1111/j.1460-9568.2011.07793.x.

Vanneste S, Plazier M, der Loo Ev, de Heyning PV, Congedo M, De Ridder D. The neural correlates of tinnitus-related distress. Neuroimage. 2010 Aug 15;52(2):470-80. doi: 10.1016/j.neuroimage.2010.04.029.

Vaughan JT, Adriany G, Garwood M, Yacoub E, Duong T, DelaBarre L, Andersen P, Ugurbil K. Detunable transverse electromagnetic (TEM) volume coil for high-field NMR. Magn Reson Med. 2002 May;47(5):990-1000. doi: 10.1002/mrm.10141.

Wagner AD. Cognitive control and episodic memory: Contributions from prefrontal cortex. In LR Squire, DL Schacter (Eds.), Neuropsychology of memory (3rd ed., pp. 174-192). New York: Guildford.

Wangemann P. K+ cycling and the endocochlear potential. Hear Res. 2002 Mar;165(1-2):1-9. doi: 10.1016/s0378-5955(02)00279-4.

Weinberger NM. New perspectives on the auditory cortex: learning and memory. Handb Clin Neurol. 2015;129:117-47. doi: 10.1016/B978-0-444-62630-1.00007-X.

Wienbruch C, Paul I, Weisz N, Elbert T, Roberts LE. Frequency organization of the 40-Hz auditory steady-state response in normal hearing and in tinnitus. Neuroimage. 2006 Oct 15;33(1):180-94. doi: 10.1016/j.neuroimage.2006.06.023.

Wiethoff S, Wildgruber D, Grodd W, Ethofer T. Response and habituation of the amygdala during processing of emotional prosody. Neuroreport. 2009 Oct 7;20(15):1356-60. doi: 10.1097/WNR.0b013e328330eb83.

Winer JA. The functional architecture of the medial geniculate body and the primary auditory cortex. In “The mammalian auditory pathway: Neuroanatomy”, Webster DB, Popper AN, Fay RR. Springer, New York, NY, 1992. 222-409.

Woolnough O, Forseth KJ, Rollo PS, Tandon N. Uncovering the functional anatomy of the human insula during speech. Elife. 2019 Dec 19;8:e53086. doi: 10.7554/eLife.53086.

Yacoub E, Van De Moortele PF, Shmuel A, Uğurbil K. Signal and noisecharacteristics of Hahn SE and GE BOLD fMRI at 7 T in humans. Neuroimage. 2005 Feb 1;24(3):738-50. doi: 10.1016/j.neuroimage.2004.09.002.

Yang S, Bao S. Homeostatic mechanisms and treatment of tinnitus. Restor Neurol Neurosci. 2013;31(2):99-108. doi: 10.3233/RNN-120248.

Yang S, Weiner BD, Zhang LS, Cho SJ, Bao S. Homeostatic plasticity drives tinnitus perception in an animal model. Proc Natl Acad Sci U S A. 2011 Sep 6;108(36):14974-9. doi: 10.1073/pnas.1107998108.

Yoo HB, De Ridder D, Vanneste S. The Importance of Aging in Gray Matter Changes Within Tinnitus Patients Shown in Cortical Thickness, Surface Area and Volume. Brain Topogr. 2016 Nov;29(6):885-896. doi: 10.1007/s10548-016-0511-5.

Zaitsev M, Hennig J, Speck O. "Automated online EPI distortion correction for fMRI applications." Proceedings of the 11th annual meeting of the International Society for Magnetic Resonance in Medicine. Vol. 1042, 2003.

Zeng FG. An active loudness model suggesting tinnitus as increased central noise and hyperacusis as increased nonlinear gain. Hear Res. 2013 Jan;295:172-9. doi: 10.1016/j.heares.2012.05.009.

Zhang JS, Kaltenbach JA, Wang J, Kim SA. Fos-like immunoreactivity in auditory and nonauditory brain structures of hamsters previously exposed to intense sound. Exp Brain Res. 2003 Dec;153(4):655-60. doi: 10.1007/s00221-003-1612-4.

7 Appendix

7.1 Time course correlation matrix for auditory pathway regions

Mean values of Pearson correlation coefficients for each significant connectivity ($p < 0,05$). To provide a clearer overview, non-significant correlations have been intentionally omitted.

CN-R/SOC-R	0,687
CN-R/IC-R	0,094
CN-R/MGB-R	-0,063
CN-R/BA41-R	-0,043
CN-R/BA42-R	-0,041
CN-R/BA22A-R	-0,06
CN-R/BA22P-R	-0,012
CN-R/BA21P-R	-0,045
CN-R/BA21A-R	-0,018
CN-R/Hipp-R	0,129
CN-R/BA13P-R	-0,068
CN-R/BA13P-L	-0,079
CN-R/Hipp-L	0,138
CN-R/BA21A-L	-0,028
CN-R/BA21P-L	-0,035
CN-R/BA22P-L	-0,089
CN-R/BA22A-L	-0,061
CN-R/BA42-L	-0,066
CN-R/BA41-L	-0,088
CN-R/MGB-L	-0,027
CN-R/IC-L	0,173
CN-R/SOC-L	0,311
CN-R/CN-L	0,419
SOC-R/IC-R	0,096
SOC-R/MGB-R	-0,044
SOC-R/BA41-R	-0,029
SOC-R/BA42-R	-0,006
SOC-R/BA22A-R	-0,06
SOC-R/BA22P-R	-0,009
SOC-R/BA21P-R	-0,044
SOC-R/BA21A-R	-0,013
SOC-R/Hipp-R	0,084
SOC-R/BA13P-R	-0,054
SOC-R/BA13P-L	-0,061
SOC-R/Hipp-L	0,11

SOC-R/BA21A-L	-0,072
SOC-R/BA21P-L	-0,046
SOC-R/BA22P-L	-0,052
SOC-R/BA22A-L	-0,035
SOC-R/BA42-L	-0,081
SOC-R/BA41-L	-0,058
SOC-R/MGB-L	-0,039
SOC-R/IC-L	0,175
SOC-R/SOC-L	0,373
SOC-R/CN-L	0,422
IC-R/MGB-R	0,05
IC-R/BA41-R	-0,054
IC-R/BA42-R	-0,097
IC-R/BA22A-R	-0,03
IC-R/BA22P-R	-0,041
IC-R/BA21P-R	-0,053
IC-R/BA21A-R	-0,037
IC-R/Hipp-R	0,101
IC-R/BA13P-R	-0,068
IC-R/BA13P-L	-0,042
IC-R/Hipp-L	0,104
IC-R/BA21A-L	0,014
IC-R/BA21P-L	0,015
IC-R/BA22P-L	-0,041
IC-R/BA22A-L	-0,055
IC-R/BA42-L	-0,049
IC-R/BA41-L	-0,056
IC-R/MGB-L	0,047
IC-R/IC-L	0,419
IC-R/SOC-L	0,107
IC-R/CN-L	0,13
MGB-R/BA41-R	0,088
MGB-R/BA42-R	0,086
MGB-R/BA22A-R	0,033
MGB-R/BA22P-R	0,016
MGB-R/BA21P-R	0,017
MGB-R/BA21A-R	0,022
MGB-R/Hipp-R	-0,022
MGB-R/BA13P-R	0,144
MGB-R/BA13P-L	0,174
MGB-R/Hipp-L	-0,028
MGB-R/BA21A-L	0,037
MGB-R/BA21P-L	-0,01

MGB-R/BA22P-L	-0,01
MGB-R/BA22A-L	0,05
MGB-R/BA42-L	0,035
MGB-R/BA41-L	0,102
MGB-R/MGB-L	0,437
MGB-R/IC-L	0,027
MGB-R/SOC-L	-0,058
MGB-R/CN-L	-0,046
BA41-R/BA42-R	0,429
BA41-R/BA22A-R	0,222
BA41-R/BA22P-R	0,201
BA41-R/BA21P-R	0,029
BA41-R/BA21A-R	0,162
BA41-R/Hipp-R	-0,027
BA41-R/BA13P-R	0,211
BA41-R/BA13P-L	0,228
BA41-R/Hipp-L	-0,034
BA41-R/BA21A-L	0,028
BA41-R/BA21P-L	0,002
BA41-R/BA22P-L	0,119
BA41-R/BA22A-L	0,195
BA41-R/BA42-L	0,209
BA41-R/BA41-L	0,281
BA41-R/MGB-L	0,044
BA41-R/IC-L	-0,033
BA41-R/SOC-L	-0,034
BA41-R/CN-L	-0,037
BA42-R/BA22A-R	0,334
BA42-R/BA22P-R	0,436
BA42-R/BA21P-R	0,154
BA42-R/BA21A-R	0,274
BA42-R/Hipp-R	-0,155
BA42-R/BA13P-R	0,207
BA42-R/BA13P-L	0,268
BA42-R/Hipp-L	-0,132
BA42-R/BA21A-L	0,088
BA42-R/BA21P-L	0,067
BA42-R/BA22P-L	0,189
BA42-R/BA22A-L	0,288
BA42-R/BA42-L	0,326
BA42-R/BA41-L	0,327
BA42-R/MGB-L	0,022
BA42-R/IC-L	-0,046

BA42-R/SOC-L	-0,046
BA42-R/CN-L	-0,071
BA22A-R/BA22P-R	0,252
BA22A-R/BA21P-R	0,149
BA22A-R/BA21A-R	0,281
BA22A-R/Hipp-R	-0,028
BA22A-R/BA13P-R	0,118
BA22A-R/BA13P-L	0,206
BA22A-R/Hipp-L	-0,078
BA22A-R/BA21A-L	0,114
BA22A-R/BA21P-L	0,07
BA22A-R/BA22P-L	0,137
BA22A-R/BA22A-L	0,287
BA22A-R/BA42-L	0,228
BA22A-R/BA41-L	0,265
BA22A-R/MGB-L	-0,039
BA22A-R/IC-L	0,017
BA22A-R/SOC-L	-0,086
BA22A-R/CN-L	-0,094
BA22P-R/BA21P-R	0,47
BA22P-R/BA21A-R	0,334
BA22P-R/Hipp-R	-0,081
BA22P-R/BA13P-R	0,024
BA22P-R/BA13P-L	0,087
BA22P-R/Hipp-L	-0,11
BA22P-R/BA21A-L	0,181
BA22P-R/BA21P-L	0,236
BA22P-R/BA22P-L	0,244
BA22P-R/BA22A-L	0,226
BA22P-R/BA42-L	0,162
BA22P-R/BA41-L	0,122
BA22P-R/MGB-L	-0,03
BA22P-R/IC-L	-0,046
BA22P-R/SOC-L	-0,055
BA22P-R/CN-L	-0,065
BA21P-R/BA21A-R	0,475
BA21P-R/Hipp-R	-0,031
BA21P-R/BA13P-R	-0,063
BA21P-R/BA13P-L	-0,045
BA21P-R/Hipp-L	-0,114
BA21P-R/BA21A-L	0,128
BA21P-R/BA21P-L	0,261
BA21P-R/BA22P-L	0,21

BA21P-R/BA22A-L	0,136
BA21P-R/BA42-L	0,046
BA21P-R/BA41-L	0,045
BA21P-R/MGB-L	0,017
BA21P-R/IC-L	-0,036
BA21P-R/SOC-L	-0,081
BA21P-R/CN-L	-0,077
BA21A-R/Hipp-R	-0,016
BA21A-R/BA13P-R	0,045
BA21A-R/BA13P-L	0,065
BA21A-R/Hipp-L	-0,012
BA21A-R/BA21A-L	0,182
BA21A-R/BA21P-L	0,198
BA21A-R/BA22P-L	0,209
BA21A-R/BA22A-L	0,28
BA21A-R/BA42-L	0,132
BA21A-R/BA41-L	0,117
BA21A-R/MGB-L	-4E-04
BA21A-R/IC-L	-0,048
BA21A-R/SOC-L	-0,055
BA21A-R/CN-L	-0,056
Hipp-R/BA13P-R	-0,042
Hipp-R/BA13P-L	-0,043
Hipp-R/Hipp-L	0,37
Hipp-R/BA21A-L	-8E-04
Hipp-R/BA21P-L	0,002
Hipp-R/BA22P-L	-0,046
Hipp-R/BA22A-L	-0,008
Hipp-R/BA42-L	-0,039
Hipp-R/BA41-L	-0,064
Hipp-R/MGB-L	-0,043
Hipp-R/IC-L	0,105
Hipp-R/SOC-L	0,072
Hipp-R/CN-L	0,103
BA13P-R/BA13P-L	0,458
BA13P-R/Hipp-L	-0,085
BA13P-R/BA21A-L	0,066
BA13P-R/BA21P-L	0,007
BA13P-R/BA22P-L	0,041
BA13P-R/BA22A-L	0,19
BA13P-R/BA42-L	0,179
BA13P-R/BA41-L	0,224
BA13P-R/MGB-L	0,103

BA13P-R/IC-L	-0,077
BA13P-R/SOC-L	-0,086
BA13P-R/CN-L	-0,121
BA13P-L/Hipp-L	-0,032
BA13P-L/BA21A-L	0,024
BA13P-L/BA21P-L	0,018
BA13P-L/BA22P-L	0,121
BA13P-L/BA22A-L	0,206
BA13P-L/BA42-L	0,223
BA13P-L/BA41-L	0,304
BA13P-L/MGB-L	0,142
BA13P-L/IC-L	-0,024
BA13P-L/SOC-L	-0,122
BA13P-L/CN-L	-0,161
Hipp-L/BA21A-L	-0,02
Hipp-L/BA21P-L	-0,051
Hipp-L/BA22P-L	-0,102
Hipp-L/BA22A-L	-0,028
Hipp-L/BA42-L	-0,069
Hipp-L/BA41-L	-0,117
Hipp-L/MGB-L	-0,045
Hipp-L/IC-L	0,052
Hipp-L/SOC-L	0,075
Hipp-L/CN-L	0,091
BA21A-L/BA21P-L	0,378
BA21A-L/BA22P-L	0,208
BA21A-L/BA22A-L	0,187
BA21A-L/BA42-L	0,142
BA21A-L/BA41-L	0,031
BA21A-L/MGB-L	0,007
BA21A-L/IC-L	-0,05
BA21A-L/SOC-L	-0,093
BA21A-L/CN-L	-0,083
BA21P-L/BA22P-L	0,282
BA21P-L/BA22A-L	0,167
BA21P-L/BA42-L	0,082
BA21P-L/BA41-L	-0,048
BA21P-L/MGB-L	0,013
BA21P-L/IC-L	-0,031
BA21P-L/SOC-L	-0,003
BA21P-L/CN-L	-0,017
BA22P-L/BA22A-L	0,158
BA22P-L/BA42-L	0,414

BA22P-L/BA41-L	0,186
BA22P-L/MGB-L	-0,031
BA22P-L/IC-L	-0,038
BA22P-L/SOC-L	-0,063
BA22P-L/CN-L	-0,086
BA22A-L/BA42-L	0,298
BA22A-L/BA41-L	0,257
BA22A-L/MGB-L	0,002
BA22A-L/IC-L	-0,041
BA22A-L/SOC-L	-0,035
BA22A-L/CN-L	-0,067
BA42-L/BA41-L	0,396
BA42-L/MGB-L	0,017
BA42-L/IC-L	-0,037
BA42-L/SOC-L	-0,094
BA42-L/CN-L	-0,123
BA41-L/MGB-L	0,11
BA41-L/IC-L	-0,039
BA41-L/SOC-L	-0,127
BA41-L/CN-L	-0,151
MGB-L/IC-L	0,052
MGB-L/SOC-L	0,015
MGB-L/CN-L	-0,014
IC-L/SOC-L	0,145
IC-L/CN-L	0,206
SOC-L/CN-L	0,765

7.2 Time course correlation matrix for auditory-limbic regions

Mean values of Pearson correlation coefficients for each significant connectivity ($p < 0,05$). To provide a clearer overview, non-significant correlations have been intentionally omitted.

MGB-R/Amyg-L	0,089
BA22A-R/Amyg-R	0,177
BA22A-R/Amyg-L	0,151
BA21P-R/BA13A-R	-0,148
Amyg-R/BA28-R	0,414
Amyg-R/BA28-L	0,31
Amyg-R/Amyg-L	0,385
Amyg-R/BA22A-L	0,127
Amyg-R/BA42-L	0,133
BA28-R/BA28-L	0,287

BA28-R/Amyg-L	0,238
BA28-R/IC-L	0,175
BA13A-R/BA13A-L	0,426
BA13A-R/BA21P-L	-0,123
BA13A-R/BA42-L	0,165
BA13A-R/BA41-L	0,112
BA13A-L/Amyg-L	0,098
BA13A-L/BA21P-L	-0,156
BA13A-L/BA42-L	0,138
BA28-L/Amyg-L	0,55
BA28-L/BA21A-L	0,11
Amyg-L/BA21A-L	0,093
Amyg-L/BA22A-L	0,135
Amyg-L/BA41-L	0,09

7.3 Time course correlation matrix for temporofrontal attentional regions

Mean values of Pearson correlation coefficients for each significant connectivity ($p < 0,05$).

To provide a clearer overview, non-significant correlations have been intentionally omitted.

IC-R/BA45-R	-0,073
BA22P-R/BA46-L	-0,144
BA21P-R/BA9M-R	0,198
BA21P-R/BA9M-L	0,215
BA21P-R/BA46-L	-0,112
BA21A-R/BA45-R	0,057
BA21A-R/BA46-R	-0,12
BA45-R/BA46-R	0,131
BA45-R/BA9DL-R	0,212
BA45-R/BA9M-L	0,157
BA45-R/BA9DL-L	0,156
BA45-R/BA45-L	0,229
BA46-R/BA9DL-R	0,302
BA46-R/BA9M-L	-0,168
BA46-R/BA9DL-L	0,186
BA46-R/BA46-L	0,33
BA47-R/BA47-L	0,189
BA47-R/BA21P-L	-0,089
BA9DL-R/BA9DL-L	0,328
BA9M-R/BA9M-L	0,571
BA9M-R/BA46-L	-0,162
BA9M-R/BA21A-L	0,134

BA9M-R/BA21P-L	0,176
BA9M-L/BA21A-L	0,116
BA9M-L/BA21P-L	0,169
BA9DL-L/BA46-L	0,15
BA9DL-L/BA45-L	0,231
BA47-L/BA45-L	0,128

8 Declaration of Own Contribution

The work was carried out at the University Clinic for Otolaryngology in Tübingen, under the supervision of Prof. Dr. Marlies Knipper, Hearing, Cognition, and Tinnitus Research Group. The study was developed in collaboration with Prof. Dr. Uwe Klose, Diagnostic and Interventional Neuroradiology, MR Research Division, University Clinic Tübingen. The statistical analysis was independently conducted by me. I assure that I have written the manuscript independently, following guidance from Prof. Dr. Marlies Knipper and Prof. Dr. Uwe Klose, and that I have not used any sources other than those cited by me.

Tübingen, May 19, 2024

Giulio Mendola

9 Acknowledgments

I would like to express my deepest gratitude to my professors for their invaluable guidance and support throughout the course of my dissertation.

I am profoundly grateful to Prof. Dr. Marlies Knipper for her exceptional mentorship, insightful feedback, and unwavering encouragement. Her expertise and dedication have been instrumental in shaping this work.

I also extend my heartfelt thanks to Prof. Dr. Uwe Klose for his collaborative spirit, constructive suggestion, and continuous support in the development of the study. His knowledge and experience have been essential for this research.

Finally, I am thankful to all my colleagues, friends and relatives who have offered their assistance and moral support during this journey.

Thank you all for your contributions to this dissertation.

Sincerely,

Giulio Mendola